CHRONIC SHEAR STRESS EFFECTS ON ENDOTHELIAL CELL RESPONSE

by

Selim Elhadj

Chemical Engineering Department, Virginia Polytechnic Institute and State University, Blacksburg, VA

Doctor of Philosophy

In

Chemical Engineering

Approved:

_____

Kimberly E. Forsten, Chair

_____

William H. Velander

_____

Michael R. Akers

_____

Aaron Goldstein

_____

Rick Howard

10 December, 2001

Keywords: shear stress, endothelial cells, proteoglycans, IGF-I, IGF-binding proteins, strain

Chronic shear stress effects on endothelial cell response

by

Selim Elhadj

Kimberly E. Forsten, Chair

Chemical Engineering Department

Abstract

The overall focus of this dissertation is on how chronic shear stress alters the synthesis and secretion of important regulatory molecules by endothelial cells. Our hypothesis was that inclusion of chronic pulsatile shear stress in our model would lead to changes in endothelial cell release of regulatory molecules. We distinguished between high arterial shear stresses and low venous shear stresses and used static cell cultures as reference. The first part of this research thus entailed the complete characterization of the flow dynamics in our experimental biomechanical model. Cell stretching can have a physiological effect on endothelial cells; hence we implemented a laser based optical technique for real time strain measurement of the growth fibers used in our culture system, and found that no significant strains were occurring during shear treatment. After characterization of the mechanical environment of the cells, we focused the scope of our research on metabolism of proteoglycans and insulin-like growth factor-I (IGF-I) and related IGF binding proteins (IGFBPs) in bovine aortic endothelial cells cultured under chronic pulsatile shear. We found that shear stress increased the release of proteoglycans and significantly altered proteoglycans distribution. We also found that there was an inverse relationship between the shear level treatment used to obtain the purified proteoglycans from endothelial cells and their potency in inhibiting coagulation. IGF-I release and message (IGF-I mRNA) was decreased at high shear stress compared to low shear stress. Further, the levels found under shear were significantly greater than those observed in the static cell culture model. IGFBPs released were also significantly increased by shear. This research thus establishes a link between chronic pulsatile shear stress and the metabolism of both primary (IGF-I) and secondary (IGFBPs, proteoglycans) regulators of vascular cell activity. The improved realism of our experimental biomechanical model has proved to be a valuable tool in improving the relevance of this study to vascular research. Ultimately, this research calls for further investigation in the molecular mechanisms underlying the phenomenological effects documented, which may help in

understanding fundamental aspects in cardiovascular disease and its link to hemodynamics but our work is an important first step.

Table of Contents

List of Figures

Chapter V: Chronic Pulsatile Shear Stress Increases Insulin Like Growth Factor-I (IGF-I) and IGF Binding Protein Release *in vitro*

List of Tables

Chapter I: Introduction and Overview

Cardiovascular disease - atherosclerosis

The amount of literature related to cardiovascular disease (CVD) is staggering. Nevertheless, CVD remains the number one killer amongst the more developed nations [1] (Figure 1). Vascular intervention (angioplasty, bypass surgery, vascular implants) provides a temporary, *ad hoc* relief, however restenosis, reocclusion of the blood vessel, occurs within a month to a year in as many as 50 % of the patients treated requiring further intervention. Vascular grafts less than 6 mm in diameter have patency rates below 30 % after 5 years [2]. While systemic factors that include life style, smoking and predisposing conditions such as hypertension, diabetes, and individual genetic make-up are major contributors of CVD, the location of atherosclerotic lesions is not random within the vasculature [1]. Hemodynamic factors have been implicated in the occurrence of these lesions because they occur at well defined regions of the vasculature characterized by bifurcation, bends, and in locations where blood flow re-circulation, flow separation, and low oscillating shear stresses appear [3-6] (Figure 2). However the mechanism by which hemodynamics act to generate or favor these lesions are still very much subject to ongoing research.

Endothelial (EC) and smooth muscle cells (SMC) within the vascular wall are essential to vascular physiology and their metabolism of blood components and response to vessel mechanical forces can determine the progression of vascular disease [7-9]. Endothelial cells line the inside of all type of blood vessels including arteries, veins, and microvascular blood vessels although specific characteristics may differ between cells from these altered environments [10]. As a monolayer, they separate the blood flow from the underlying cells and tissue and participate actively in the various functions of the blood vessel wall. The EC monolayer and its basal laminae constitute the intimal layer of the blood vessel. The medial layer is comprised of multiple layers of SMC and secreted extracellular matrix (ECM), while the adventitial layer is comprised of SMC, fibroblasts, ECM, blood vessels, and nerves. Hence, as the main components of the vascular wall, EC and SMC biology is key in the development of atherosclerosis [11].

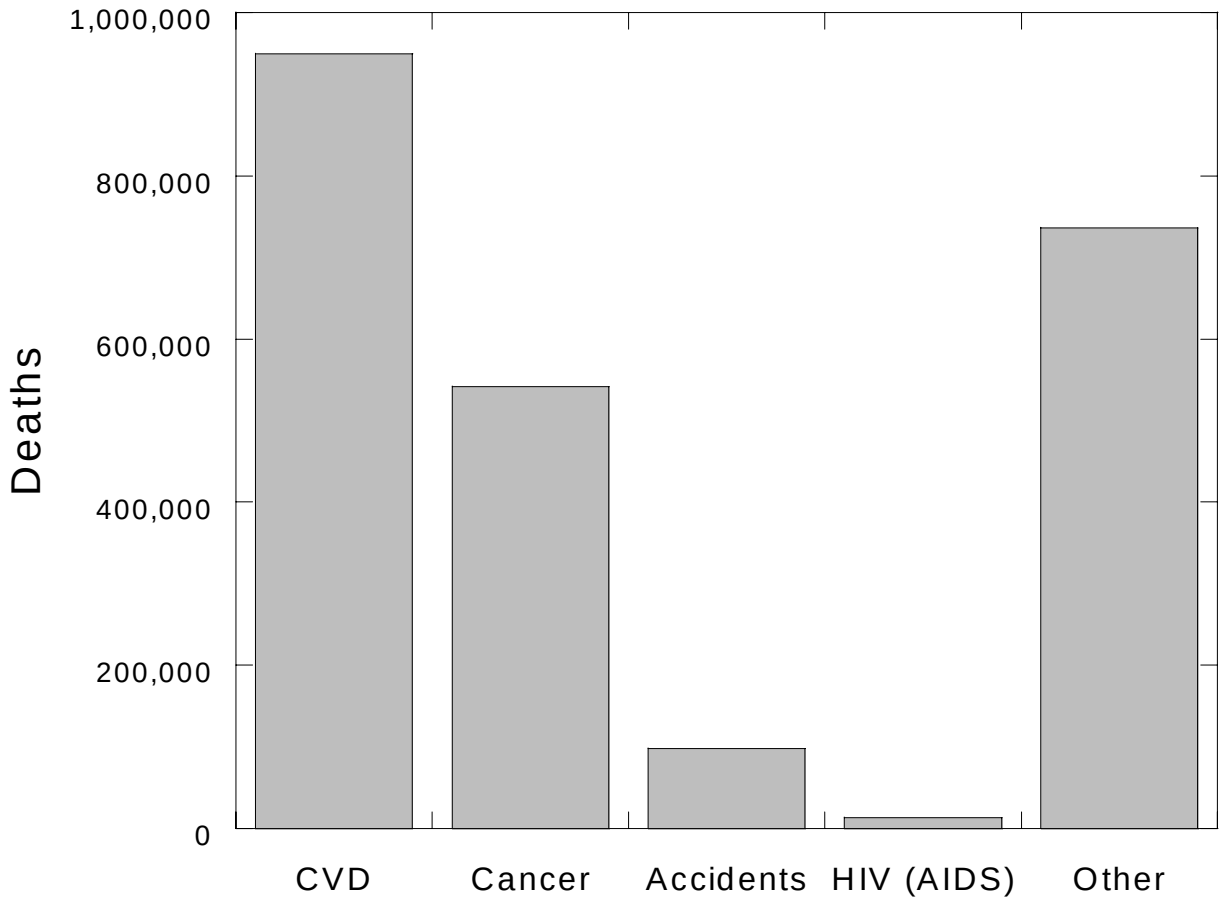

Figure 1. Cardiovascular disease (CVD) is the leading cause of death in the US. Data from the American Heart Association (1998).

Atherosclerosis is characterized by a thickening and occlusion of blood vessel that can lead to tissue damage, aneurysm, stroke, and heart malfunction. The prevalent hypothesis on the formation of atherosclerotic lesions lies in the response to injury model [10, 11]. In this model, chemical and/or mechanical injury, as occurs during hypoxemia, coronary angioplasty or within high shears stress gradients regions in the vasculature, disrupt the endothelium and alter permeability. Fatty components (low density lipoproteins (LDL)) deposition follows as well as a promotion of inflammatory reactions. A compromised endothelium resulting from desquamation or partial denudation exposes the cellular matrix leading to platelet aggregation and thrombosis. In addition, a growth factor driven migration within the intima of monocytes and smooth muscle cells contributes to intimal hyperplasia. At this point, the luminal protuberance created affects blood flow patterns by creating regions of re-circulation and flow separation where the velocities

are necessarily reduced. This increased residence time favors plaque deposition by augmenting monocyte and endothelial cell interaction, platelet binding to the denuded substrate, and further increases lipid permeation inside the arterial wall [12]. Macrophages and SMC augment their LDL uptake as intimal LDL concentrations increase, contributing to the lipid and cholesterol deposition process [7]. Increases in connective tissue production by SMC also contribute significantly to intimal thickening. Ultimately, necrosis of the neointimal cells (SMC, EC, and monocyte derived macrophages), cholesterol deposition, and calcification of the tissue leads to a hypertensive condition and predisposes the patient to life threatening cardiovascular diseases. Other complications at these sites may include hemorrhages and even breaks of the atherosclerotic plaques that can cause embolism and tissue ischemia downstream [10]. This suggests that hemodynamics can affect the injury-state of the endothelium and can alter the transport characteristics of relevant blood components that favor the acceleration of atherosclerosis. It is unclear how these altered dynamics are initiated, however, our interest is on how endothelial response may be altered once changes in shear have occurred.

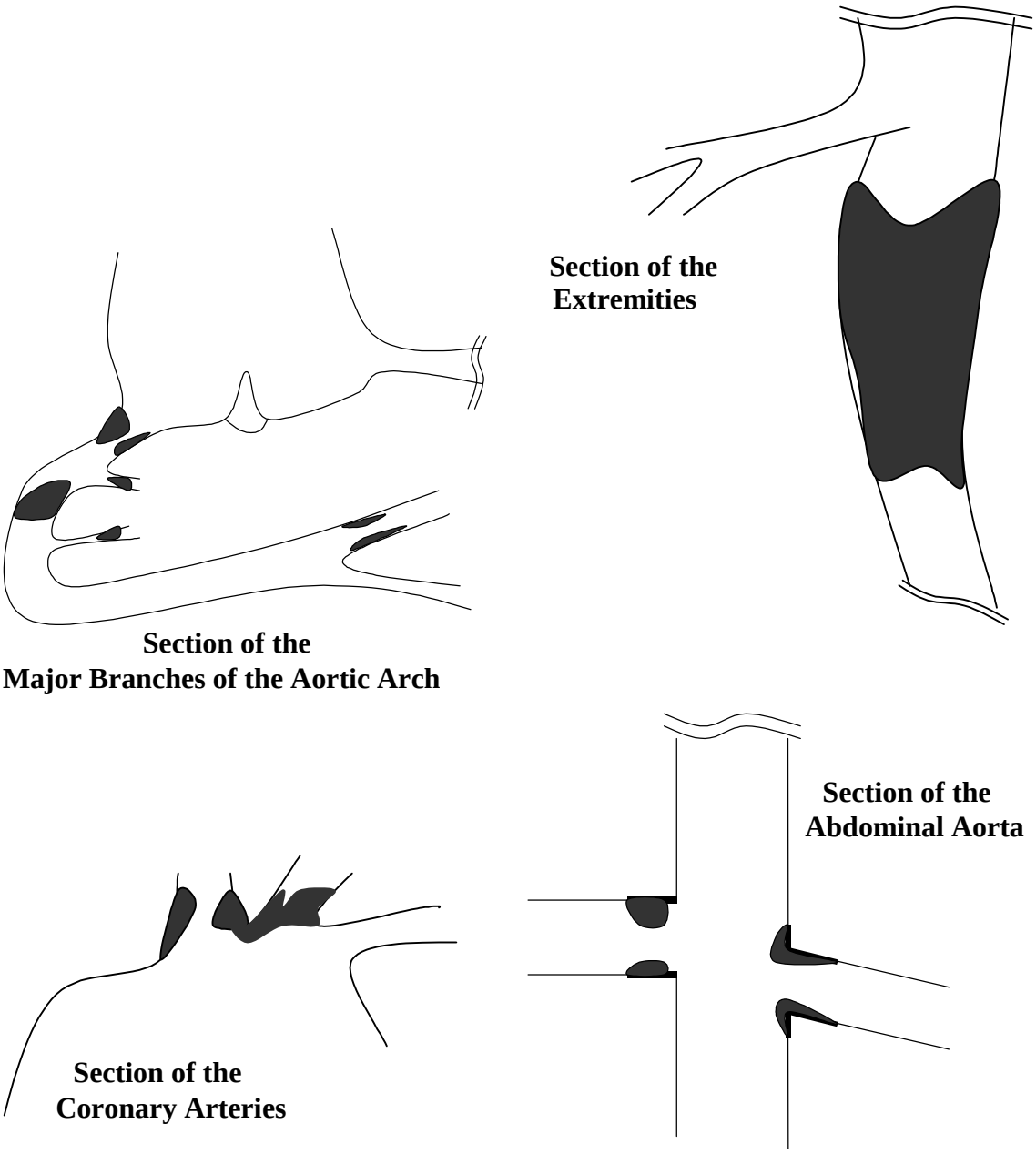

Figure 2. Vasculature configuration – darkened areas show the preferred locations for atherosclerotic lesions. Most atherosclerotic lesions occur in bifurcations or downstream from bifurcations. These regions often include disturbed blood flow mechanics. Redrawn from DeBakey et al. (1985) [13].

Endothelial cells (EC) and smooth muscle cells (SMC) and their implications in atherosclerosis

The vasculature consists of three type of cells: endothelial cells (EC), smooth muscle cells (SMC), and fibroblasts. The EC monolayer and its basal laminae constitute the intimal layer of the blood vessel. The medial layer is comprised of multiple layers of SMC and secreted extracellular matrix (ECM), while the adventitial layer is comprised of SMC, fibroblasts, ECM, blood vessels, and nerves. Both *in vivo* and *in vitro* studies have focused on EC and SMC activity primarily due to their importance with regard to the development and progression of arteriosclerotic lesions [1, 3, 4, 14-31]. Both EC and SMC are known to secrete cellular and extracellular proteoglycans (PGs) and glycosaminoglycans (GAGs) [30, 32-49 15, 18, 36, 39, 50-54], but we focused on the EC model in this dissertation. EC are also quite active in modulating myogenic responses [19], vasoactivation [55], vascular remodeling [9], and influence vascular tone through SMC contraction and relaxation effected by endothelial relaxing factors (e.g., nitric oxide, endothelin, prostacyclin) [56]. Furthermore, angiogenesis and metastasis are related to EC secreted growth factors [57], matrix components [49], and cell surface receptors [58]. The configuration of a segment of an arterial wall is shown in Figure 3A and 3B along with the principal hemodynamic force components acting on it.

Major matrix components within the arterial wall are collagen, elastin, proteoglycans, and basal surface anchoring proteins such as fibronectin, laminin, and vitronectin [59]. The majority of these cell-anchoring proteins can interact with transmembrane integrins that provide a continuum between cytoskeletal elements and the extracellular matrix [60]. The EC layer and the underlying matrix primarily generated by EC and SMC act as a filtration barrier for blood flow components such as proteins, water, and various ions. In general lipid-soluble compounds and smaller molecules permeate with relative ease compared to lipid-insoluble compounds and large plasma proteins [61]. Larger molecules undergo a more controlled permeation that is tissue dependent, and may rely on specific channels or fenestrea [52] in addition to vesicle mediated transcytosis for transport [62]. Blood components transported across the arterial wall include growth factors, inflammatory cytokines, lipoproteins, and various blood pathogens [30]. The glycocalyx associated with EC is thought to play an important role in the filtration process of permeation of these molecules [63]. For example, PGs and GAGs confer a negatively charged

barrier to the glycocalyx that acts to allow selective vessel permeation [63]. The same process was shown to be involved in the occurrence of hypercholesterolemia in rabbits [64]. Hormones (e.g., prostacylcin [65] and bradykinin [66]) produced by EC and regulated by shear stress also influence permeability or molecular influx, indicating that EC take an active role in arterial wall permeation. The combination of monocyte recruitment and LDL uptake and metabolism by EC is, perhaps, the most significant process in the progression of arterial lesions [7]. EC PGs are known to interact with LDL [35] thereby determining the metabolic fate of LDL in conjunction with monocyte-derived macrophages [67].

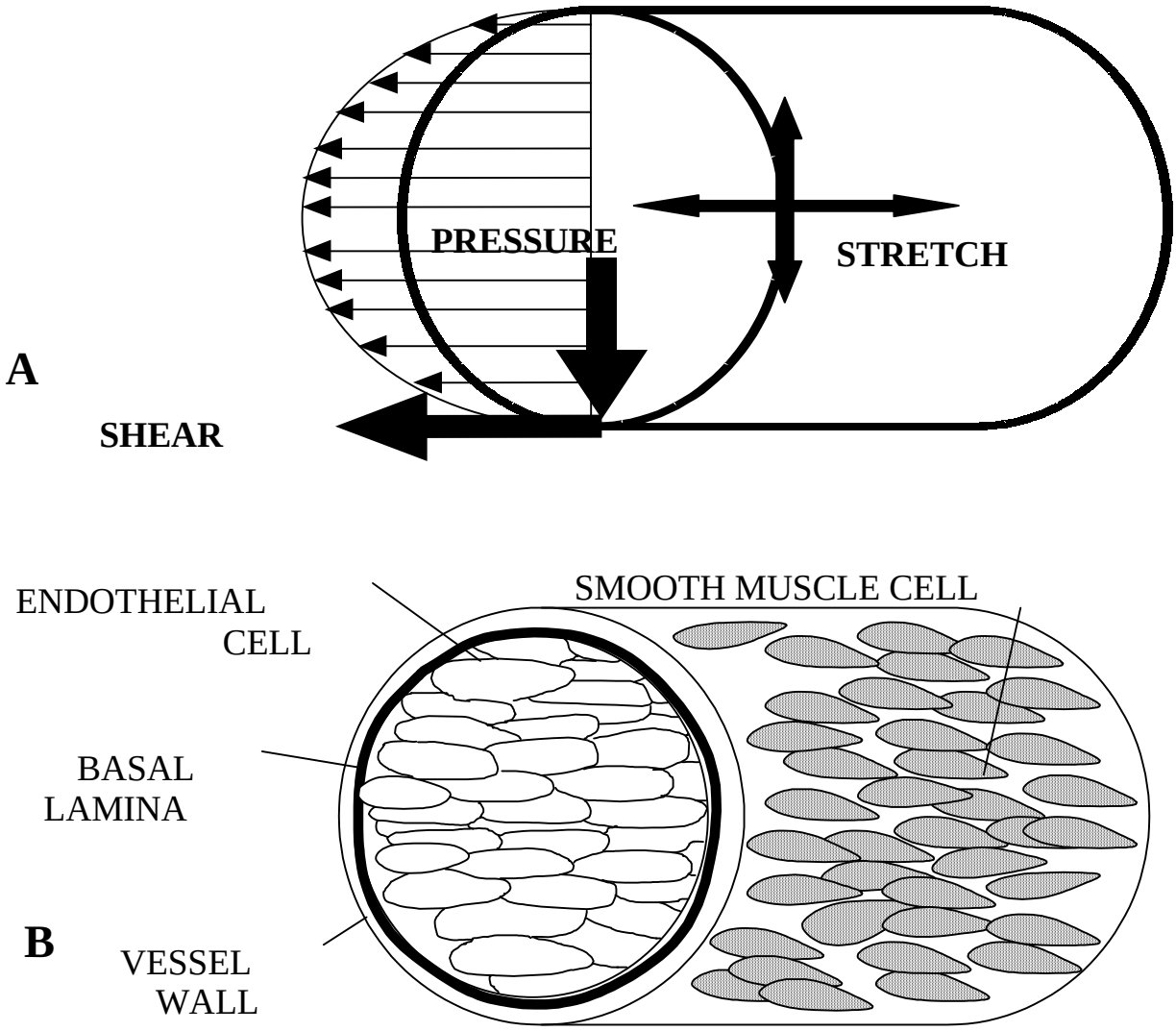

Figure 3. Schematic of a section of a blood vessel wall. Arrows indicate the hemodynamic force components acting on the vessel wall (A). The main vascular wall components are also shown (B).

An essential role of the endothelium is to maintain a clot-free environment in healthy blood vessels. This antithrombic property results from isolating the perfusing blood components from the highly thrombogenic underlying tissue and reducing activation of coagulation factors [68, 69]. In a related way, endothelial cell surface and soluble PGs and GAGs potentiate the inhibition of proteases involved in the clotting cascade [30]. EC are also involved in the response to injury by promoting the formation of thrombus that act as plugs. EC secrete proteins that

favor platelet aggregation (e.g. endothelin and Factor VIII-VWF [70]) and wound healing. The wound healing process itself depends on the attachment of circulating leukocytes through pseudopod formation [71] and secretion at the endothelial cell surface of adhesion molecules [72], both phenomena having been shown to be altered by shear stress. Further responses to chronic injury include the migration of SMC into the intima of the artery caused by chemotactic gradients and multiple growth factors [7, 73] that favor the proliferation of SMC. These growth factor activities are themselves modulated by EC secreted PGs either by sequestration/release or by potentiation [36, 74]. The evidence so far discussed strongly suggests that EC are actively involved in the pathogenesis of atherosclerosis and that this pathology can be influenced by both shear stress applied to EC and proteoglycans expressed by EC.

Smooth muscle cells respond to platelet derived growth factors (PDGF) and basic fibroblast growth factor (bFGF) [7] by proliferating especially after "injury" to the endothelium lining. Regulation of these heparin-binding growth factors by EC proteoglycans is critical. However, non-heparin-binding growth factors, such as insulin-like growth factor-I (IGF-I), may also have a role. In normal arteries IGF-I – a potent growth regulator of vascular smooth muscle cells – expression is limited, however increased IGF-I gene expression occurs in the rabbit model of balloon injury [75] and in the coronary arteries of allografts undergoing chronic rejection [76]. These observations led to studies on the role of IGF-I in modulating intimal hyperplasia in IGF-I treated grafts [77]. It was found that grafted arterial tissue treated with IGF-I and immunostained for α-actin, showed a significant thickening over control in a rat model. Concomitantly, IGF-I deposition in the intima increased in a dose dependent manner with IGF-I concentration treatment. That data suggests that SMC proliferation and migration is linked to IGF-I presence at the locations of tissue formation, especially after injury.

Intimal/arterial thickening is also further induced by uptake of LDL by SMC and generation of excess connective tissue [78] such as collagen and proteoglycans [54]. This dynamic interaction between endothelial cells and SMC is evident in the effects of increased permeation as in "minor" injury and desquamation in more serious chronic injuries of EC [79]. Not only is the attachment of platelets enhanced and their survival decreased [80] but blood components normally confined to the blood stream now interact with SMC to lead, possibly, to advanced lesions that, in time, will occlude the blood vessel [10].

Hemodynamics

The focus of this research was on how shear stress affects endothelial cell function since endothelial cells *in vivo* are constantly exposed to shear forces stemming from blood flow. Numerous studies have reported an endothelial cell function dependence on shear stress, which can be linked to vascular wall physiology [17]. Hemodynamic forces from blood flow and the interaction between fluid frictional forces and the vascular wall result in wall shear stress. By definition shear stress is the ratio between tangential force per unit surface area. Shear stress on endothelial cells is determined from the velocity gradient at the wall and the ability of the perfusing fluid to transmit shear forces through frictional contact. This property of the fluid to transmit fluid shear forces is the fluid viscosity. A gradient in the fluid velocity profile (how the velocity of the fluid elements changes with position) exists because, typically, fluids do not slip at the wall, hence the velocity at the wall is negligible. For a non-turbulent laminar flow in a tube that would approximate a segment of an artery, the velocity is maximal at the cylindrical axis and is symmetrical with respect to that axis. Conservation of momentum equations are used to determine the specific expression for the velocity profile and then the shear stress calculated by evaluating the gradient at the wall position. While fluid viscosity may depend on shear rate (the rate at which the fluid is moving per unit length), aqueous fluids such as cell media typically do not vary significantly with shear rate. Hence the simple product of shear rate or velocity gradient with the fluid viscosity allows the calculation of shear stress. It should be noted that the exact shear stress applied at the wall due to blood flow might not be known in detail since endothelial cell shape at the lumen of an artery will alter the flow. Therefore, only bulk shear stress values are used that do not reflect exactly the actual shear stress distribution, which could only be calculated if the cell topography was experimentally determined [81].

As an interface between blood circulation and underlying tissue, EC constitute a major component of the arterial biology. EC regulation of cellular metabolic activity and physiologic responses of the underlying tissue is conditioned by the nature of the flow it is exposed to. The hemodynamic environment in blood vessels is complex and, while flow patterns and blood velocities can be measured [82-84] or determined by computational fluid dynamics [85-87], the state of the mechanical stress *in vivo* at the cellular level is rarely known. With specialized imaging techniques of the cell topography, estimates of the shear stress distribution and the shear stress

gradients can be obtained [81]. However, most studies on shear stress effects focus only on average shear stress near the wall as the functional variable.

Typical experimental models used to date utilize flow chambers and plate-and-cone apparatus that generate a sustained laminar flow [88]. The ease of use of parallel flow chambers has led to their extensive use since cells can be visualized in real time and the shear stress levels can be readily calculated. Their rectangular geometry, however, does not replicate the more typical cylindrical configuration seen *in vivo*. Plate-and-cone experimental models have the advantage of inducing flow with a moving upper conical boundary and, thus, do not generate any pressure gradients that could alter cell function [89, 90]. Still, their use is limited by an unconfined lateral boundary and the generation of complicated flow patterns at high rates of strain [88]. Culture systems based on hollow fibers are useful especially in vascular research since they replicate better the configuration in blood vessels. Calculation of shear stress levels is also readily achieved, but the visualization in real time is not possible without the use of transparent fibers and a specialized setup to flatten the fiber [91]. The surface to volume ratio of the cylindrical geometry increases the number of cells that can be seeded per unit volume, and increases the amount of metabolite obtained per experimental unit thus facilitating analysis. Whatever the experimental model used, typical *in vitro* shear stress levels are < 6 dynes/cm^2 [3, 92-95] for low shear stress treatments, while high shear stress treatments are approximately 35 dynes/cm^2 [6, 96, 97] or greater. The low and high shear distinction reflects typical values for a spectrum of arterial shear stresses and have been documented to be in the order of a few dynes/cm^2 for low shear and around 25 dynes/cm^2 for high shear [83].

In contrast with the shear stress models discussed so far, the Cellmax® capillary system is a relatively new biomechanical experimental model used in this research to allow for chronic shear stress treatments of bovine aortic endothelial cells (BAEC). Its feasibility for sustained cell culture has been demonstrated in previous studies and has been used to simulate blood flow and to apply shear stress to endothelial cells seeded in the lumen of capillaries. Redmond *et al.* (1995) showed that endothelial cells grown under chronic pulsatile shear stress conditions (for up to 7 wk) exhibited a typical elongated profile and grew as a confluent monolayer [98]. Further studies using the same model demonstrated that shear stress could alter endothelin receptor regulation and G-protein expression [56, 99]. Capaddona *et al.* (1999) used the Cellmax® to study

the effects of pulsed pressure on SMC phenotype and found significant differences in various differentiation markers in SMC depending on whether cells were subjected to pulsed pressure or not [100]. The Cellmax® was also used to determine flow effects on endothelial nitric oxide synthase and ethanol mediated SMC migration [101, 102]. More recently, Redmond *et al.* (2001) demonstrated the role of plasminogen activator inhibitor-1 in endothelial cell mediated growth inhibition of SMC migration [103].

These experiments were carried under chronic shear stress conditions and further reinforce the Cellmax® system as a valuable tool in vascular biology, especially in its ability to duplicate vascular wall configuration and for its use in prolonged sustainable growth. The positive displacement pump system used to drive the flow in the Cellmax® generates some level of pulsatility in the flow depending on the flow regime specified. Since blood flow pulsatility is a natural and important component of the mechanical signaling to endothelial cells [92], a model that incorporates pulsatile flow is advantageous. However, the velocity profile and thus the shear stress is now time dependent and requires monitoring of the pressure gradient in real time and the use of the Womersley equations [104, 105] to resolve them.

Hemodynamic parameters that have been correlated with atherosclerotic lesion location are the oscillating shear index, maximum wall shear stress, and mean wall shear stress [22]. These parameters are thus useful for a more complete characterization of shear stress treatment *in vitro*. For instance, variations in shear stress have been shown to result in increased levels of active transcriptional factors [5] and increases in EC permeability [6]. Interestingly, work by Ziegler *et al.* (1998) demonstrated that sustained laminar low shear stress increased endothelin (a strong vasoconstrictor and SMC mitogen) expression less than an oscillatory shear stress with the same time-averaged shear stress [92]. This evidence reinforces the importance of spatial and temporal variations of flow on EC biology.

The emphasis in most studies to date has been on shear stress effects on endothelial cells under acute conditions. Cells are typically seeded and grown to confluence in a static cell culture plate before applying specified levels of shear stress lasting up to 24 hrs [65, 81, 92, 106-108]. For example Arisaka *et al.* (1995) [106] and Grimm et al. (1988) [32] studied shear stress effects on proteoglycan metabolism under acute conditions and subjected endothelial cells to shear treatment for up to 24 hr. Studies on growth factor regulation by shear stress such as PDGF [109]

and TGF-β1 [110] were also performed under acute conditions. The metabolic fate of these molecules beyond the 24 hr shear treatment used is not clear and may vary as the cells reach a more differentiated state over prolonged period of time [111, 112]. Acute shear stress conditions are rarely seen *in vivo* since some level of blood flow is always present in the vasculature. The importance of chronic shear stress treatment where EC are cultured under shear is illustrated in studies where cells are shear-conditioned to improve vascular graft performance upon transplantation [111-113]. Further, morphological and structural alterations occur approximately within the first 24 hours after onset of flow [17] and thus shear stress forces at the cell surface will change during acute application of shear treatment. Basal response to flow is more likely to occur after cells are set and aligned in the direction of flow and all cytoskeletal and focal adhesion sites have been formed. Hence the advantage of studying cells under chronic shear stress conditions lies in the cells being closer to their natural state of differentiation *in vivo*, where basal response to shear forces are more likely and more pertinent to vessel wall physiology and pathology.

EC interact directly with forces associated with blood flow in addition to stretch forces driven by transmural pressure gradients [111]. Other cells present within the vascular wall, such as SMC and fibroblasts, are subjected to limited interstitial shear stresses [52] but are continuously strained in a cyclical fashion. This strain combined with shear stress synergically enhances morphological changes at the cytoskeletal levels [108] in SMC and promotes cell proliferation by augmenting IGF-I expression in EC [114]. The details of blood flow have been shown to be important in determining phenotype and cellular metabolism [17] and significant efforts have been made to model them for specific configurations and locations in the arterial tree [52, 85-87, 115, 116]. Responses to flow occur within seconds after a perturbation or can be generated over period of a few hours to a few days [17]. While flow and stretch physiological effects have been well documented [2, 60, 117, 118], it is not yet clear how those forces are sensed and transmitted by cells to generate a response. Regions of endothelial cells focal adhesion may be important in that process as they tend to realign in the direction of sustained flow forces, thus allowing for the adjustment of cell morphology to flow [107]. These structural changes are accompanied by a streamlining of the cells that reduces - as indicated by computational fluid dynamics - the effective shear stress and shear stress gradient on the cells [81]. Interestingly, those adhesion sites

are also associated with increased kinase activity [59] that would suggest that focal adhesion sites might be, at the least, one of the shear stress mechanosensors available to the cell.

The mechanotransduction of signals from surface and body forces to transcription effectors are better understood. Secondary messengers, such as calcium [119], inositol trisphosphate [120, 121], and arachidonic acid [65] have been implicated in the activation of key enzymes in signaling cascades involving protein kinases [119]. Morphological changes of EC - occurring hours after onset of a sustained flow - are related to stress induced signaling since inhibitors of cytoskeletal formation inhibited the cells response to flow effects [122]. Therefore the cytoskeleton has been proposed as the mediator of force transmission to various locations within cells where cell responses are activated [123]. Structures of the cytoskeleton that are associated with the nucleus may generate - through shear stress response element (SSRE) – early and sustained responses to blood flow characteristics [95, 124, 125].

Shear stress has been shown to be a potent regulator of gene expression [126] and has suggested the use of vascular EC as ideal candidates for targeted cardiovascular gene therapy using specific shear stress response elements [124]. To date, few studies on gene regulation of shear induced PGs expression have been performed. Thrombomodulin (a cell surface PGs) mRNA levels increased with flow in human umbilical vascular endothelial cells [17], however, arterial flow conditions applied to saphenous vein EC decreased significantly the presence of immunostained thrombomodulin [127]. At this point it should be noted that shear stress not only affects gene expression but it also determines the differentiated state of the EC. In a study by Ballermann *et al.* [112], using both BAEC and glomerular capillary EC cultured under shear stresses of up to 15 dynes/cm^2, significantly more pronounced differentiation features such as reduced turnover, increase in Weibel Palade bodies (storage sites for Willebrand factor), increase acetylated LDL up-take, and rearrangement of the cytoskeletal structure in the direction of flow were demonstrated. All of these EC features were shown to be brought about by shear stress treatments and are present in their *in vivo* counter-parts. Thus, EC cultured under shear constitutes an improved model for the study of EC biological functions, based on their state of differentiation that more closely resembles that present *in vivo.*

Proteoglycans (PGs) and glycosaminoglycans (GAGs)

PGs are ubiquitous molecules present in all mammalian tissues, consisting of a protein core and at least one unbranched, GAGs chain [128]. Six types of GAGs are currently known: heparan (HS), chondroitin (CS), dermatan (DS), keratan sulfate (KS), as well as heparin and hyaluronic acid (HA) [128] (Figure 4). These GAGs are defined by specific types of modified disaccharide repeat units such as iduronic and hexosamines and other saccharride units [128]. Typically, GAGs are attached to the core protein through a serine xylosyl covalent bond although, in some instances, an asparagine is substituted for the serine residue. PGs are post-translationally N- or O-sulfated and glycosylated by various enzymes in the Golgi apparatus [128]. GAGs are highly heterogeneous even amongst members of the same core protein family. Interestingly, heparan sulfate and heparin contain the most negatively charged structures produced by vertebrate cells [129] and this property of PGs is critical for their biological function. PGs are present in relatively small amounts in vascular tissue (2 to 5 % by dry weight) particularly when compared to the large amounts found in cartilage (50 % by dry weight) [30]. PGs are found as transmembrane molecules, cell membrane associated molecules via covalent binding to a membrane phosphoinositol, incorporated within the extracellular matrix or released into the perfusing media. Many of the mechanisms by which PGs and GAGs perform the functions discussed below remain speculative or rely on circumstantial evidence, primarily because genetic manipulation, function blocking antibodies, GAGs-protein interfering reagent, and adequate drug that can intervene with GAGs biosynthesis remain limited [130]. However, significant advances in the understanding of the cellular functions of PGs have been made over the years and some of them will be discussed below. A schematic representation of a typical PGs is shown in figure 4.

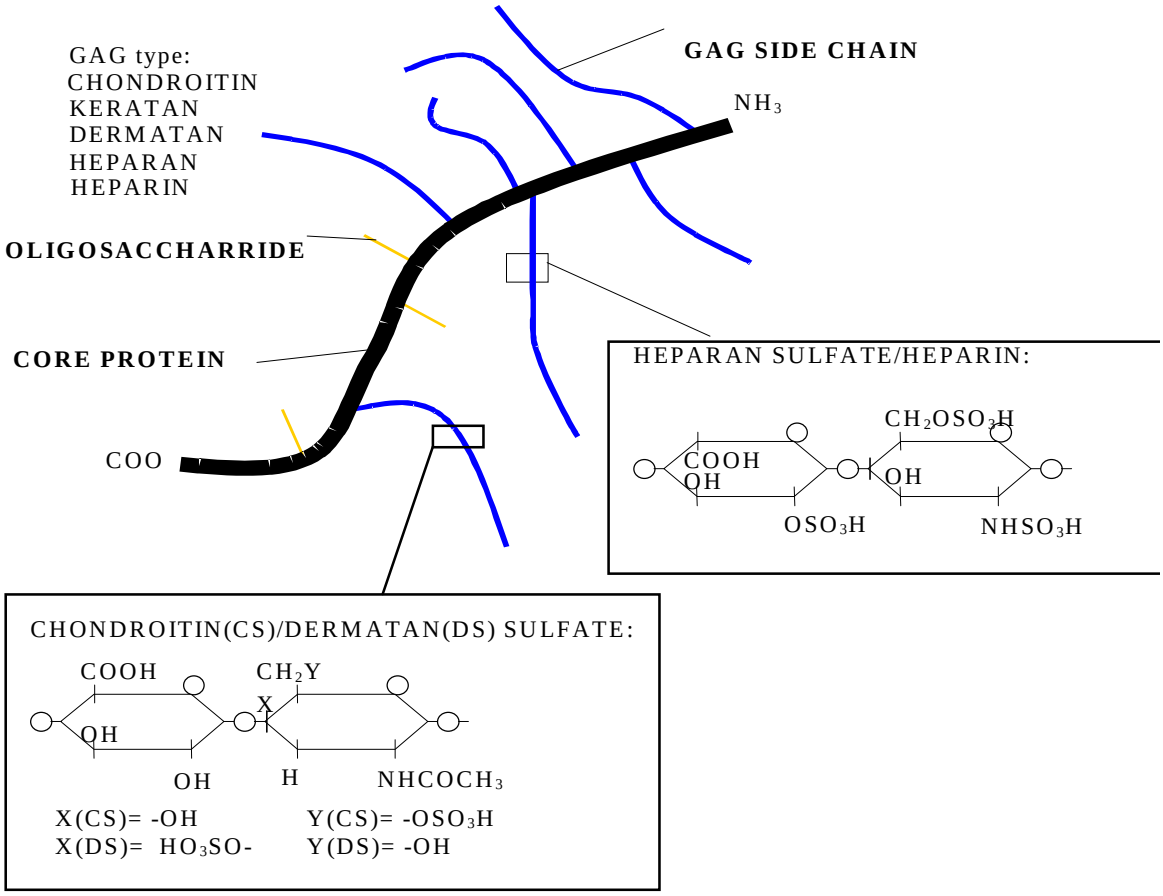

Figure 4. Schematic representation of a prototype proteoglycan. Included is the basic structure of representative disaccharide units for heparan sulfate and heparin, as well as chondroitin (CS) and dermatan sulfate (DS).

PGs functions include both spatial and temporal management of growth factors by increasing their half-life *in vitro* and either by sequestering them within the extra cellular matrix (ECM), or by specifically targeting bound growth factors to nuclear sites [131, 132]. Since ECM associated PGs can act as growth factor "sinks" via reversible growth factor binding, it is not surprising that soluble forms of PGs can control the release and activity of growth factors by competing for bound ligands [30]. Similarly, secreted enzymes such as heparanase can digest HS from ECM bound PGs thus releasing growth factors. This release of growth factors is important in vascular remodeling and repair [133] and may also be involved in angiogenesis [47]. For example, the combination of acidic fibroblast growth factor (aFGF) and PGs accelerated the repair process in confluent human vascular endothelial cells *in vitro* [133]. Furthermore,

metastasis, as it involves the formation of new capillaries that sustained tumor growth, was inhibited by heparanase treatment [49]. In this study [49], heparanase activity was shown to correlate with the metastatic potential of various tumor cells and heparanase inhibiting molecules significantly reduced the occurrence of lung metastasis in experimental animals. Conversely, growth factors may themselves affect PGs function. It has been suggested that transforming growth factor-beta (TGF-β) protects blood vessels from atherosclerosis by preventing SMC proliferation [73]. However, TGF-β also contributes to the pathogenesis of lipid-rich atherosclerotic lesions by stimulating the production of arterial PGs that trap lipoprotein [15]. There is little doubt that, due to the ubiquitous nature of PGs, they effectively bind most of the growth factors and cytokines that have GAGs and/or protein core binding domains. Thus, PGs play an important role in tissue formation, modeling, and in various pathologies.

The diversity of PGs mainly stems from the variety of protein cores and post-translational modifications within the GAGs of the PGs [128]. This diversity might explain how PGs can influence so many arterial functions including, hemostasis [134], wall permeability [61], LDL metabolism in EC [30] and SMC [45], thrombosis [30], wall viscoelasticity [30], inflammatory response [48], and vascular remodeling since PGs can act as modulators of growth factor activity [74]. Many of these functions result from the interaction of PGs with secreted, cell membrane, and extracellular cell matrix proteins also referred to as heparin binding proteins since many of the studies of PGs interaction use heparin as a model glycosaminoglycan [129]. However, PGs and GAGs can be very specific in their mode of action. For example, the enhancement of bFGF activity results from specific interactions with the growth factors GAGs binding domains of surface heparan sulfate PGs (HSPG) [36]. Targeted enzyme digestion of heparan sulfate abrogates the potentiation of bFGF while treatment with chondroitin sulfate specific enzyme does not.

Specific sugar residue sequence with well defined sulfation sites within HS or heparin have been shown to be essential in the acceleration of antithrombin III inhibition of thrombin protease (clotting factor) [128]. PGs and heparin have been shown to participate in the coagulation process (Figure 5).

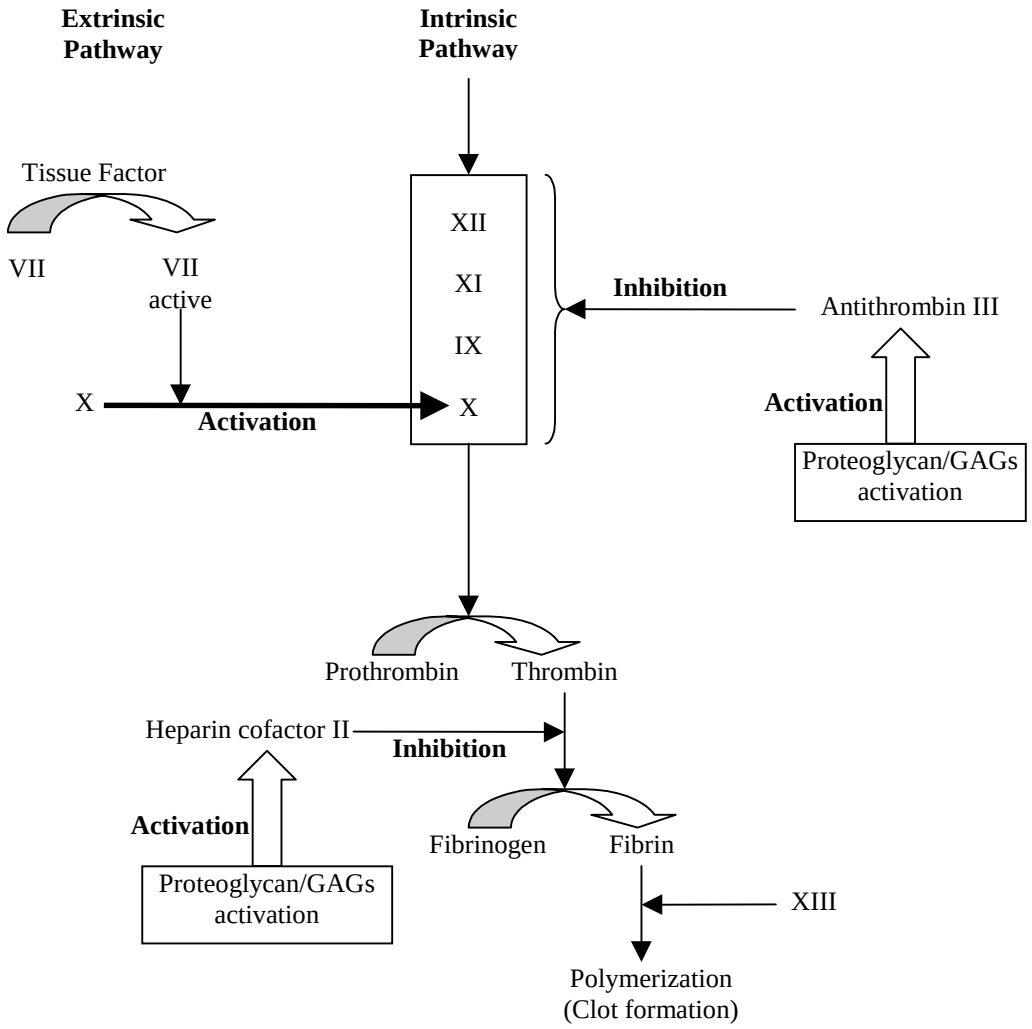

Figure 5. Intrinsic and extrinsic coagulation pathways inhibition mechanism by proteoglycans and glycosaminoglycans (GAGs). Antithrombin III and Heparin cofactor II activity is significantly increased by heparin and heparin like proteoglycans/GAGs. The inhibition of coagulation cascade proteases shown (factors XII, XI, IX, X) results in inhibition of clot formation. Thrombomodulin is a proteoglycan with inhibitory properties that enhances inactivation of Factor VIII and V within the intrinsic pathway via activation of Protein C and S (not shown). Redrawn from Nader et al. (2001) [135].

Within the intrinsic coagulation pathway, PGs can inhibit thrombus formation by activating various serpins or protease inhibitors, including antithrombin III [136], heparin co-factor II [128], and leuserpin [128]. While heparin and heparin like GAGs such as heparan sulfate can promote thrombin inhibition 1000 fold through antithrombin III activation, other proteases

(factors IX, X, XI, and XII) can also be inactivated but to a lesser extent (4-15 fold) [30, 128]. Heparin cofactor II, however, is specific to thrombin inactivation but can also be activated by dermatan sulfate GAGs in contrast to antithrombin III, which requires heparin and heparan sulfate specific sequences. Both releasable and surface bound PGs can impact hemostasis as outlined above however, even PGs and GAGs that do not promote thrombus inhibition *in vitro*, can be effective coagulation inhibitors *in vivo* [135]. Endothelial cells exposed to heparin increase the synthesis of antithrombic heparan sulfate on the cell surface and into the medium [137-139]. Some of the heparin and heparan sulfate sequences that failed to have significant effects on serine proteases still resulted in stimulation of antithrombic activity, presumably, by enhancing the release of antithrombic PGs and GAGs [135]. Finally, PGs also interact with blood borne pathogens [140, 141] and influence the viscoelastic properties at substrate interfaces [142]. By all indications, PGs are involved in most if not all cellular functions.

Since proteoglycans are involved in many of the vascular processes relevant to CVD and, particularly, in coagulation and cell migration to the intima of the arterial wall, it is natural to suggest that changes in shear stress might regulate PGs via altered cellular metabolism. Our laboratory [36] and others [18, 30, 39] have already shown that specific types of endothelial-secreted PGs and GAGs inhibit SMC proliferation mediated by growth factors. These *in vitro* studies, however, were performed with static cultures, a condition not normally found *in vivo* for vascular cells. Furthermore, heparin treatment of rat carotid artery following balloon angioplasty endothelial denudation reduced restenosis or re-occlusion of the blood vessels by limiting *in vivo* SMC proliferation [143]. This anti-proliferative effect was shown to be independent of the anti-coagulating property of heparin by specifically altering the pentasaccharide sequence responsible for coagulation. Heparin is also routinely administered to prevent thrombosis [144]; and EC surface PGs also maintain a non-thrombogenic lining. However, cell surface PGs can also act as pro-thrombogenic substances and heparin treatment of EC can lead to cell proliferation [143]. It is thus conjectured that a functional endothelium is essential to maintain hemostasis and for regulation of underlying cell proliferation. PGs are thought to play an important role in these regulatory processes [30].

Insulin like growth factor -I (IGF-I)

Growth factors, such as is insulin-like growth factor - I (IGF-I), can have a significant effect on both the normal and pathologic proliferation and migration found within the vasculature. IGF-I belongs to the IGF peptide hormone family along with insulin and IGF-II. Six known IGF binding proteins (IGFBPs) modulate IGF-I function, including IGFBP-3. EC are a significant source of IGFBP3 in the circulating blood [145] and have been shown to secrete IGFBP-3 in culture when confluent [146]. The binding of IGFBP-3 to IGF-I increases IGF-I half-life and also sequesters it from cell surface receptors [147], thus altering its biological functions. Further, IGF-I is secreted by EC and SMC [77, 148] and was shown to be a potent SMC mitogen, which suggests a significant role in arterial wall response to injury [149]. These mitogenic properties also suggest that IGF-I may contribute to intimal hyperplasia. For example, pretreatment *ex vivo* of allograft from rat aorta with IGF-I led to an increase in the expression of IGF-I and its receptor within the vascular wall, while also up-regulating IGFBP-3 and various other growth factors [77]. The authors speculated that this could, in part, explain the occurrence of accelerated transplant arteriosclerosis, especially considering that IGF-I is up-regulated during graft rejection [77] and in the rabbit model of balloon injury [75]. Increased IGF-I receptor expression has been found in atherosclerotic plaque specimens and, hence, the implication would be that IGF-I has a role in the formation or regulation of atherosclerotic lesions. Further, the interaction of circulating monocytes with the endothelium can involve an IGF-I regulated secretion of cellular adhesion molecules at the cell surface [14]. These molecules allow the recruitment of the monocytes to the inside of the blood vessel wall, which is an early step in the pathogenesis of atherosclerosis. In light of all the above data it is reasonable to assume that IGF-I can play a significant role in the pathology of vascular diseases. The abundance of growth factors known to be regulated by shear stress [65, 110, 150, 151] suggests the possibility that shear stress may also regulate IGF-I metabolism in endothelial cells. Shear stress regulation of IGF-I may then point to one mechanism by which hemodynamics contributes to vascular proliferative disorders.

Overview of this Dissertation

We focused the research presented in this dissertation on how chronic shear stress impacts IGF-I and proteoglycans metabolism in bovine aortic endothelial cells. Growth factors

such as IGF-I have been shown to promote SMC proliferation and migration [114, 147, 152, 153] and can potentially influence proliferative vascular disorders, while proteoglycans can contribute to hemostasis via their antithrombic properties [30, 136]. Hence, with IGF-I and proteoglycans both having a potential role in physiological and pathological vascular processes, we sought to determine if shear stress could affect their metabolism, thereby providing a possible link between the documented correlation between atherosclerosis focal localization and specific features of blood flow that include reduced average shear stresses.

To date, no research has been carried out to look at long term chronic shear stress treatment effects on endothelial cells IGF-I and proteoglycans metabolism by endothelial cells. In a study by Arisaka *et al.* (1995) shear stress applied to porcine aortic confluent EC up-regulated the amount of cellular and extracellular PGs [106]. Grimm *et al.* (1988) showed that the pattern of proteoglycan production changed with application of shear stress on bovine aortic EC and that these patterns resembled those found *in vivo* as shear stress levels were increased [32]. In contrast with our studies, these results were obtained under acute conditions in parallel flow chambers and led to seemingly contradictory observations. For example, whereas Arisaka *et al*. found an increase in PGs release, Grimm *et al*. found a decrease with increased shear stress treatment. While this discrepancy may stem from a variety of parameters such as the source of endothelial cells, differences in shear conditioning time between the two studies may have contributed to this inconsistency as well. These ambiguities reinforce the need to utilize long term shear conditions to establish physiological chronic shear conditions. We used a relatively new biomechanical model that allows for the sustained growth of BAEC cultured and seeded in the luminal side of capillaries under flow, in a configuration similar to that found in the vasculature.

Short-term acute shear stress treatments (<24 hr) may not be physiological and can lead to artifactual results and were thus discarded. Instead, we focused on basal response of BAEC under shear, as it is more relevant to vascular conditions found *in vivo*. The analysis in the proteoglycan studies focused on media proteoglycans released during shear stress conditioning. We do however acknowledge that surface proteoglycans may also play an important role in hemostasis, but their isolation and characterization is more difficult given the limited amounts of cells available in each experiment. Further, IGF-I is only one of many growth factors

participating in autocrine and paracrine cell stimulation and, therefore, the results must be interpreted in light of what these other growth factors can contribute to cellular response.

The mechanical environment seen by endothelial cells *in vivo* often includes significant stretch forces in addition to shear forces [154]. However our biomechanical model was simplified in that it did not include any significant stretch of the cells during perfusion. While stretch forces can impact vascular function and can favor or antagonize endothelial response to shear stress [108, 154, 155], it was important to determine its contribution to our system. However, since the capillaries used as growth substrate were made of polypropylene, there was a potential for capillary deformation during perfusion due to the pressure driven flow. Hence, to determine whether cells might be subjected to stretch forces, we implemented a custom built laser optical technique and data acquisition system to measure real time diameter changes.

Pulsatility of the flow, an inherent feature of our experimental model, simulates some features of the cardiac cycle flows that would be expected in the natural environment of endothelial cells. This pulsatility was thoroughly characterized using harmonic analysis of the pressure waveforms along with a complete modeling of the velocity profiles. These steps insured that flow was laminar and thus fully definable and specified the scope of the shear treatments applied. Two shear stress levels were selected: a high shear stress representative of arterial shear of 23±8 dynes/cm^2 and a low shear of 5±2 dynes/cm^2 representative of low venous shear often associated with atherogenic conditions in arterial branches [22]. Static cultures were used as a reference to which shear results could be compared, but also to explore the adequacy of this model in vascular biology research. Our experimental model approximates both the dynamic and geometric set up that would be experienced by cells in the vasculature, since hollow fibers and a pulsatile pump are used to perfuse and *culture* the EC under shear.

In the first part of this dissertation the mechanical environment and the modeling of the pulsatile flow in our cell culture flow system were analyzed to better define the mechanical parameters during the low and high shear stress treatments of the BAEC (Chapt. II). First, the modeling of the flow was carried out using the Womersley solution of the Navier-Stokes equations and, second, to insure that no significant strain was occurring during the pump driven media flow, a laser optical method was implemented to measure changes in capillary diameter (Chapt. III). The harmonic analysis of these waveforms established the frequency content of the

flow and pressure waveforms, in addition to determining the phase angle difference between pressure and flow. Phase angle differences and flow frequency have both been linked to specific endothelial response hence the need to quantitate them for our system [90, 92, 156]. A custom built data acquisition system is described in this thesis for the measurements of capillary intraluminal pressure and capillary diameter (Chapt. III). The results demonstrated that, under low or high shear stress treatment, EC were subjected to similar and purely sinusoidal frequencies and, in addition, that no significant strain or phase angle differences occurred. Further, the pulsatility of the pressure waveform, the capillary dimensions, and fluid properties were such that a simple Poiseuille flow description of the laminar flow was adequate to model the fluid mechanics of the perfusate in our cell culture system during high and low shear experiments. The analysis of the fluid mechanics indicated that flow rates and phase angle between pressure and flow can be significantly altered depending on the values of these parameters. Hence, the derived Womersley equations for flow modeling are required under these conditions and will be useful in future experiments for alternate experimental models.

Following the mechanical environment characterization, we sought to elucidate effects of chronic shear stress on secreted PGs from BAEC (Chapt. IV). Our hypothesis was that chronic shear stress treatment affects the metabolism of released proteoglycans. It was proposed that shear stress is a regulator of PGs secretion and that this regulation could be reflected in altered inhibition of human blood coagulation and human platelet aggregation. We thus first characterized purified PGs using various chromatographic techniques as well as enzyme digestions and alkaline borohydride treatments of PGs for GAG content analysis. The PGs obtained from the shear treated and non shear treated cells were evaluated on the basis of their anticoagulant effects on thrombin induced human platelet aggregation using aggregometry and tissue factor induced blood clot dynamics using a Thromboelastograh™. The data demonstrate a functional relationship between coagulation inhibition potency in a dose dependent manner and the shear stress levels used to obtain the PGs from shear and non shear treated BAEC. Coagulation experiments were performed at Dupont Pharmaceuticals (DE) with the kind assistance of Dr. Shaker A. Mousa who provided access to the necessary equipment and materials for this part of the research.

This research represents a natural extension of previous studies done in our laboratory [36] and can also be useful for understanding the inherently atheroprotective nature of high shear stresses [8, 157]. Indeed, as described in more detail later in this thesis, our laboratory has found a PGs fraction that appears in the conditioned media at low shear stress but not at high shear stress treatment of BAEC. The released GAG and PGs profiles and amounts were also altered by shear stress treatment as demonstrated by size exclusion and ion exchange chromatography. This study identified a high and low molecular weight (MW) PGs fraction in shear and non-shear treated BAEC that is consistent with previous findings from Forsten *et al.* (1997) [36]. In that study a difference in the potency of low MW PGs versus high MW PGs from BAEC grown under static conditions was found. The high MW PGs were 20 times more potent in inhibiting FGF-2 induced proliferation compared to the low MW fraction. In this thesis we demonstrate a decrease in the relative amount of the high MW PGs fraction with increased shear stress, which could thus suggest, unexpectedly, a more atheroprotective phenotype of the low shear treated EC.

Since PGs do not have inherent growth factor activity and since growth factors are important in proliferative vascular pathologies [73 77, 114, 158, 159], a study of the regulation of IGF-I metabolism by shear stress was performed (Chapt. V). We hypothesized that shear stress alters IGF-I expression and its regulatory proteins: the IGF binding proteins. This study was carried out in conjunction with Dr. R. Michael Akers laboratory, Erika Hensley (Ph.D. candidate, Dairy Science Dept., Blacksburg, VA) and Pat Boyle (senior lab technician, Dairy Science Dept., Blacksburg, VA) in his laboratory. Culturing and shear treatments of BAEC was undertaken in our laboratory using the same experimental protocol used for PGs studies. Using a radioimmunoassay to determine IGF-I concentration in the conditioned media and Northern blotting for IGF-I mRNA message, we found a tendency for IGF-I downregulation with increased shear treatment. Further, IGFBP profiles were also dependent on shear stress levels applied as determined using Western ligand blotting. Thus, alterations in IGF-I secretion and IGFBP profiles were found as a result of shear treatment in contrast with static cultures where IGFBP and IGF-I levels were significantly reduced on a per DNA basis compared to shear treated cells.

A conclusion chapter is provided at the end of this dissertation that summarizes and analyzes experimental results from all studies presented (Chapt. VI).

Chapter II: Characterization and modeling of the experimental flow

Hemodynamics characterization

Measurements of the pulsatile pressure drop and average volumetric flow rates allow modeling and characterization of the flow within our experimental model. Since endothelial cells reside at the interface between the perfusate and the capillary luminal wall, all hemodynamic components can be sensed and ultimately transduced to affect cellular metabolism, cell phenotype, and vascular wall physiology [17]. Hence, a determination of the specific features of the experimental flow is required to properly characterize the mechanical environment pertaining to the cells. These features include whether the flow is laminar or turbulent, the frequency and amplitude of the flow waveform, and whether significant phase angle difference exists between flow and pressure waveforms.

Using the Navier-Stokes equation, the modeling of the velocity profile within our experimental capillary was performed for steady and pulsatile pressure driven flow. Once the velocity profiles were known the wall shear stresses were calculated based on the spatial gradient of the velocity profile at the lumen boundaries. In the case of a constant pressure drop across the capillary, the Poiseuille solution is well known and the velocity profile readily determined from the vessel geometry, the fluid viscosity, and the magnitude of the pressure drop. In the case of pulsatile pressure drops across our growth capillaries, the measured pressure gradient waveform was represented by a Fourier series using discrete Fourier transform (DFT) and used as input in the Navier-Stokes equations. These equations were first solved and described by Womersley [104] to analyze flow in arteries modeled as straight, rigid tubes. We thus describe the modeling of our experimental pulsatile flow and a characterization of the flow mechanics based on these results.

Hemodynamic effects on vascular cells

As an interface between blood circulation and underlying tissue EC constitute a major component of the arterial biology. EC regulation of cellular metabolic activity and physiologic responses of the underlying tissue is conditioned by the nature of the flow the endothelium is exposed to. The hemodynamic environment in blood vessels is complex and while flow patterns and blood velocities can be measured [82-84] or determined by computational fluid dynamics [85-87], the state of the mechanical stress *in vivo* at the cellular level is rarely known. With specialized

imaging techniques of the cell topography some estimates of the shear stress distribution and the shear stress gradients have been obtained [81]. Most studies on shear stress effects however only control for average shear stress near the wall as the functional variable. Typical experimental models used to date utilize flow chambers and plate-and-cone apparatus that generate a sustained laminar flow.

Additional hemodynamic parameters that have been correlated with atherosclerotic lesions location are the oscillating shear index, maximum wall shear stress, and mean wall shear stress [22]. These parameters are thus useful for a more complete characterization of shear stress treatment *in vitro*. For instance, variations in shear stress have been shown to result in increased levels of active transcriptional factors [5] and increases in EC permeability [6]. Interestingly, a recent study by Ziegler *et al.* [92] demonstrated that sustained laminar "low" shear stress increased endothelin (a strong vasoconstrictor and SMC mitogen) expression less than a oscillatory shear stress with the same time-averaged shear stress. This evidence reinforces the importance of spatial and temporal variations of flow on EC biology.

Mass transport considerations further complicate the isolation of shear stress effects. Ecto-enzymes that metabolize ATP at the EC surface are regulated by the concentration profile at the luminal surface [12, 160]. In turn, flow regimes affect convective transport of this agonist and subsequently control the intra-cellular calcium concentration since it is shear rate dependent as a secondary messenger. Controversy, however, persists in light of conflicting data indicating that calcium concentration varies solely because of shear forces applied to the endothelium [97], while others emphasized that ATP convective transport and metabolism at the cell surface is at the origin of the generated response [161]. Thus, whether metabolite transport and/or fluid shear forces elicit EC response to altered blood flow conditions, their quantification and modeling can only be achieved by determining the velocity profile.

The study of shear stress effects on cellular function is challenged by the fact that no clear "mechanosensor" has been found and isolating the effect of shear stress, *per se*, has proven difficult. However, EC cultured under shear constitutes an improved model for the study of EC biological functions based on their state of differentiation that more closely resembles that present *in vivo.* Further, a model that includes mechanical forces is more relevant based on the effective control of cellular functions by shear as attested by the multitude of proteins whose

expression depends on the mechanical environment of the cells. It thus becomes important to be able to model the fluid velocity profiles since it can indicate both, the extent of shear stress on endothelial cells and the magnitude of the convective transport of agonists and antagonists.

Shear stress modeling: assumptions

The Navier-Stokes equations are based on the general principle of conservation of momentum but are simplified in that the fluid is assumed incompressible and the viscosity independent of shear rate. Fluids such as blood are known to exhibit shear thinning such that its effective viscosity at higher shear rates can reduce its viscosity as much as four fold. In this case, constitutive equations are required to relate viscosity to shear rate using, for example, a power law type model and the more fundamental Cauchy momentum equations are then used instead of the simplified Navier-Stokes equations. However, the solutions to these equations become more difficult to solve since the equations are non-linear and require numerical modeling. In our experimental model the perfused aqueous media is incompressible at the low pressures used (<16psia). Further, the viscosity of the media is independent of the rates of shear since no colloidal or fibrous material is present (as opposed to blood, which contains red blood cells, platelets, fibrin, etc.). Therefore the Navier Stokes equations were used to derive the velocity profiles, resulting in insignificant error compared to the measurement errors of pressure, volumetric flow rates, and vessel geometry. In modeling the flow we also assumed no slip conditions at the luminal surface since the media is viscous and that the surface was smooth. Volumetric flow rate is inversely related to the cube of the vessel radius and is thus is thus very sensitive to the capillary radius. However, optical measurement of the radial distention of the capillary was shown to be negligible under experimental pressures (see Chapt. III).

Solution to Navier-Stokes equations: Poiseuille and Womersley flow

The momentum conservation equations as described by the Navier-Stokes equations are:

$$\frac{\partial \bar{V}}{\partial t} + (\bar{V} \bullet \nabla)\bar{V} = -(\frac{1}{\rho})\nabla p + (\frac{\mu}{\rho})(\nabla \bullet \nabla)\bar{V} \qquad \text{Eq. 1}$$

Where $\bar{V}$ is the velocity vector along the main axis of the capillary, p is the scalar pressure field, μ is the viscosity, and ρ is the constant media density. Uniaxial flow is present and so Eq. 1 can be simplified to:

$$\frac{d^2V_z}{dr^2} + (\frac{1}{r})\frac{dV_z}{dr} + (\frac{1}{\mu})\frac{\Delta p}{L} = 0 \qquad \text{Eq. 2}$$

The pressure drop across the length L of the capillary is independent of time and the solution thus becomes the Poiseuille velocity profile where Vz is a function of the radial position "r":

$$V_z(r) = \frac{\Delta p}{4\mu L} R^2 (1 - (\frac{r}{R})^2) \qquad \text{Eq. 3}$$

Note that Eq. 3 does not apply at the very entrance of the capillaries where the flow is constricted upon entry in the capillaries, however entrance effects can be neglected since they would occur only over the first ≈ 0.1 cm of 13 cm of total capillary length. The calculation of the entrance length was obtained from [162] the following empirical equation:

$$L_e = 0.226\frac{\rho Q}{\pi\eta} \qquad \text{Eq. 4}$$

Where, ρ is the fluid density, Q the volumetric flow rate, and η the fluid viscosity. From Eq. 3 the fluid velocity is a function of the radial position and the experimental parameters are the capillary radius and length (R and L, respectively), the viscosity, and the constant pressure driven flow. The volumetric flow rate can then be obtained by integrating the dot product of the velocity with the transversal cross sectional surface of the capillary

$$\int dQ = \int V \bullet dA \qquad \text{Eq. 5}$$

From the definition of shear stress in cylindrical coordinate, the wall shear stress can be calculated from the velocity profile:

$$\tau_w = -\mu \left. \frac{\partial V}{\partial r} \right|_{r=R} \qquad \text{Eq. 6}$$

Thus all fluid flow characteristics of interest can be derived once the velocity profile is known.

Similarly, deriving the velocity profile for a time varying or pulsatile pressure drop, as is the case in our Cellmax® pump driven flow, can be done starting from the Navier-Stokes equations (Eq. 1) and the fluid flow characteristic derived from Eq. 5 and 6. However, to solve the problem analytically, the pressure drop data term needs to be represented as a harmonic Fourier series of the form:

$$\left. \frac{\Delta p}{L}(t) \right|_{measured} = \sum_i f_i \,, \qquad f_i = A_i \exp[j\varpi_i t + \Delta] = A_i \exp[j\varpi_i t] \qquad \text{Eq. 7}$$

Where the "i" index represents the summation over all terms in the series, j an imaginary number, Δ_i he phase lag, and ϖ the angular frequency (A_i is also imaginary and contains the phase angle of the waveform). This term can then be substituted in the Navier-Stokes differential equation to lead to:

$$\frac{\partial^2 V}{\partial r^2} + \frac{1}{r}\frac{\partial V}{\partial r} - \frac{\rho}{\mu}\frac{\partial V}{\partial t} = -\sum_i f_i \qquad \text{Eq. 8}$$

The partial differential equation (Eq. 8) can then be converted to a second order linear ordinary differential equation by using the separation of variable method where a solution of this form is assumed:

$$V_i(r,t) = U_i(r)\exp[j\varpi_i t] \qquad \text{Eq. 9}$$

Upon substitution, Eq. 7 then becomes:

$$\frac{d^2 U}{dr^2} + \frac{1}{r}\frac{dU}{dr} - \frac{\rho}{\mu} j\varpi U = -\frac{A_i}{\mu}$$

Since for linear differential equations the principle of superposition is applicable [163], individual solution to each term of the series representation of the pressure drop data can be summed to lead to the general solution of the differential equation (Eq. 8). The Womersley solution for each term contains Bessel functions of order zero (J_0) with complex argument and is given by [104]:

$$V_i(r,t) = \frac{A_i}{\rho}\frac{1}{j\varpi_i}\left\{1 - \frac{J_0(\alpha y j^{3/2})}{J_0(\alpha j^{3/2})}\right\}\exp[j\varpi_i t] \qquad \text{Eq. 10}$$

Where,

$$y \equiv r/R$$

$$\alpha \equiv R\sqrt{\frac{\varpi\rho}{\mu}} \qquad \text{Eq. 11}$$

α represents the dimensionless Womersley number, a measure of pulsatility, and the complete solution of the oscillatory components is given by the real (Re) component of the imaginary solutions:

$$V(r,t) = \mathrm{Re}\sum_i V_i(r,t) \qquad \text{Eq. 12}$$

Note that equation 12 also must include the solution for the steady or average pressure drop given by Eq. 3 since Eq. 3 is one solution of Eq. 8 with a constant instead of a time varying pressure drop term (see Eq. 2). The solutions are additive since the differential equations are linear. Therefore, the pulsatile pressure drop data was scaled by subtracting the constant time-averaged pressure drop to lead to the purely oscillatory component of the pressure waveform that was fitted to a Fourier series.

Discrete Fourier transform: series representation of the pressure data

In order to use equation Eq. 8 to obtain the velocity profile for our flow system where the pressure drop was pulsatile, the discrete Fourier transform (DFT) of the data was performed [163].

The inverse DFT of the transformed data was then carried out to generate the harmonic series representation of the data and to obtain the coefficients of the series expansion (G[i]):

$$S(t)\big|_{10} = \sum_i G[i]\exp(j2\pi t) \qquad \text{Eq. 13}$$

In this representation only ten terms in the series were used since they were sufficient to reconstruct the waveform for one cycle of the pressure drop. Both the fitted data and the data are shown in figure 1.

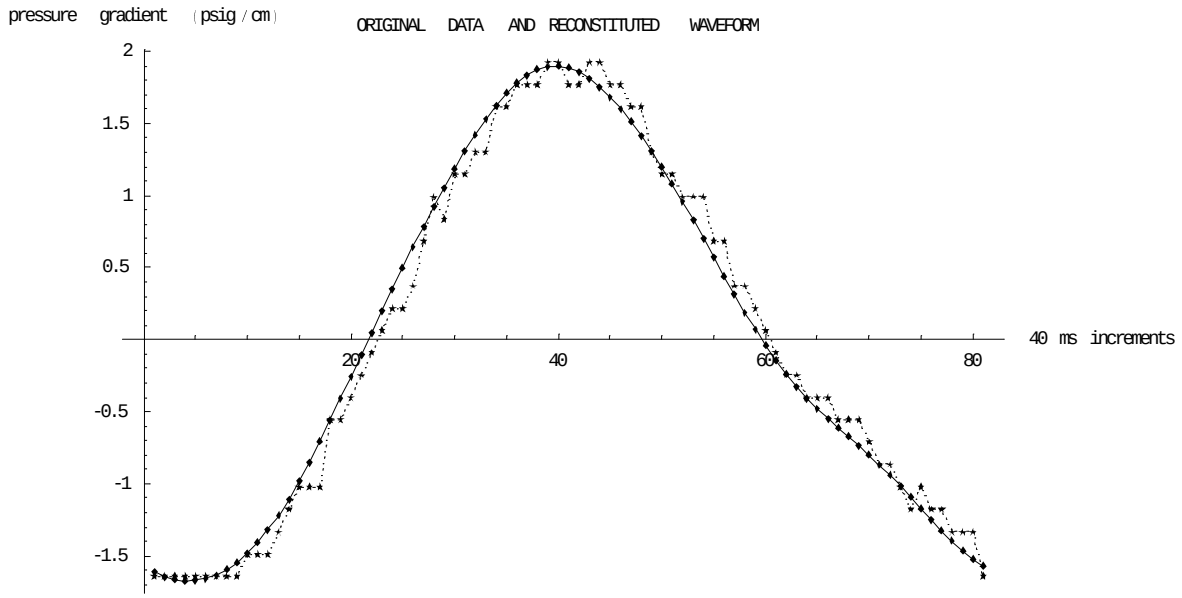

Figure 1. Fourier series representation of pressure drop data. Using a differential pressure transducer the pulsatile pressure drop across the cell culture capillaries was recorded (∗). One cycle of the data was then fitted to a harmonic series with 10 terms using DFT (♦). Note that the data was scaled by subtracting the contribution from the time averaged pressure drop component.

A Fast Fourier Transform (FFT) algorithm could also have been used to reduce CPU time for the calculations, however, given the relatively small amount of data to be processed (<100 per cycle) and the longer time required to implement the coding for the FFT method, a DFT method was sufficient to carry out the required calculations.

Substituting Eq. 12 for the velocity profile into Eq. 6, the time dependent wall shear stress was calculated and a representative figure of shear stress as a function of time was obtain for the high shear stress treatment in our experimental model (Figure 2).

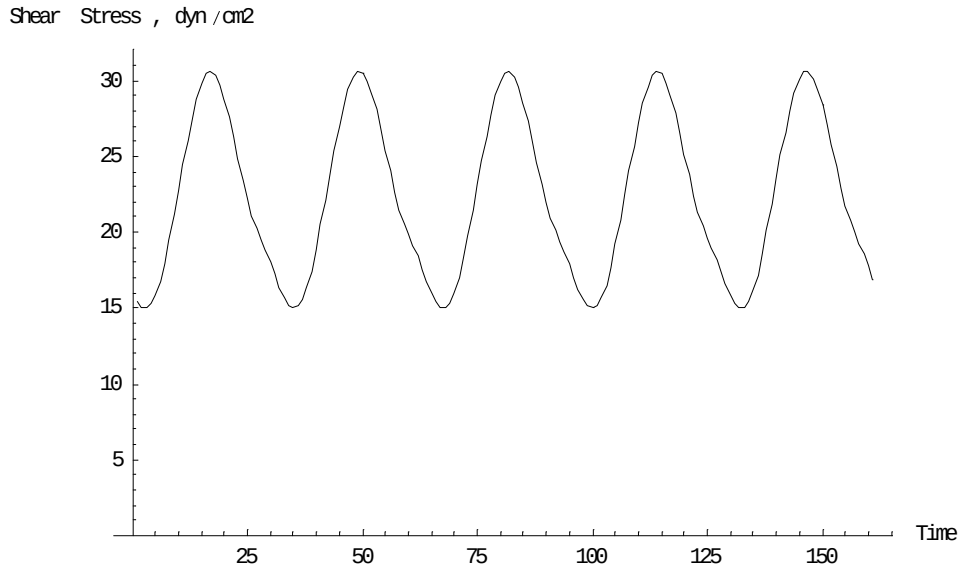

Figure 2. Calculated shear stress from pressure drop measurements. Pressure drop data obtained during cell culture in the Cellmax® capillary system were used to calculate the time-dependent wall shear stress. Shear stress was obtained from the gradient of the velocity profile at the wall determined from the Womersley solution of the Navier-Stokes equation.

The calculations in our model were validated by comparing the average volumetric flow rate calculated from Eq. 5 and 12 with measurements of the volumetric flow rate (Table 1). The instantaneous volumetric flow rate can be calculated using Eq. 4 and 11 without averaging over time. The results are in good agreement with experimental data, thus supporting the validity of our model with errors of $\approx \pm 5\%$.

Table 1. Comparison between measured and calculated time-averaged volumetric flow rates in Cellmax® cartridges (containing 50 capillaries per cartridge). Volumetric flow rate measurements were obtained by timing the collection of dionized water at room temperature for at least one minute. Calculations of average volumetric flow rates were based on the Womersley solution of the Navier-Stokes for pulsatile pressure drop generated by the Cellmax® pump.

	Measured Volumetric Flow Rate (mL/min)	Calculated Volumetric Flow Rate (mL/min)
High shear stress experiments	24.9	23.6
Low shear stress experiments	3.9	3.8

Harmonic analysis of the pressure waveform

For additional characterization of the fluid mechanics in our flow system, we analyzed the pressure waveform data to determine the frequency content of the measured waveforms. The power spectrum was thus calculated using FFT with Mathematica™ (Wolfram Research Inc., Champaign, IL) software to resolve the energy contribution of individual waves making up the measured waveform (Figure 3). Only one significant wave was observed at a frequency of ≈ 0.3 Hz for the high shear stress (23±8 dynes/cm^2) treatment regiment during our cell cultures. At our low shear stress regiment (5±2 dynes/cm^2), a similar frequency was obtained of ≈ 0.27 Hz (data not shown) thus eliminating any possibility that differences in frequency components were responsible for changes in cell metabolism seen from our cell culture shear studies. The relatively small higher frequency content observed is likely the result of low level noise generated by pump vibration and surrounding electromagnetic fields interfering with our data acquisition system. This noise, however, does not significantly affect our results since it is an order of magnitude smaller then our main frequency component and can thus be neglected. It should be noted that, with the sampling frequency used to acquire the data (25 Hz), the highest frequency content observable would be half the sampling frequency (also known as the Nyquist frequency [163]). However, the frequency content of our pressure waveform is unlikely to include any frequency above a few Hertz since the frequency of the positive displacement pump in the Cellmax® system is less than a few Hertz. Sampling at higher frequencies would only resolve higher frequency noise that has already been shown to be insignificant. Given that our main frequency component was ≈ 0.3 Hz, the minimum sampling rate would thus be 0.6 Hz. We

choose to sample at frequencies higher than required since it is advantageous in reconstituting the measured waveform and simple linear interpolation can be used for accurate reconstitution of the waveforms. Therefore we have shown that the main component of our pressure waveform is approximately 0.3 Hz for both our low and high shear stress experiments and that, furthermore, this waveform is almost purely sinusoidal.

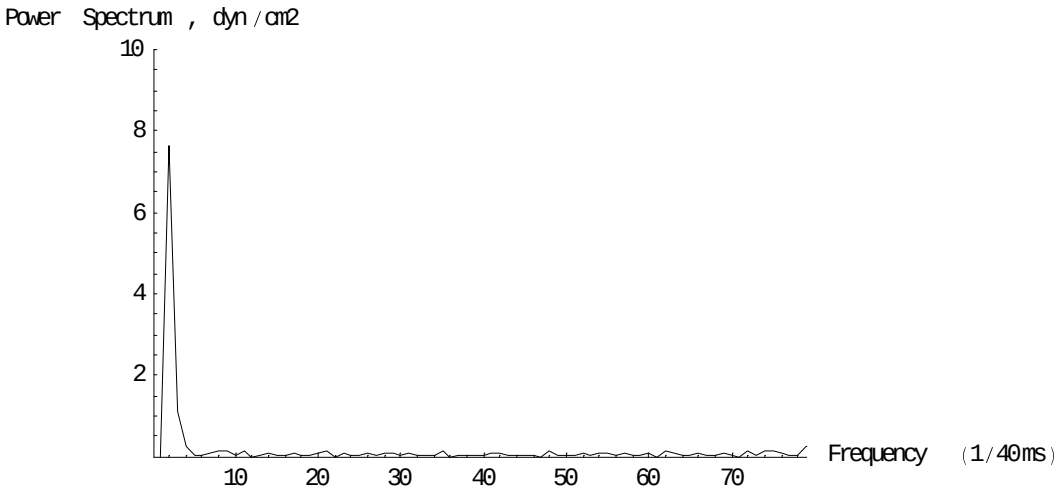

Figure 3. Power spectrum of the pressure waveform data. Pressure drop data were obtained during the high shear stress treatment in our cell culture system and analyzed using FFT. The sampling frequency was 25 Hz.

Phase angle difference between pressure and flow

Phase angle differences between wall deformation and shear stress can have physiological effects and can alter vascular cells metabolism [156, 164]. Lag between pressure and flow is known to occur in the vasculature (pressure leading flow) [156, 164]. Therefore it is important to be able to determine the extent of phase angle difference between pressure and flow waveforms, especially since pressure and flow affect wall deformation and shear stress, respectively. The phase angle between the main component of pressure and the flow waveform were calculated using the Womersley solution [104] of the velocity profile, and from the Fourier series representation (Eq. 13). The fluid inertia and viscosity retards its convective transport relative to the pressure applied causing the pressure to lead the flow. The resulting phase angle can be resolved from the magnitude of the imaginary amplitudes of the waveforms (f_i) represented by:

$$f_i = A_i Exp[\, j(\varpi_i t + \Delta_i)] = A_i Exp[\, j\Delta_i\,] Exp[\, j\varpi_i t] \qquad \text{Eq. 14}$$

Where A_i is real in this case and the "i" index represents the i^{th} component of the pressure and flow waveforms. Further, from the harmonic representation of the imaginary amplitude term:

$$A_i Exp[\Delta_i] = A_i[\cos(\Delta_i) + j\sin(\Delta_i)] \qquad \text{Eq. 15}$$

Thus, the phase angles for the main component of each waveform can be calculated from:

$$\Delta_i = \tan^{-1}\left[\frac{A_i \sin(\Delta_i)}{A_i \cos(\Delta_i)}\right] \qquad \text{Eq. 16}$$

And the phase angle difference can then be obtained from the difference between the phase angle for each waveform. In our cell culture system the phase angle differences between pressure and flow were calculated to be $\approx 3^{o}$ for low and high shear experiments. Thus these waveforms are about 1 in 100 parts out of phase for our main frequency of 0.3 Hz. Since higher frequency components were negligible in our system (Figure 3) the phase angle difference can be neglected in terms of its impact on cellular function. In addition, since the magnitude of the velocity increases away from the wall with a maximum at the axis, the phase lag will be reduced closer to the wall. Indeed, viscous forces become relatively more important at lower velocities, thus closer to the wall, compared to near the axis where higher velocities occur and inertial forces dominate. Therefore our estimate of the phase difference between pressure and flow is conservative since, at the wall, this difference is even further reduced.

It should also be noted that phase angle differences will increase significantly with increased magnitude of the Womersley number (see Eq. 11). However, our Womersley numbers (α) were between 0.2 and 0.7 compared to ≈ 3 for blood *in vivo* [104, 105] and thus the phase angle does not vary significantly in this range ($<10^{o}$). For α between 1 and 5 the phase angle drops off sharply (a drop of $\approx 70^{o}$)[104]. Therefore, frequency, density, viscosity, and capillary radius that are used to calculate α are important experimental parameters when performing pulsed or

oscillatory flow experiments in biomechanical models. The pulsatility in our model has little effect on phase lag however.

A specific feature of the Womersley flow is that the ratio of the flow due to a given oscillating pressure to the corresponding steady Poiseuille flow changes with α. In a similar fashion as the phase angle above, this ratio for steady non-pulsatile flow (α=0) is one as expected and about 0.95 for α equal to one. Thus, as the Womersley number increases up to 5 the ratio can become as small as 0.2 [104]. Hence only a fraction of the volumetric or shear stress can be achieved under pulse driven flow compared to steady flow. In our experiments however since α was much less than 1 (0.29 at the main frequency component) little effect is expected. Thus the Poiseuille flow equations can be used with little error as long as α is less than about 1 as was the case in our low and high shear experiments.

We thus used the Poiseuille equations to derive the predicted average pressure drop in our low and high shear experiments using measurements of the average volumetric flow rates:

$$\Delta P = \frac{8Q\mu L}{\pi R^4} \qquad \text{Eq. 17}$$

The calculated pressure drops were then compared to the time averaged pressure drop data obtained during cell culturing under shear (Figure 4). The pressure drops predicted and measured are nearly equal indicating laminar flow (Figure 4). If turbulent flow had occurred, the measurements would have been greater then predicted since in the turbulent regime flow is multidirectional and thus the integrand in Eq. 5 would be reduced. Therefore more energy (which stems from the Pressure-Volume work in the fluid) per unit of volumetric flow rate is required compared to uniaxial flow, where only one component of the flow is present. Since the flow is laminar it is thus well defined and shear stress profiles can accurately be obtained. This demonstration of laminar flow is consistent with a Reynolds number less than 100 in our low and high shear experiments and is thus much lower than 2100, where the transition to turbulent flow typically occurs. In pulsatile flows, however, the Reynolds number required for transition to turbulence is much lower for Womersley numbers less than approximately two [105]. With our Womersley number less than one the ordinary Reynolds number can be used as an indication of laminar flow.

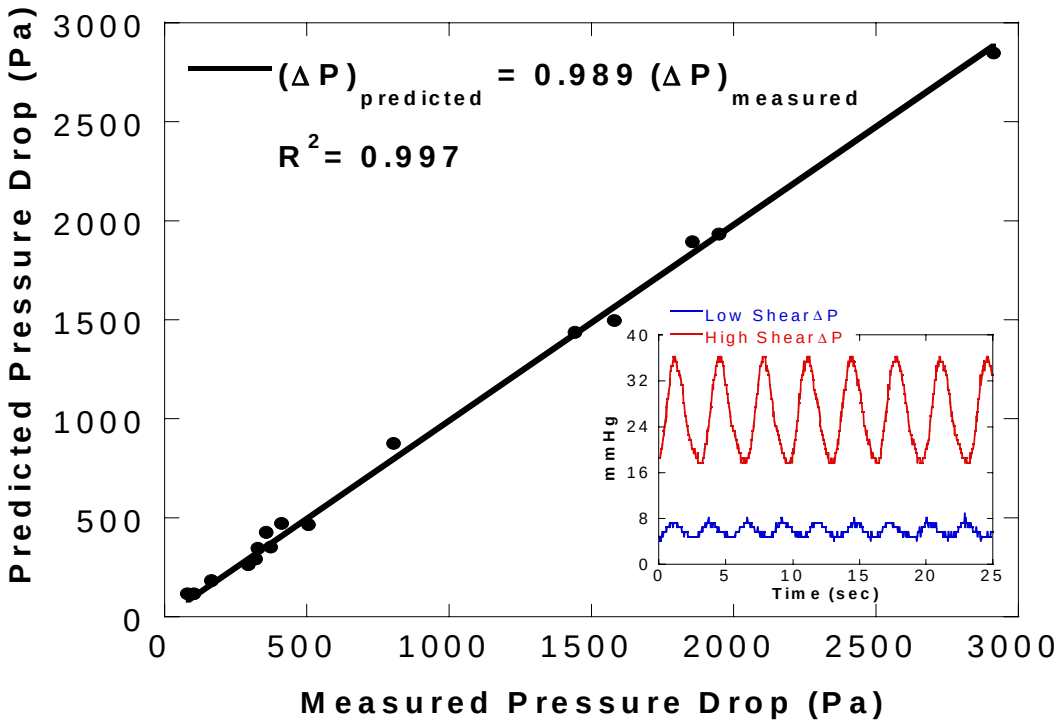

Figure 4. Pressure drop was calculated from the laminar flow equations and compared to average pressure drop measured for low and high shear experiments in our cell culture model. The pressure drops are equal indicating that the flow is laminar. Inset shows the measured pressure drops as a function of time for low and high shear experiments.

Summary

In summary we have modeled the flow in our low and high shear experiments using the Womersley solution of the Navier-Stokes equations to calculate the wall shear stress, the main mechanical factor in this thesis. The pressure and flow waveforms were represented using discrete Fourier transforms and a Fourier series expansion. The spectral analysis of the pressure waveforms indicated that only one component at a frequency of about 0.3 Hz was important and that they were similar in the low and high shear experiments. Phase angle differences between the pressure and flow waveforms were shown to be negligible ($<3^{o}$) and, further, since the Womersley numbers were relatively small in our experiments (<1) the Poiseuille equations can be used to model our flow. However, care must be taken in pulsatile flow experiments with significantly different frequencies, viscosity, or fluid density, since flow and phase angle will be altered beyond a Womersley number of one, compared to what would occur in a Poiseuille type flow. Entrance effects could also be neglected since they occur in less than 1% of the capillaries length. Finally, the flow in our cell culture system was shown to be laminar and can thus be

modeled predictably. The type of analysis presented here is essential in characterizing the flow in shear stress type biomechanical models, so as to avoid ambiguous interpretation of results from measurements of cell function.

Chapter III: Implementation of an optical method for the determination of uniaxial strain and dynamic vessel mechanics

Selim Elhadj, Riley Chan, Kimberly E. Forsten

Abstract

The determination of the mechanical properties of vascular growth substrates has seen increasing interest in the bioengineering field. Mechanical features such as rupture strength, compliance characteristics, and viscoelastic properties of vascular grafts are important in their design and can determine their success *in vivo*. Since vascular transplant patency rates depend on robust bioengineered or synthetic grafts that match the mechanical properties of the host tissue, a measurement technique for these parameters would be useful. In the case of grafts using vascular cells and biodegradable material as growth support, it also becomes important to be able to monitor vessel dynamic loading and maintain a sterile growth environment, hence a non-contact measurement method would be ideal. In this report we describe the implementation of an optical method for the deterministic measurement of vessel distention under a pulsatile or steady transluminal pressure gradient. This method is based on the concept of laser light occlusion and allows for non-contact diameter measurements. The laser light occlusion method is well suited for applications requiring real time circumferential measurement in vascular type vessels (<6mm) although, as designed, the largest measurable diameter is ≈2 cm. Low level changes in diameter of a fraction of a micrometer can be recorded and related to the vessel's circumferential strain. This method can thus be used to ascertain the dynamic mechanical properties of any opaque vessel subjected to transluminal pressure gradients. Using this method we demonstrate precise and reproducible measurements of diameter changes of less than ≈5 μm, which translates into microstrain measurements under dynamic loading. Further, with the simultaneous determination of both strain and luminal pressure we were able to determine the elastic modulus of the vessels tested. A 630 μm (OD) microporous polypropylene fiber and a 2600 μm (OD) Pharmed® tube were used as test samples under dynamic loading. Matching calculated modulus from strain/pressure measurements against known values validated our experimental results and

our dynamic strain measurement method. One attribute of this technique is its relative low cost, ease of implementation, high resolution, and flexibility stemming from its modular setup.

Introduction

Mechanical forces are known to significantly affect the metabolism, phenotype, and secretory pathways of vascular cells [17]. Amongst these forces, shear stress and circumferential stretch are the most commonly suspected mechanical regulatory agents for endothelial and smooth muscle cells metabolism [108, 154, 165]. Endothelial cells (EC) constitute a natural interface between blood flow and the underlying tissue, while smooth muscle cells (SMC) are normally present in the deeper layer of arteries and veins. The focal nature of atherosclerotic lesions within the vasculature is well established and correlates with specific blood flow patterns and stress forces [1, 22]. An understanding of the mechanisms relating hemodynamics and diseased arteries can not be obtained without careful studies relating the response of vascular cells to the dynamics of blood flow and arterial mechanics. In addition, attempts to grow vascular graft using endothelial and/or smooth muscle cells could benefit significantly from the determination of the mechanical properties during growth, thus allowing for the systematic analysis of various growth parameters on graft mechanics critical for matching the mechanical properties of the graft to those of the host tissue. Mismatch of the mechanical properties has been suggested to be a contributing factor for lower patency rates, especially for grafts less than 6 mm in diameter [2, 166] where thrombosis and vascular hyperplasia are prominent.

In vitro vascular cell models predominantly utilize static cell cultures. Non-static cell culture models such as the plate-and-cone and parallel flow chambers emulate shear stress forces, and these type of models have increasingly been used in research seeking to reproduce better the natural *in vivo* environment of vascular cells [167-170]. We and others [98, 102] have used the Cellmax® hollow fiber unit system to mimic chronic shear stress effects. However, vascular cells typically experience stretch forces as well as shear forces [108] and stretch forces effects are typically studied using a membrane support for cell growth that is stretched with specified boundary loads or by bending [88]. However, these models can be difficult to utilize experimentally [88]. For example, stretch gradients within the membrane must be calculated or shown to be negligible since the presence of unmonitored stretch gradients during stretch loading

can render experimental results ambiguous where cells may not be uniformly loaded. Further, the spatial resolution of these strains is difficult to ascertain and often requires numerical modeling or must be calibrated with specialized samples.

Given that stretch forces are known to have significant effects on EC and SMC metabolism, there is a need to develop a reliable and precise method to make a direct measurement of vessel stretch in vascular models. Vessel radii in biomechanical models have been measured using relatively costly ultrasonographic equipment [171, 172] or laser micrometers [91, 173]. Bergel (1961) [174] originally implemented a technique with low resolution, and low sampling rates that utilized a light source and collimating lens for radius measurements in arteries *ex vivo*. This technique was similar in principle to that used by Ramesh *et al*. (1996) [175]. In that study, a method was outlined to measure the radial deformation of a specimen subjected to compression in the split-Hopkinson bar. While their focus was on the measurement of the plastic deformation of the specimen at intermediate strain rates (10^2-10^4 s^{-1}) under dynamic loading, the method can be adapted to our specific purposes of measuring the circumferential strain of cell culture type vessels under elastic deformation. An adaptation of the Laser Occlusive Radius Detector apparatus was implemented for this study. Further, we suggest that this method can easily be expanded to provide a convenient and well-defined experimental model for the study of the effects of stretch forces on vascular cells. The method is based on measuring the occluded light from cylindrical fibers obstructing a laser sheet. Hollow fibers used as growth substrates are advantageous in that they mimic the geometry of a blood vessel and provide a good model system for *in vitro* vascular biology studies. The cylindrical symmetry of the fibers permits a uniform uniaxial stretch over the entire surface of the vessel, thereby eliminating limitations associated with some of the current stretch apparatus. We validated the method using non-cell seeded polymeric fibers but suggest that the method can be adapted to provide a biomechanical experimental model where microscale strains and strain regiments can be measured and monitored continuously. The main attributes of the described are its low cost, ease of implementation, high resolution, and its modular setup that provides flexibility in the study of vascular biomechanics.

Experimental Design

Optics setup

The optical system consists of a 1 mW semiconductor diode class II line generator laser (SNF-501L-650-1-5, StokerYale Inc., Salem, NH) directed towards an achromatic collimating lens (PAC 552, Newport, Irvine, CA) which focuses the laser light onto the receptive surface of a photodiode (Devar Inc., Bridgeport, CT) that converts light energy into electrical energy. The setup is designed so that the test vessel is placed perpendicular to the line of sight of the beam leading to the occlusion of a fraction of the light emitted by the laser (Figure 1). As the vessel deforms and its diameter changes, a change in the portion of light not occluded by the vessel results. Any variation of the energy output of the photosensor can be correlated with a change in the light received and, therefore, with a change in the diameter of the vessel. The laser has a 5^{o} fan angle and generates a non-Gaussian line that results in negligible variation in light intensity over angular emission (manufacturer manual, StokerYale Inc., Salem, NH). However, light intensity drops off sharply at the edges of the laser line, thus care must be taken to keep the sample within the laser line boundary and away from the edge of the laser line to avoid non-linearity in laser light intensity reaching the photodiode. A bandpass filtering lens (P10-650, Thermo Corion, Franklin, MA), also in line with the laser beam path, reduces any light energy contribution outside of that of the laser (coherent monochromatic light at 650 nm). The optical rail and carriers (Newport, Co., Irvine, CA) allow for the proper alignment of the laser/vessel/lens/diode system.

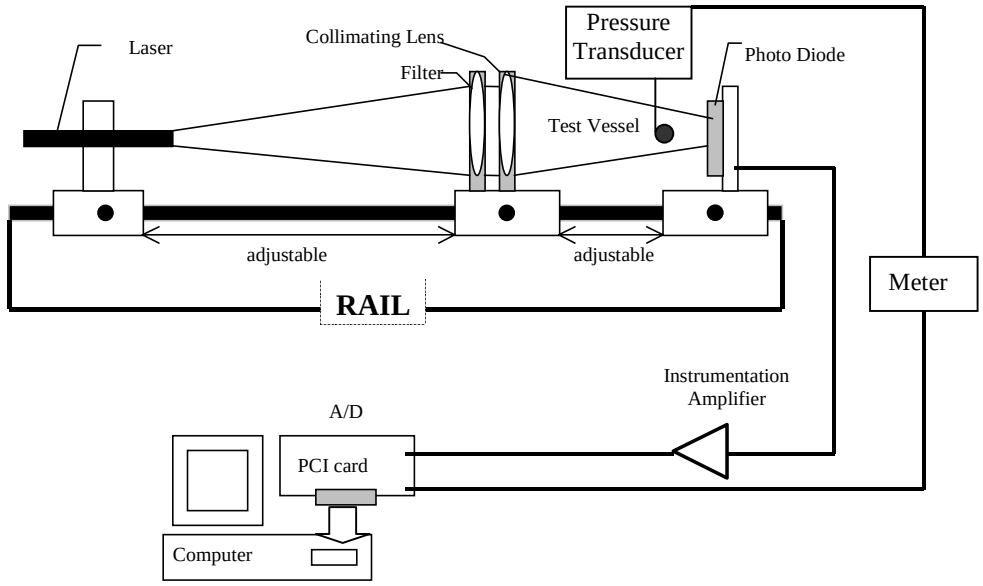

Figure 1. Schematic of the optical apparatus for radial strain and pressure measurement. A laser sheet, obstructed by the test vessel, is collimated to a photodiode. Any change in the vessel diameter caused by luminal pressure variations alters the amount of light reaching the photodiode. The light energy is transformed to a voltage output by the diode and recorded using a data acquisition card fitting a PCI slot on the computer main board. An operational amplifier is used to set the baseline and scale voltage output to the A/D board. Simultaneous recording of the luminal pressure is achieved using a gage pressure transducer and a variable analog output meter to the A/D board. The three dimensional translational stage for the test vessel is not shown (see Figure 2).

A vessel holder screwed onto the diode carrier allows for three-dimensional translational positioning of the vessel (Figure 2). The closer the vessel is positioned relative to the diode, the more light is occluded per unit change in vessel diameter. Care must be taken such that, even with distention, the vessel cross section remains within the aforementioned boundaries of the laser to avoid any significant contribution from scattered light, which can result in a non-linear signal. Our data acquisition system consists of a 200 kHz, 12-bit input A/D card (PCI-6023E, National Instruments, Austin, TX) with eight differential inputs and LabVIEW™ interface (National Instruments, Austin, TX). Pressure measurements are obtained with a gage pressure transducer (OMEGA Inc., Stamford, CT) and a pressure meter (DP25-S-A, OMEGA Inc., Stamford, CT) that provides transducer excitation voltage and variable analog output.

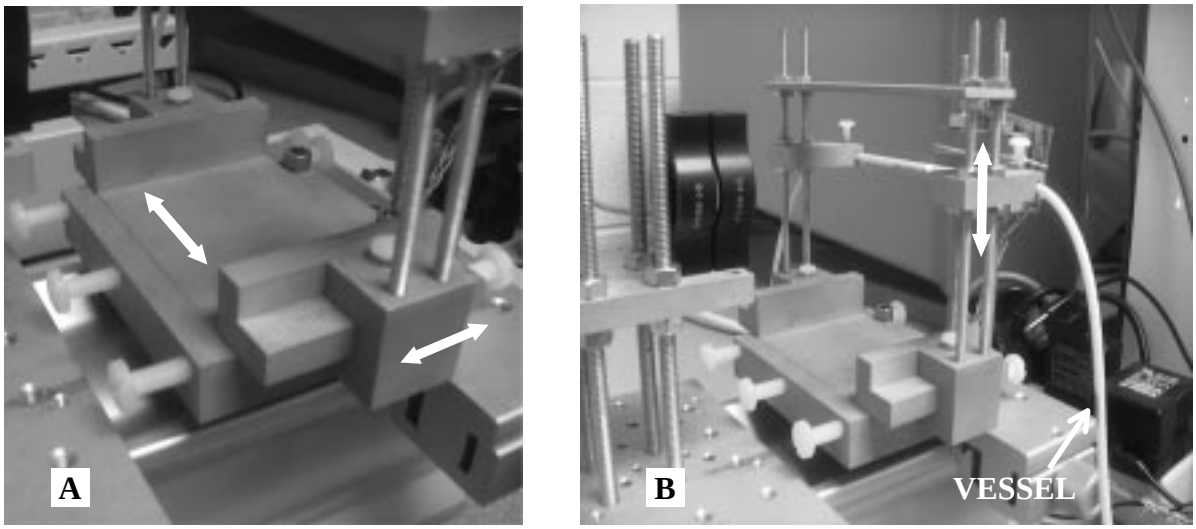

Figure 2. Picture of the vessel positioning translational stage. This custom built manual three dimensional translational stage allows the precise positioning of the test vessel by moving the test vessel in the x and y directions on the base (A), and in the z direction to adjust the height (B). The plastic white screws shown are used to secure the test vessel in position. The bandpass filter and collimating lenses are shown on the left side of the picture (B). The diode and its circuitry stand behind the test vessel as shown (Pharmed®: 2.6 mm OD, 1.6 mm ID).

Circuit design

The regulated power supply (HAD15-0.4A, Power-One®, Camarillo, CA) and associated circuitry was designed to optimize the sensitivity of the system and to provide the power requirement for the entire apparatus (Figure 3). An operational amplifier (AD542L, Analog Devices Inc., Norwood, MA) was utilized to match the sensor voltage output with that of the input of the A/D card in order to optimize the available resolution. Variable resistance elements can be used to set a specified baseline voltage output from the photodiode to the A/D card input. The photodiode has multiple connections for excitation voltage (±6V), bias voltage (set at -15 V) that can be adjusted depending on the signal frequency to be measured, grounding, and for the diode output. The diode has an active area of $5mm^2$ with a responsivity of 7,000 V/Watt. Since the optimal diode excitation wavelength is at 900 nm, the laser used in this study (650 nm wavelength) will lead to about 70% of the maximum diode output (personal communication, Devar Inc., Bridgeport, CT).

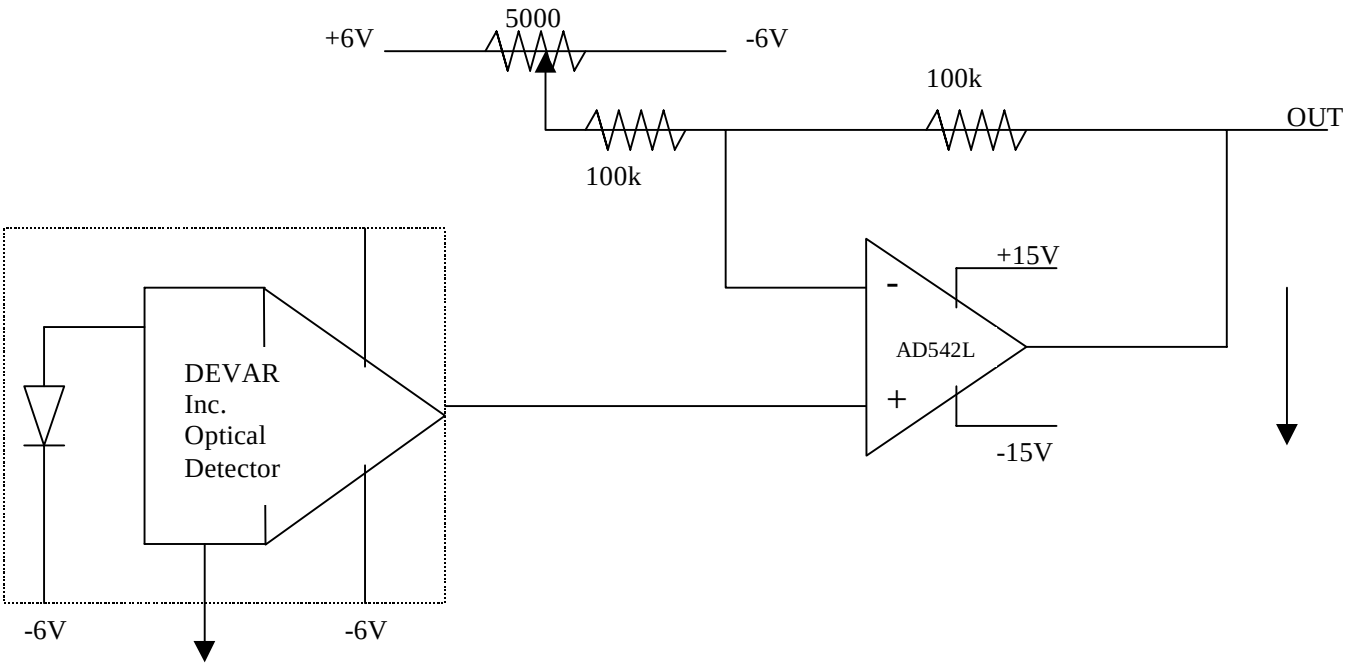

Figure 3. Optical sensor and amplifier circuit design. The photodiode uses ±6V excitation from a regulated power source and the output is an input to an op-amp and variable resistive circuit that allows baseline setting and scaling of the voltage output to the I/O board.

Laser/optics calibration

The laser optical system was calibrated to relate diode voltage output to diameter measurements. Calibration of the system was achieved by taking advantage of the collimated laser sheet shape. As the resting vessel is moved toward the diode from the lens, the fraction of occluded light is increased in a predictable fashion. In an analogous manner, at a given position between the diode and the lens, any increase in diameter will result in an increase in the fraction of occluded light. The fraction of occluded light is determined from simple geometry as described in Figure 4 below.

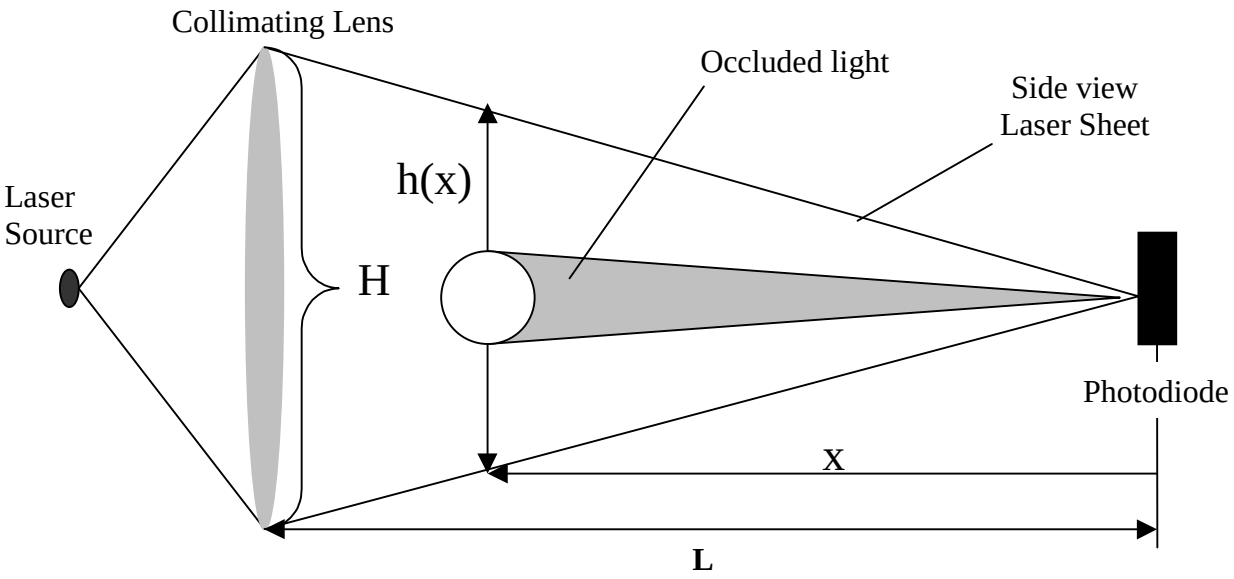

Figure 4. A schematic of the cross sectional view of the laser light geometry describing the fraction of laser light occluded. H represents the lens height, x the varying distance from the diode to the sample position, h the effective laser beam height at position x, and L the fixed focal length.

We can show that the fraction of light occluded by a test vessel at rest at any position between the diode and the lens is given by:

$$\phi(x) = \frac{d_{rest}}{h(x)} = \frac{d_{rest} L}{Hx}, \qquad \text{since} \quad \frac{H}{L} = \frac{h(x)}{x} \qquad \text{Eq. 1}$$

where d_{rest} is the resting diameter of the fiber, H is the lens height, x is the distance from the diode to the sample position, L is the fixed focal length, and $\phi(x)$ is the faction of light occluded by a vessel at position x. By varying the position of the vessel, we calculated the fraction of occluded light and calibrated it to a voltage output from the diode enabling us to obtain the fraction of occluded light as a function of voltage ($\phi(V)$). Calibration of the system was done for both, a microporous flexible plastic polypropylene capillary (630 μm OD, 330 μm ID) and a larger non-porous Pharmed® elastomer vessel (2.6 mm OD, 1.6 mm ID). A linear relationship between fraction of light occluded (ϕ) and diode voltage output was found for both samples (Figure 5). Since the diameters for the two vessels tested were known, fractional occlusion was calculated from the specified distance (x) between the diode and the lens (Eq. 1).

Typical coefficient of determination values (r^2) for the calibrations were greater than 0.99 as shown for a representative calibration using a polypropylene fiber in Figure 5.

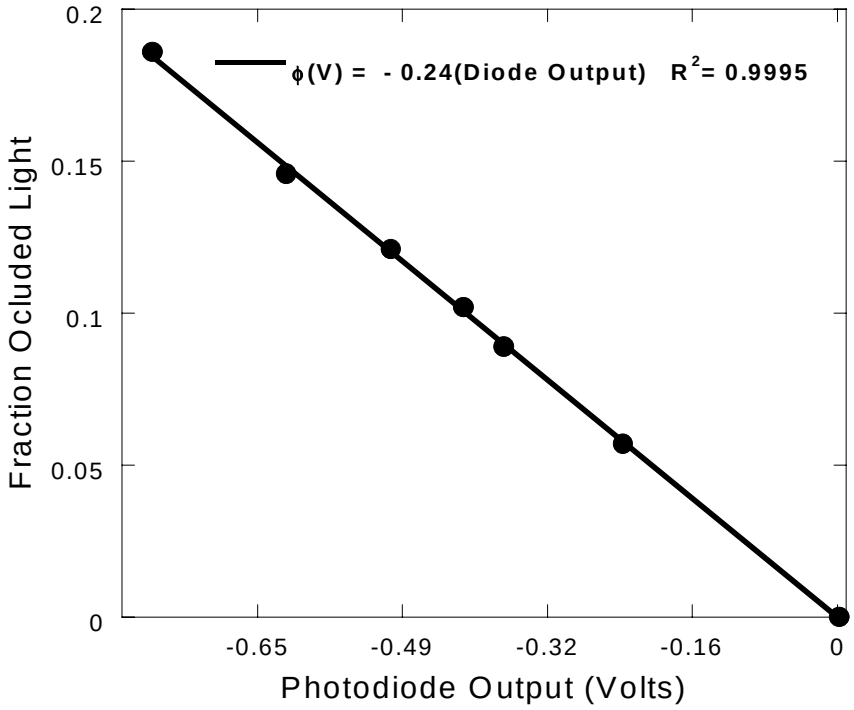

Figure 5. Calibration curve for the laser occlusion apparatus. The test polypropylene capillary (630 μm OD, 330μm ID) was used to calibrate the photodiode output to the fraction of laser light occluded, which can then be related to the vessel radius using Eq. 2. The change in fraction of light occluded was achieved by positioning the capillary at specified intervals between the lens and the photodiode, and the fraction of light occluded calculated using Eq. 1.

Vessel diameter measurements using optical laser setup

Calibration of the diode output to the fractional occlusion was done using test vessel at rest, however, the change in vessel diameter for a vessel undergoing diameter change due to increased luminal pressure at a fixed position (x_o), can be obtained based on our $\phi(V)$ calibrations. The magnitudes of physiologically relevant strains within the vasculature reside between 0 and 20% [176] and, typical experimental strains used for cell testing are ~10% [88]. Intraluminal strain can be determined indirectly by using the principle of mass conservation provided the sample is incompressible within the loading range. Thus the surface circumferential strain (ε) is defined as:

$$\varepsilon \equiv \frac{\Delta r}{R} \qquad \text{Eq. 2}$$

where Δr is the change in radius and R is the vessel radius at rest [176]. We experimentally measured the amount of occlude light and then determined the change in diameter by solving for d(t) based on the change in diode output. This can be related to the strain recalling that the radius is simply half of the diameter:

$$\varepsilon \equiv \frac{d(t) - d_i}{d_i} = \frac{\phi(V(t)) - \phi_i(V_i)}{\phi_i(V_i)} \qquad \text{Eq. 3}$$

where the subscripts "i" indicates the initial state of the vessel at rest and where the diameter d(t) and the recorded diode output V(t) are a function of time. If the vessel initial or resting diameter is known then an absolute measurement of the diameter can be obtained. Otherwise, only the strain (ε) or relative change in diameter can be determined.

Since the pressure in the vessel can vary with time due to the dynamic pressure resulting from a pump driven flow or by applying varying levels of hydrostatic pressure, the real time dynamic stretch needs to be determined in conjunction with the simultaneous measurement of the luminal pressure. To test our optical system, changes in vessel diameter were obtained by setting the vessel position close to the photodiode insuring, by visual inspection, that the laser sheet spans the entire cross section of the vessel. The Pharmed® vessel was manually pressurized with a syringe and water and the luminal pressure measured using a pressure transducer. The data was collected using LabVIEW™ interface with a Pentium I, 200 MHz, IBM PC compatible computer and the data recorded at a 20 Hz sampling frequency. For improved time resolution and to reduce data file size for long term monitoring applications, the data was streamed as a binary file directly to the hard drive. The recorded binary file was later converted to a text file for analysis or plotted directly from the binary data records for visual inspection using LabView™. A representative sample of the processed data obtained of a Pharmed® vessel diameter change under manual pressure loading is shown in figure 5. The average pressure load, in addition to the oscillating component, was 2 psig with resting intraluminal pressure at 0 psig. While the pressure load peaks appeared similar variations in vessel radius were not reproduced as well.

Reasons for these variations may be the result of residual strains that occur following rapid strain and relaxation regiments.

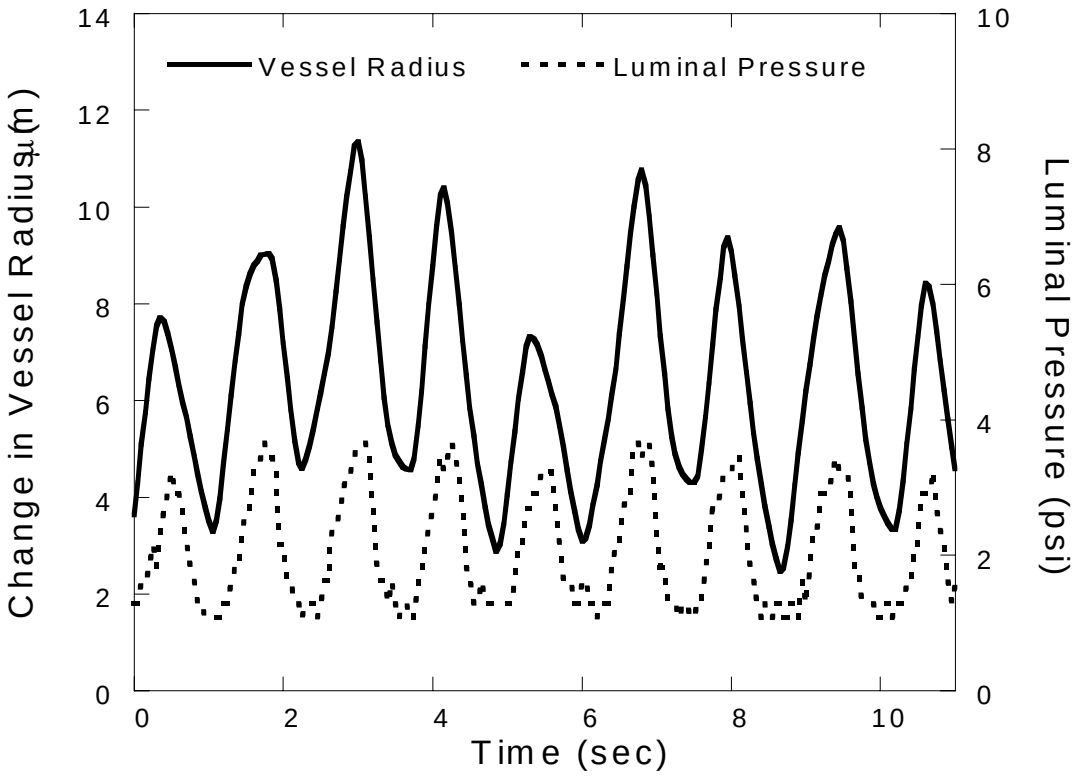

Figure 6. Measurement of a Pharmed® vessel distention under transluminal pressure gradient. A Pharmed® vessel was subjected to a manual transluminal pressure gradient and the vessel change in radius was measured using a laser occlusion non-contact optical method. This data set is representative of dynamic testing of the Pharmed® vessel (2.6 mm OD, 1.6 mm ID) under no luminal flow conditions and was repeated at least three times with three different vessels.

Similarly, a polypropylene capillary (630 μm OD, 330 μm ID) was tested under luminal flow (0-30 mL/min) specified using a syringe pump (KDS230, kdScientific, New Hope, PA) with water. Because flow was pressure driven, luminal pressure was determined using a pressure gage (OMEGA Inc., Stamford, CT) and radius change determined using the laser occlusion apparatus. Tests were conducted under sustained flow conditions at a sampling frequency of 25 Hz. Since radius change is related to strain (Eq. 2), we plotted the measured luminal pressure and the strain (Figure 7). As expected, the stress-strain plot describes a linear relationship (r^2 =

0.997) since, at low strain regiments, polymers typically exhibit pure elastic behavior [177]. It should be noted that the laser occlusion apparatus can measure small changes in vessel diameter corresponding to small levels of strain (Figure 6, 7). This level of detection is comparable to many high-end laser micrometers (Beta Lasermike, Dayton, OH). High-end laser micrometers, however, are over three times more costly than the laser occlusion apparatus presented here and are not built as modular elements, which restricts the number of applications they can be used for. The low cost and modular setting of the laser occlusion apparatus is thus advantageous compared to commercially available laser micrometers.

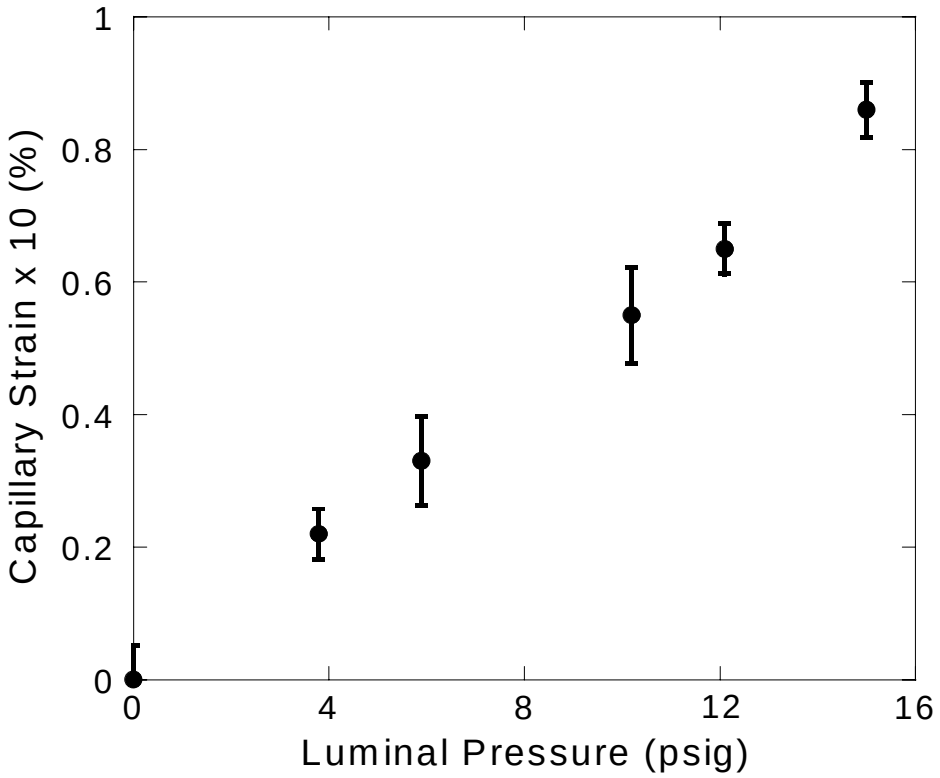

Figure 7. Strain vs luminal pressure plot for a polypropylene capillary. Polypropylene capillaries were tested under sustained luminal pressure driven flow (with a syringe pump). Pressure and capillary radius were measured using a pressure gage and the laser occlusion apparatus. Data points represent the mean ± standard deviation for 8 separate capillaries. The error in pressure measurement is less than 0.01 psi (OMEGA, Inc., Stamford, CT).

Mechanical properties determination

In order to validate the performance of the laser occlusion apparatus we used the measured changes in diameter and luminal pressure (Figure 6, 7) to calculate the dynamic elastic modulus of our test vessel samples and compare them to known values. The dynamic elastic modulus can be calculated using diameter and pressure measurements [91]:

$$E_{inc} = \frac{2(1-\sigma^2)\mathrm{Ri}^2\mathrm{Ro}\Delta\mathrm{Pi}}{(\mathrm{Ro}^2-\mathrm{Ri}^2)\Delta Ro} \qquad \text{Eq. 4}$$

where σ is Poisson's ratio (0.5 for isotropic materials), Ri and Ro represent inside and outside radius of the vessel, and ΔPi is the transluminal pressure gradient. This expression is valid for simple viscoelastic materials, i.e., if the viscous component of the modulus ($\eta\varpi$) is less than about 10% of the modulus amplitude [174]. Assuming the coefficient of viscosity (η) is constant or the phase angle (φ) between pressure and distention is less than 6°, then Eq. 4 is a good approximation of the elastic modulus since [174]:

$$|E| = \left[(E_{inc})^2 + (\eta\varpi)^2\right]^{1/2} \approx E_{inc} \qquad \text{Eq. 5}$$

where ϖ is the angular frequency and,

$$E_{inc} = E\cos\varphi,$$
$$\eta\varpi = E\sin\varphi, \qquad \text{Eq. 6}$$

The phase angle between pressure (ΔP leading) and vessel distention can be determined from the corresponding waveform data and the Fourier series representation of these waveforms (Figures 6, 7). Thus, from the imaginary amplitude of the distention and pressure waveform for the main frequency component of these waveforms, the phase angle (φ) was calculated to be <5° (data not shown). Therefore, under our experimental conditions of relatively low rate of strain, strain magnitude, and frequency (see Figure 6), and given the viscoelastic properties of our polypropylene and Pharmed® test vessels, Eq. 5 can be used with no significant error.

Calculations of the elastic modulus of the polypropylene and Tygon Pharmed vessels, based on our measurements of pressure and vessel radius, are in good agreement with reported values. The polypropylene microporous capillaries were found to have a modulus of 70±14 kpsi while the Tygon Pharmed vessel a modulus of 3.16±0.35 kpsi (compared to 3.2 kpsi (Norton Plastic Performance, City, State)). Our polypropylene capillary results are significantly lower than bulk polypropylene known values (150-250 kpsi [178]), however, this was not unexpected given that the capillaries were porous with a porosity of approximately 0.9 (Mettler Toledo Density Kit, Columbus, OH), which reduces fiber modulus [178]. The ability to measure the mechanical properties of vascular graft type vessels is useful since there is a strong positive correlation between graft vessel compliance and patency rates for various biological and prosthetic grafts [166]. Therefore, vascular graft design could benefit from a simple assessment measure of the mechanical parameters based on easy to obtain vessel radius and intraluminal pressure measurements.

Conclusions

An inexpensive PC-based non-contact optical method has been described that can allow for the real-time measurement of circumferential strain in vascular type vessels. This apparatus can provide valuable information on the magnitude of pressure driven stretch and can thus be used to determine vessel mechanical properties such as the elastic modulus, even under dynamic loading conditions. For applications employing cells cultured in vessels, the risk of contamination would be reduced since physical contact is not required for vessel diameter measurement. It is, however, important that the laser/diode calibration be performed each time the optical system is altered to insure that quantitative results are obtained. The described method allows for a reproducible determination of vessel mechanical properties even for small radius vessels on the order of a few hundred microns (Figure 7). Further, the system is effective regardless of whether variations in luminal pressure are from application of hydrostatic pressure or from luminal flow. Therefore, this system could be used in vascular type application where luminal flow of media is required to satisfy the metabolic need of the seeded vascular cells. Brant *et al.* (1987) [173] reported the successful use of a laser micrometer to measure changes in radius of arterial segments under pulsatile transmural pressure where arteries were kept in a transparent tissue-housing chamber containing physiological fluids. We suggest that the method

described here, which is based on the same principle of laser light occlusion as in the Brant *et al.* study, could also be applied to study vascular biomechanics under dynamic loading.

One of the main advantage of our system is its comparatively lower cost. Whereas our entire system was built for less than $2,000, commercially available micrometer cost start at around $5,000, which does not include data acquisition hardware such as a D/A card likely raising the cost to $6-7,000 per unit. Another advantage of this system is its flexibility in setup since, by adjusting the size of the collimating lens and its focal length, vessels of various sizes can be tested. In addition, enough space between the lens and the diode can be created to accommodate housing chambers of different size. Commercial units typically have factory set dimensions and optics, which can not be altered to accommodate vessel chambers of varying dimensions. Because of the geometry of the laser light sheet, the test vessel itself can be used as a standard for calibration (see Eq. 1-2), which is useful in studies requiring the use of "small" diameter vessels (in the order of a few hundred μm) where calibrating standards can be difficult to obtain or manufacture.

If only strain measurements are required, then the actual dimensions of the test vessel need not be known, since the ratio of the diode signal of a vessel under dynamic loading to the signal from a vessel at rest are sufficient to obtain the relative change in vessel diameter. In commercial laser micrometers relative changes can also be measured, however the linearity of response from the diode can not be tested as in the laser occlusion apparatus described here. The triangular shape of the laser sheet in the latter allows for a check of linearity since the translation of the vessel, along the axis between the diode and the lens, is expected to generate a varying linear diode output. In contrast, commercial laser micrometers have a rectangular laser sheet shape hence no changes would be observed during translation of the vessel.

There are several limitations with regard to the applicability of the system. This method can only obtain measurements of uniaxial strain and is not suited for *in vivo* data collection, in contrast with ultrasonic equipment. Also, it is preferable that the test vessel material not be transparent or problems with laser light scattering and refraction may occur rendering the system difficult to calibrate. Similar restrictions apply to commercially available laser micrometers. With regard to applications making use of cell culture, it may be necessary to maintain the vessel in an aqueous environment. The currently described system, as is, was not designed for this type

of application. However, by upgrading to a more powerful laser, one should be able to overcome the energy loss that would occur at the interfaces of the fluid chamber and within the liquid phase itself. Because of changes in refractive index that the laser light sheet would encounter when going from air to the liquid phase, there is a need to adjust the diode positioning so that it would meet the incident light. This capability is built-in the described apparatus, thus the use of a fluid containing housing chamber is feasible in principle. We are currently working on implementing a method for vessel radius measurement in aqueous type media that will include vascular cell seeding.

In summary, we have described a relatively straightforward system for analyzing strain due to fluid flow through cylindrical vessels and hydrostatic pressure loading. The metabolism of vascular cells is strongly influenced by the dynamics of blood flow and related vascular biomechanics, thus an inexpensive, high resolution, tool for the characterization and monitoring of the vascular cells mechanical environment should prove advantageous.

Chapter IV: Endothelial Cells Alter Proteoglycan Release in Response to Chronic Pulsatile Shear Stress: Effects on Platelets Aggregation and Coagulation

Selim Elhadj, Shaker A. Mousa#, and Kimberly E. Forsten*

Department of Chemical Engineering
Virginia Polytechnic Institute and State University
Blacksburg, VA 24061

DuPont Pharmaceuticals Company
Experimental Station
Route 141 & Henry Clay Road
Wilmington, DE 19880

*To whom correspondence should be addressed

133 Randolph Hall

Department of Chemical Engineering

Virginia Polytechnic Institute & State University

Blacksburg, Virginia 24061

540-231-4851 (tel) 540-231-5022 (fax) kforsten@vt.edu

Subject Codes: Coagulation Inhibitors [182], Platelet [178], Other vascular biology [97]

Abstract

The primary objective of this study was to determine the effect of chronic shear stress on the release of proteoglycans from bovine aortic endothelial cells (BAEC) cultured under pulsatile flow. Proteoglycans were purified from BAEC conditioned media and analyzed using both anionic exchange and size exclusion chromatography. While overall size and composition of the proteoglycans and glycosaminoglycan side chains were not altered by shear, the relative proportion of the high MW species was inversely related to the shear stress. Moreover, a unique proteoglycan peak was isolated from low shear stress (5±2 dynes/cm^2) conditioned media when compared to no or high shear conditions (0 and 23±8 dynes/cm^2, respectively) via anionic exchange chromatography. Further, glycosaminoglycans from non-shear treated samples had a higher fraction of the low cation-binding fraction compared to shear treated samples. In order to characterize whether these changes impacted proteoglycan function, we studied the effects of shear specific proteoglycans on the inhibition of thrombin-induced human platelet aggregation as well as on platelet-fibrin clot dynamics. Proteoglycans from shear treated samples were less effective inhibitors of both platelet aggregation and blood coagulation inhibition. IC_{50} values for platelet aggregation inhibition increased from 0.15 to 0.24 μg/dose, while IC_{50}'s for blood coagulation inhibition similarly increased from 0.080 to 0.30 μg/dose as higher shear proteoglycans were used. Our data suggests that shear stress, by altering proteoglycans release profiles that impact platelet aggregation and coagulation, may play a role in vascular pathologies that are related to hemodynamics and hemostasis.

Keywords: shear stress, proteoglycan, glycosaminoglycan, coagulation, platelets

Introduction

Endothelial cells constitute a natural active boundary between blood and the underlying vascular tissue. Under normal conditions, transluminal pressure gradients and stretch forces act on the entire vascular wall, including underlying fibroblast and smooth muscle cells, while shear stress acts primarily on the endothelium [179]. Hemodynamic forces represent an essential modulator of vascular function via, in part, release of active molecules by endothelial cells targeted to control vasomotor tone, wall remodeling, and cell to cell interactions [17]. Ultimately, the goal is to maintain hemostasis and to sustain normal baseline functional vascular responses to the pervasive hemodynamic environment. Disturbed flow conditions are prevalent in vascular bifurcations and following surgical interventions [3, 180]. These disturbances often include significant spatial and temporal gradients [85], regions of recirculation [24], low average shear stresses [4, 20, 181], and transient back flow [182]. While systemic factors contribute to vascular disease, a strong positive correlation exists between these local hemodynamic conditions and the focal nature of atherosclerotic plaque formation [183].

Numerous studies document the relation between shear stress and the release of vasoactive agents [17]. For example, prostaglandin I_2, a potent smooth muscle cells (SMC) growth inhibitor, platelet aggregation inhibitor, and vasodilator, is transiently up-regulated by increasing shear stress [65]. In contrast, increasing shear stress down-regulates endothelin-1 [56], which has the opposite effects of promoting SMC growth [17] and increasing vessel vasoconstriction [184]. Further, nitric oxide is part of the early response to increased shear stress as a SMC growth inhibitor and by augmenting vessel luminal diameter [185]. In a non-compromised vasculature, these vasoactive agents tend to maintain a "setpoint" shear stress, acutely via the release of vasomotor agents and chronically by modulating vessel wall remodeling [17]. In this study, we have focused on chronic shear stress treatment and the effects on bovine aortic endothelial cells (BAEC) synthesis of proteoglycans.

Proteoglycans are ubiquitous glycoproteins that are composed of a protein core with sulfated glycosaminoglycans (GAGs) side chains as their main constituents [128, 186]. These highly negatively charged GAGs are important for the interactions of proteoglycans with growth factors and enzymes involved in the coagulation pathway [136]. Proteoglycans have been implicated in the process of intimal hyperplasia and thrombosis [38], both major events in

atherosclerosis development. Two previous studies have examined proteoglycans metabolism under conditions of non-pulsatile sustained laminar flow. Grimm *et al* (1988) found that proteoglycans were differentially polarized amongst the medium, plasma membrane, and matrix when bovine aortic endothelial cells (BAEC) were exposed to flow for 2 hr, noting that the chromatograph profiles of the proteoglycans resembled those found *in vivo* as shear rate was increased [32]. Arisaka *et al* (1995) studied proteoglycan metabolism from porcine endothelial cells post shear stress treatment and found that, in contradiction with Grimm's results, GAGs synthesis increased with shear stress [106]. Both experiments focused on the effect of shear treatment for 24 hr or less and, hence, were focused on acute responses rather than chronic effects. In contrast, our experimental model is geared toward the study of the release of the proteoglycans from BAEC under long-term physiological flow rates.

In our studies, we have used the Cellmax® capillary system that is based on endothelial cell culture on the walls of hollow fibers having the general dimensions of blood vessels [98]. With this model, we cultured BAEC under flow conditions resulting in shear stresses of either 5±2 or 23±8 dynes/cm^2 in order to ascertain the effects of shear stress on endothelial cell metabolism of proteoglycans. We compared our flow system proteoglycans with samples isolated from endothelial cells cultured in the absence of flow in tissue culture conditions. Furthermore, we evaluated how these proteoglycans impact platelet aggregation as an indicator of the possible effect on hemostasis. Our data show that shear stress can alter important characteristics of proteoglycans released from BAEC, which ultimately can regulate platelet activity and coagulation in whole blood.

Materials and Methods

Materials

Bovine aortic endothelial cells (BAEC), cryopreserved at passage 8, were obtained from the Coriell Institute (Camden, NJ). All chromatography supplies and general chemicals as well as dimethylmethylene blue dye (DMMB), blue dextran (2,000,000 MW), human thrombin, chondroitinase ABC (C.ABC), and unfractionated heparin (ovine intestinal mucosa) were purchased from Sigma-Aldrich (St. Louis, MO). Heparinase III (Hep III) was a generous gift from IBEX Pharmaceuticals (Montreal, Canada). Beef lung unfractionated heparin used for the

aggregation studies was purchased from Pharmacia&Upjohn (Peapack, NJ). Recombinant human tissue factor was purchased from Dade Behring (Deerfield, IL). Fetal bovine serum (FBS) was purchased from Hyclone (Logan, UT). Media supplements with the exception of acidic fibroblast growth factor (aFGF) and all tissue culture supplies were purchased from Fisher Scientific (Suwanee, GA). aFGF was obtained from GibcoBRL Life Technologies (Carlsbad, CA). Aqueous sodium sulfate ($Na_2{}^{35}SO_4$) was purchased from NEN Life Science (Boston, MA). Dialysis cassettes (3,500 MWCO) were from Pierce (Rockford, IL). The Cellmax® High Flow Quad Artificial Capillary Cell Culture System was from Cellco® Spectrum Laboratories (Rancho Dominguez, CA) and the hollow fibers cartridges used were made of porous polypropylene (0.5 μm pore size) and were coated by the manufacturer with pronectin-F™ to facilitate cell adhesion.

Conditioned Media Collection

BAEC, passage 10, were seeded on the luminal surface of pronectin-F™ coated polypropylene capillaries contained in a sealed cartridge at 2.9×10^4 cells/cm^2 as described previously [98]. A total of 50 capillaries (9.6 cm long, 330 μm ID, 150 μm wall, 0.5 μm pore size) are contained within each cartridge and the system can handle four independent cartridges simultaneously. Culture media (Ham's F12, supplemented with 10% FBS, 1% L-glutamine, penicillin (100 U/mL), streptomycin (100 μg/mL), and aFGF (3.5×10^{-3} μg/mL) was directed within the extra-capillary space to allow for cell attachment for 24 hr before initiating exposure of the cell culture to flow (4 ml/min). Seeding efficiency in the cartridges was ≈ 85%. The cells were cultured for 7 days under low shear stress (< 0.5 dynes/cm^2) before gradually ramping up the flow rate for the high shear samples. The culture was maintained for 14 days including the treatment shear stresses (final 72 hr). Prior to conditioning, a 1 hr wash with serum-free Ham's F-12 media was then followed by conditioning with $Na^{35}SO_4$ (30 μCi/mL) supplemented serum-free Ham's F-12 at the desired flow rate. The conditioned media was collected 24 hr later and centrifuged (Jouan CR412, Wincester, VA) at 1865 × g for 10 min at 4 °C to remove any cell debris. The treatment shear stresses were 5±2 and 23±8 dynes/cm^2. The pulsatile flows had similar frequencies for low and high shear treatments of ≈ 0.3 Hz and were essentially sinusoidal. The intraluminal average pressure gradients across the cartridges for low and high shear cultures

were 9.6 and 26 mmHg, respectively. The non-flow cultures involved seeding BAEC on polypropylene membranes placed in 12 well tissue culture plates at an identical seeding density as used in shear stress cultures. Cells were grown for 7 days including the 1 hr wash and 24 hr conditioning with $Na_2^{35}SO_4$ (30 μCi/mL). Following collection, all conditioned media was centrifuged to remove any cell debris, and processed for purification as described below. Purified samples were frozen at -80 °C and thawed as needed.

Isolation of proteoglycans and GAGs

Isolation of proteoglycans from conditioned media was performed as described previously [36]. Briefly, urea (1 mol/L) was added to the conditioned media prior to loading on a Q-sepharose anionic exchange column (1.5 × 3.5 cm) at 1 mL/min. A step salt gradient (Tris buffer, (50 mmol/L Tris, pH 8.0)), 0.3 mol/L NaCl) was followed by the elution of the target proteoglycans using Tris buffer, 1.5 mol/L NaCl. Flow rates were maintained at 1.0 mL/min for all elutions.

Dialysis against TBS (Tris buffer, 0.15 mol/L NaCl) using dialysis cassettes (MWCO 3,500) was performed to remove urea, any unincorporated sulfate, and to reduce salt concentration. Proteoglycan fractions from shear treated BAEC were concentrated by lyophilization. Concentrations were determined in triplicates using the DMMB spectrophotometric assay [187] with beef lung or ovine intestinal mucosa unfractionated heparins as standards. Media not exposed to cell cultures were subjected to the same purification and concentration protocol to generate control samples. GAGs from purified proteoglycans fraction were obtained using an alkaline β-elimination reaction as described previously [188]. Briefly, purified proteoglycans were incubated for 24 hr at 37 °C in 1 mol/L $NaBH_4$, 0.05 mol/L NaOH at pH 12.5. Glacial acetic acid was used to quench the solution to pH 7.0.

Enzymatic Digestion

Proteoglycan fractions were analyzed using differential enzyme digestion with heparinase III (Hep III) and chondroitinase ABC (C. ABC) as described previously [36]. Hep III was used at working concentration of 0.25 U/mL and C.ABC at 1 U/mL. Tris-HCl buffer (50 mmol/L Tris, pH 7.52, 0.15 mol/L NaCl) was prepared for all digestions. Samples were incubated with Hep III

alone, C.ABC alone or both enzymes for 4 hours at 37 °C and then assayed using spectrophotometry and DMMB. Control samples were incubated without enzymes.

Chromatography

[$^{35}SO_4$]-incorporated proteoglycans and GAGs were passed over Sepharose CL-2B (1.0 × 40 cm) and Sepharose CL-6B (1.0 × 40 cm) size exclusion columns equilibrated in TBS at an elution flow rate of 1 mL/min. The radioactivity per fraction (1 ml) was determined using a Packard Liquid Scintillation Analyzer 2100 TR (Meriden, CT). The void and total volumes of the columns were determined using blue dextran and $Na_2{}^{35}SO_4$ respectively. Average MW of proteoglycans and GAGs were obtained from derived correlations based on the Kav values [189, 190].

DEAE ion exchange column (1.0 × 3.5 cm) was used as the stationary phase to characterize elution profiles of isolated proteoglycans and GAGs. Samples were loaded and eluted using a linear gradient (0.15 to 1.5 mol/L NaCl) in 95 min at 1mL/min with fractions collected every min. The eluent stream was monitored for its conductance with a Bio-Rad conductance meter EG1 Gradient Monitor (Hercules, CA). Samples were quantified using a liquid scintillation analyzer.

Platelet Aggregation Studies

Blood samples were obtained fresh from healthy male human donors who had not taken aspirin for at least 2 weeks prior to blood collection. Venous blood was collected in sodium citrate (3.2%) vacutainers tube. The platelet-rich-plasma (PRP) fraction was extracted following centrifugation at 150 × g for 10 minutes with a Sorvall RT6000 Tabletop centrifuge with H-1000 rotor followed by isolation of the platelet-poor-plasma (PPP) fraction by centrifugation (1500 × g for 10 minutes). The PPP was used to dilute and scale the PRP to ~4.0×10^8 platelet/mL for all samples used in the aggregation study. Blood and PPP were kept at room temperature during the study.

A Bio/Data Corporation aggregometer PAP-4 (Horsham, PA) was used to determine steady state values of percent platelet aggregation. PRP (200 µl) was mixed with purified proteoglycans (20 µl) and equilibrated at 37 °C for 8 min prior to thrombin (0.5 IU/ml, 20 µl)

addition. Readings were taken continuously for at least 4 min per sample. PPP was used as a control for 100 % transmittance. Dose response curves for thrombin-induced aggregation were generated (data not shown) to determine maximal stimulation.

Thromboelastography Studies

A computerized Thromboelastograph® (CTEG Model 3000, Haemoscope Corp., Skokie, IL) was used to determine the peak rigidity of blood samples treated with shear specific proteoglycan fractions as described previously [144]. Briefly, torque measurements on a suspended stationary piston residing inside of an oscillating cup containing whole blood and treatment samples were recorded at 37 ^{o}C with tissue factor (4 μg/mL) as a coagulation agonist and $CaCl_2$ (3 mmol/L) as a coagulation cofactor. As the fibrin/platelet fibrils form, peak-to-peak torque increases indicating an increase in overall rigidity. Blood sample elasticity measurements resulting from proteoglycan treatment was referenced to that of negative controls (media treated identically to the purified proteoglycans) to determine the % inhibition of the samples.

Results

Experimental Biomechanical Model

The flow system used for our shear stress studies has been previously described by Redmond *et al.* [98]. The system is composed of a control unit that regulates four independent positive displacement pumps that are connected to four independent cell cartridges. The system allows for the culture of endothelial cells under pulsatile flow for prolonged period of time and, thus, replicates the chronic shear stress conditions encountered by endothelial cells *in vivo*. Chronic shear stress treatment of BAEC was achieved by seeding cells inside porous polypropylene capillaries contained within a sealed plastic casing. The flow rate was steadily increased over a period of 14 days and included at least 72 hr at the desired physiological shear stress levels: low shear (5±2 dynes/cm^2) or high shear (23±8 dynes/cm^2). The shear stresses used are typical of venous type shear stresses (low shear) and arterial type shear stresses (high shear) and were calculated using measured pressure drop, flow rate, and fluid viscosity data[104]. Flow inside the capillaries was pulsatile and nearly sinusoidal at a frequency of about 0.3 Hz. Comparison with a non-shear system was made by culturing BAEC on polypropylene membranes maintained in static tissue culture plates.

Effects of Shear Stress on BAEC-released proteoglycans and GAGs Levels

The effect of acute shear stress on endothelial cell synthesis of proteoglycans has been studied [32, 106] but our focus was on how chronic shear stress impacts regulation of these molecules. Following purification from conditioned media, overall levels of sulfated proteoglycans/GAGs were determined using the DMMB spectrophotometric assay [187]. An increase in average shear stress led to a significant increase ($p < 0.01$) in proteoglycan/GAGs levels isolated (Table 1). Control media not exposed to BAEC had no detectable proteoglycans. Despite changes in overall levels, shear stress does not appear to affect overall GAGs composition. Heparan sulfate GAGs constituted ~80 % of the total GAGs content with chondroitin/dermatan sulfate GAGs making up the balance for all three samples (Table 2).

Effect of Shear Stress on BAEC-released Proteoglycan Size

Changes in overall size and GAGs content have been shown to impact proteoglycan activity [36, 136] and, thus, we investigated whether shear stress affected either of these important characteristics. Following purification from conditioned media, proteoglycan fractions were separated using a CL-2B Sepharose column. In all cases, two broad peaks were evident with a Kav values of 0.14 and 0.48, corresponding to average molecular weights of 2.2×10^6 and 6.1×10^5, respectively [189, 190](Figure 1). The elution peaks occurred at the same Kav value for all samples, however, the proportion of high to low molecular weight species decreased with increasing shear. Specifically, the percentage of high molecular weight fraction decreased from 30 ± 3% for non-shear samples to 23±2 % for low shear and 19 ±2 % for high shear samples.

To determine whether these differences in distribution were reflected in changes in the overall GAGs size profile, proteoglycans fractions were treated with alkaline borohydride to release the GAGs chains and the material was separated over a CL-6B Sepharose column. Borohydride treatment was effective in releasing the GAGs side chains as undigested fractions showed only a single peak near the void fraction (data not shown). The GAGs elution profile shows a shift in the peak elution from the void volume when the proteoglycans are intact to a primary peak at Kav = 0.43 (MW 3.0×10^4) and a secondary smaller fraction at Kav = 0.83 (MW 3.5×10^3) (Figure 2). Shear stress does not appear to affect either the distribution or the elution of the GAGs.

Effect of Shear Stress on BAEC-released Proteoglycan Ion Exchange Profile

The extent of proteoglycan sulfation can impact function [191] and may reflect changes in the overall negative charge associated with the GAGs chains [136]. Hence, we used ion exchange chromatography to separate proteoglycans and GAGs based on their ionic binding affinity as a means of characterizing shear stress induced effects. Three main GAGs peaks were found compared to only two peaks for the CL-6B column separation. The earliest bound species eluted at a salt concentration of 0.15 mol/L NaCl, followed by a peak at 0.42 mol/L NaCl and, finally, a third peak at 0.59 mol/L NaCl (Figure 3A). While low shear and high shear GAGs have similar distributions, the no shear static BAEC released relatively more GAGs that had a lower ionic affinity for the column. Both the first and second peaks of the no shear GAGs represent a significant increase in relative amount when compared to corresponding low shear and high shear GAGs peak. These observations indicate a fundamental difference in the distribution of GAGs released when BAEC are subjected to shear as opposed to when the cells are grown in static cultures.

The elution of shear specific proteoglycans from a Sepharose DEAE column showed a unique proteoglycan peak that only occurred for the low shear samples (Figure 3B). High shear and no shear proteoglycans had similar profiles and distribution, however, there was a distinct distribution for low shear proteoglycans. Specifically, only two significant peaks at 0.46 and 0.62 mol/L NaCl were found for the no shear and high shear proteoglycan samples, while three significant peaks were found with the low shear proteoglycan sample. The additional peak found at 0.30 mol/L NaCl represented ≈ 20% of the total low shear proteoglycans released. The no shear and high shear proteoglycans that eluted between the same NaCl concentrations as that unique peak represented less than 2% of the total material. The latter two low shear peaks eluted at the same position as in the no and high shear cases.

Differential Inhibition of Platelet Aggregation by proteoglycans

Shear stress treatment of BAEC did impact the released proteoglycans suggesting that proteoglycan-mediated activity, such as inhibition of platelet activation, might be shear regulated. Heparin, a GAGs similar in structure to heparan sulfate, has been shown to reduce thrombosis *in vivo* and inhibit blood coagulation [144, 192] leading to its common use clinically.

We examined the effects of purified shear specific proteoglycans on thrombin induced platelet aggregation using light transmittance aggregometry and found that platelet aggregation was inhibited by purified proteoglycans from all samples (Figure 4). The effect was specific to the cell-secreted material, as processed plain media had no inhibitory effect (data not shown). Proteoglycans from high shear samples were the least potent in inhibiting thrombin induced platelet aggregation (IC_{50} 0.24 μg/dose), followed by proteoglycans from low shear samples (IC_{50} 0.20 μg/dose). Proteoglycans from static culture samples were the most potent (IC_{50} 0.15 μg/dose) although unfractionated beef lung heparin was significantly more potent in our assay than any of our purified samples (IC_{50} 0.065 μg/dose).

Differential Inhibition of Clot Formation by proteoglycans

As an extension of our aggregometry data, we used a Thromboelastograh® to analyze proteoglycan inhibition of blood clot formation. Tissue factor (4 μg/mL) induced blood clot formation dose response curves were generated (Figure 5) and a similar trend to that seen with the inhibition of platelet aggregation was found. Specifically, proteoglycan from static culture samples were the most potent inhibitors of blood clot formation (IC_{50} 0.078 μg/dose) followed by the proteoglycans from low shear samples (IC_{50} 0.19 μg/dose). Proteoglycans from high shear samples (IC_{50} 0.30 μg/dose) were the least potent. Medium, which had not been exposed to BAEC but had been processed in parallel with the conditioned media, had no significant effect on clot formation (data not shown).

Statistics

Means were compared for significance using the method of contrasts.

Discussion

Thrombosis is involved in the pathogenesis of atherosclerosis and fluid mechanical forces stemming from blood flow favor the location of atherosclerotic plaques in disturbed regions of blood flow [20-22, 157, 181, 193]. Proteoglycans are known to be involved in the regulation of vascular thrombosis [30]. For example, heparin is a commonly administered GAGs used to reduce thrombosis in which platelets take an active role [7, 79, 144, 192, 194-197]. We wanted to study how shear stress, applied to BAEC, impacted proteoglycans metabolism and, furthermore,

whether these shear specific proteoglycans influenced the inhibition of aggregation and coagulation. The first part of this research involved the identification of proteoglycans and GAGs released from BAEC cultured under pulsatile flow. Three shear stress treatments were used: no shear static culture (0 dynes/cm^2), low shear (5±2 dynes/cm^2), and high shear (23±8 dynes/cm^2). BAEC were seeded on the luminal surface of capillaries and were subjected to pulsatile flow. The conditioned media was purified and the proteoglycans and GAGs analyzed using size exclusion chromatography as well as ion exchange chromatography.

All shear specific proteoglycans separated into two broad peaks (Figure 1) on a Sepharose CL-2B column and their sizes compared favorably with previous studies [36]. In our experiments, the relative fraction of the high MW proteoglycan fraction increased with decreasing shear. Since this fraction was found previously to be more potent in inhibiting fibroblast growth factor-2 (FGF-2) mediated vascular smooth muscle cell growth (VSMC) [36], our results indicate that with increasing average shear stress BAEC release relatively less of the more potent FGF-2 inhibitor. Whether this difference is physiologically relevant remains to be tested. FGF-2 and other growth factors are known to contribute to restenosis and intimal hyperplasia [7]. Thus, lower shear stresses may generate an endothelial cell phenotype that is more atheroprotective by releasing a higher fraction of the more potent growth factor inhibitor. This is in contradiction with *in vivo* studies that have shown that low venous shear stresses (4 dynes/cm^2 or less) are associated with intimal thickening [22]. Both the pressure waveform frequencies (approx. 0.3 Hz) and the ratio of amplitude to average shear stress were similar in our low and high shear experiments (0.4 and 0.35 respectively). However the magnitude of the amplitude of the luminal shear stress does increase from 0 dynes/cm^2 under static conditions, to 2 dynes/cm^2 at low shear, and finally to 8 dynes/cm^2 at high shear, with a concomitant increase in luminal dynamic pressure. These pulsatile forces may have a deleterious effect on the observed atheroprotective responses that are normally exhibited in EC under *sustained* higher arterial shear stresses (with 23 dynes/cm^2 being an upper bound at rest).

When shear specific GAGs obtained from the β-elimination of intact proteoglycans were separated on a CL-6B column, two peaks with a Kav = 0.43 (MW 3.0×10^4) and a Kav = 0.83 (MW 3.5×10^3) were found (Figure 2). Previous work [36] found that CL-6B elution profiles of endothelial conditioned media GAGs from high and low MW proteoglycans species eluted with

a Kav = 0.52 and a Kav = 0.32, respectively. The arithmetic average of these two Kav is 0.42 and is almost exactly equal to our pooled low and high MW proteoglycans species Kav of 0.43. In that study, the heparan sulfate GAGs (as determined by heparinase and heparitinase digestion) were found to be essential for the FGF-2 mediated growth inhibitory effect of the proteoglycans on vascular smooth muscle cells (VSMC). Similar ratios of heparan to chondroitin sulfate/dermatan sulfate were found from our samples isolated from cells cultured under flow. Grimm *et al*. [32] looked at purified proteoglycans from BAEC acutely shear treated and found a very low molecular weight heparan sulfate species similar in size to that obtained in our GAGs fraction (MW 3.0×10^4) suggesting that free GAGs may be more readily available under acute shear treatment. This study further indicated that this low MW GAGs was the only remaining labeled species following shear stress treatment above 1 dynes/cm^2, which is in contrast to our findings. These differences may stem from differences in cell culture conditions (for example: inclusion of fetal calf serum during conditioning versus plain media) or may reflect differences in acute versus chronic conditions and may relate to the metabolism of proteoglycans (1 hour versus 24 hr conditioning and 2 hr versus 14 days duration of shear culture).

Since GAGs are highly anionic and this characteristic is important for activity, we used ion exchange chromatography column to separate the GAGs in terms of their ionic binding affinity using a NaCl linear gradient for elution. Elution profiles indicated that GAGs from static culture BAEC were significantly different in their distribution than GAGs from BAEC cultured under shear, particularly for the low salt peaks (0.15 mol/L and 0.42 mol/L NaCl) (Figure 3A). Hence, there appears to be a difference in the GAGs metabolism of shear treated versus static culture of BAEC, which expresses itself in terms of an increased composition of the low cation-binding GAGs. However, bulk analysis of Hep III and C.ABC digested purified GAGs indicate no difference in terms of heparan and chondroitin/dermatan sulfate composition, making-up about 80 and 20 % respectively for all samples (Table 1). Hence, the differences shown by DEAE ion exchange separation is likely the result of variable sulfation and carboxyl group content that determines electrostatic interaction with the cationic functional groups in the DEAE matrix. Whether this is responsible for the change in activity with respect to inhibition of platelet aggregation (Figure 4) is not clear.

Additional differences were found when intact shear specific proteoglycans were run over a DEAE Sepharose column. A unique proteoglycans peak was isolated from samples of low shear treated BAEC at a NaCl elution concentration of 0.3 mol/L, which was not found amongst either static or high shear proteoglycans (Figure 3B). This difference is not related to variations in GAGs since none were found (Figure 3A) between shear-treated samples. Because the lower shear stress magnitude used in this study correlates with that found at focal localization of atherosclerotic plaques, one could speculate that this functional difference might be relevant to the pathogenesis of vascular disorders. This is reinforced by the fact that proteoglycans are involved in the regulation of growth factor activity [7, 198, 199] and platelet/coagulation activation [30, 136], with all of these factors being involved in the progression of atherosclerosis and other related vascular diseases.

Thus, having found significant differences between proteoglycan profiles from static and chronic shear stress treated BAEC, we sought to show that these differences manifested in a functional effect. Using light transmittance aggregometry, we monitored the thrombin-induced aggregation of platelets when incubated with shear specific proteoglycans (Figure 4). High shear proteoglycans were less potent in inhibiting aggregation with an IC_{50} of 0.24 μg/dose, followed by low shear proteoglycans with an IC_{50} of 0.20 μg/dose and, finally, static culture proteoglycans with an IC_{50} of 0.15 μg/dose. It is possible that the decreased relative amount of the high MW component in the shear samples (Figure 1) is responsible for the observed continuous differential inhibition. Heparin, like GAGs such as heparan sulfate and, to some extent, dermatan sulfate, have been known to enhance several hundredfold antithrombin and heparin cofactor II activity [136], both inhibitors of coagulation proteases. The larger number of heparan sulfate GAGs of the high MW component would have, presumably, a higher number of binding regions for these proteases inhibitors and thus increased potency in their activation. This could explain our data given that the high MW components are more prominent at lower shear stresses. Having shown shear specific proteoglycans effect on platelet aggregation, we wanted to show that blot clot formation in whole blood was similarly differentially affected. Since platelet activation is intimately involved in the coagulation process, we rationalized that shear specific proteoglycans effect on aggregation will be reflected in the fibrin/fibrinogen clot formation process as well. Using tissue factor as an agonist for coagulation, we generated dose response curves for

proteoglycan inhibition of blood clot formation (Figure 5). A similar order of effectiveness was observed.

Our *in vitro* data suggests that under lower pulsatile flow BAEC release more potent coagulation and aggregation inhibitor proteoglycans. This may be the result of a compensatory process that would increase the antithrombic potency of the shear specific proteoglycans that occur at lower venous shear stresses, since fewer proteoglycans are released at lower shear stresses (Table 1). Hence, hemostasis could be achieved in this way. In order to address this issue we reploted the aggregation and coagulation curves (Figure 4 and 5, respectively) as dose response curves normalized to the amount of proteoglycans released per cell. Since the amount released per cell increased continuously with increased shear stress treatment (Table 1), we found that the low and high shear dose response curves collapsed for both aggregation and coagulation, in contrast with the no shear proteoglycans (Figure 6A and 6B). This data thus indicates that, while shear proteoglycans specific potency as coagulation inhibitors decreased with shear stress treatment (Figure 4 and 5), this reduced potency was offset exactly by a corresponding increase in the amount of released proteoglycans. The no shear proteoglycans have a decreased overall potency however. This is particularly relevant since platelet deposition and activation --that would presumably be favored at higher shear stresses based on our data-- is an important step in atherosclerotic plaque development. Hence, our data may reflect either a normal regulatory hemostatic response to low shear stresses or an abnormal response to the pulsatile hemodynamic environment in our perfusion system.

A similar issue arose when we considered the *reduction* in the relative amounts of the high MW components (Figure 1) with higher shear stresses. Forsten *et al*.(1997) showed that *in vitro* FGF-2-induced VSMC proliferation was better inhibited by the high MW proteoglycans fraction, however, our data show that this fraction is reduced at higher shear stresses. By releasing relatively fewer of these high MW proteoglycans at higher shear stresses, BAEC may present conditions that could favor wall thickening since vascular wall remodeling is probably mediated, in part, by paracrine and autocrine release of growth factors such as FGF-2.

In summary, we have shown that chronic pulsatile shear stress induces the release of shear specific proteoglycans and increases the amount of proteoglycans present in the conditioned media. Differences were observed in 1) the relative amount of the high MW

proteoglycan component, 2) the relative amount of low ionic binding affinity GAGs under no shear conditions, and 3) the appearance of a unique proteoglycans species under low shear stress. Differences were shown in the potency of these purified proteoglycans samples in inhibiting platelet aggregation and blood clot formation, likely linked to the shear specific distribution of the high MW proteoglycans components. Specifically, higher shear proteoglycans were less potent in inhibiting aggregation and coagulation. However, when normalized to the amount of proteoglycans released per cell the inhibition dose response curves were similar for shear samples, but decreased for the no shear. These findings point to one possible way by which shear stress modulates growth and coagulation factors activity and may be relevant to the progression of atherosclerosis.

Acknowledgments

We are grateful for support from the Carilion Biomedical Institute, Dupont (Young Professor Grant), The National Science Foundation (BES9875626), and Sigma Xi Grant-in-Aid Program (SE) as well as the generous donation of Heparinase III from IBEX Pharmaceuticals. We appreciate the technical assistance rendered by Laura Delo and Mark Foresyth.

Tables

Shear Stress Treatment	Secreted Proteoglycans ($\mu g \times 10^5$/ng DNA)
No Shear	1.37±0.37
Low Shear	3.95±0.41*
High Shear	5.59±0.36* †

Table 1. Total proteoglycans released in the conditioned media of bovine aortic endothelial cells (BAEC) as a function of shear stress treatment. Proteoglycans were purified as described under Materials and Methods and amounts determined using a DMMB spectrophotometric assay. Proteoglycans amounts were normalized to total DNA. Error bars represent standard deviation for the results of 3 independent experiments (n=3). *$p<0.005$ vs No Shear and †$p<0.01$ vs Low Shear. The amounts of released proteoglycans followed a similar trend when normalized to cell number (data not shown).

% Composition	No Shear	Low Shear	High Shear
Heparan Sulfate	84.1±5.5	82.0±6.3	80.4±4.6
Chondroitin/Dermatan Sulfate	18.5±3.6	21.5±3.2	19.3±5.0

Table 2. Glycosaminoglycan composition of conditioned media proteoglycans from shear and non-shear treated bovine aortic endothelial cells. Proteoglycans were purified as described under Materials and Methods and incubated with heparinase III (Hep III, 0.25 U/mL) and/or chondroitin ABC (C.ABC, 1.0 U/mL) for 3 hr at 37 °C. Difference assay based on DMMB assay (heparin standard) was used to determine the glycosaminoglycan composition: heparan sulfate (control (no enzyme)-Hep III), chondroitin/dermatan sulfate (control-C.ABC). Error bars represent standard deviation for the results of 3 independent experiments (n=3).

Figures

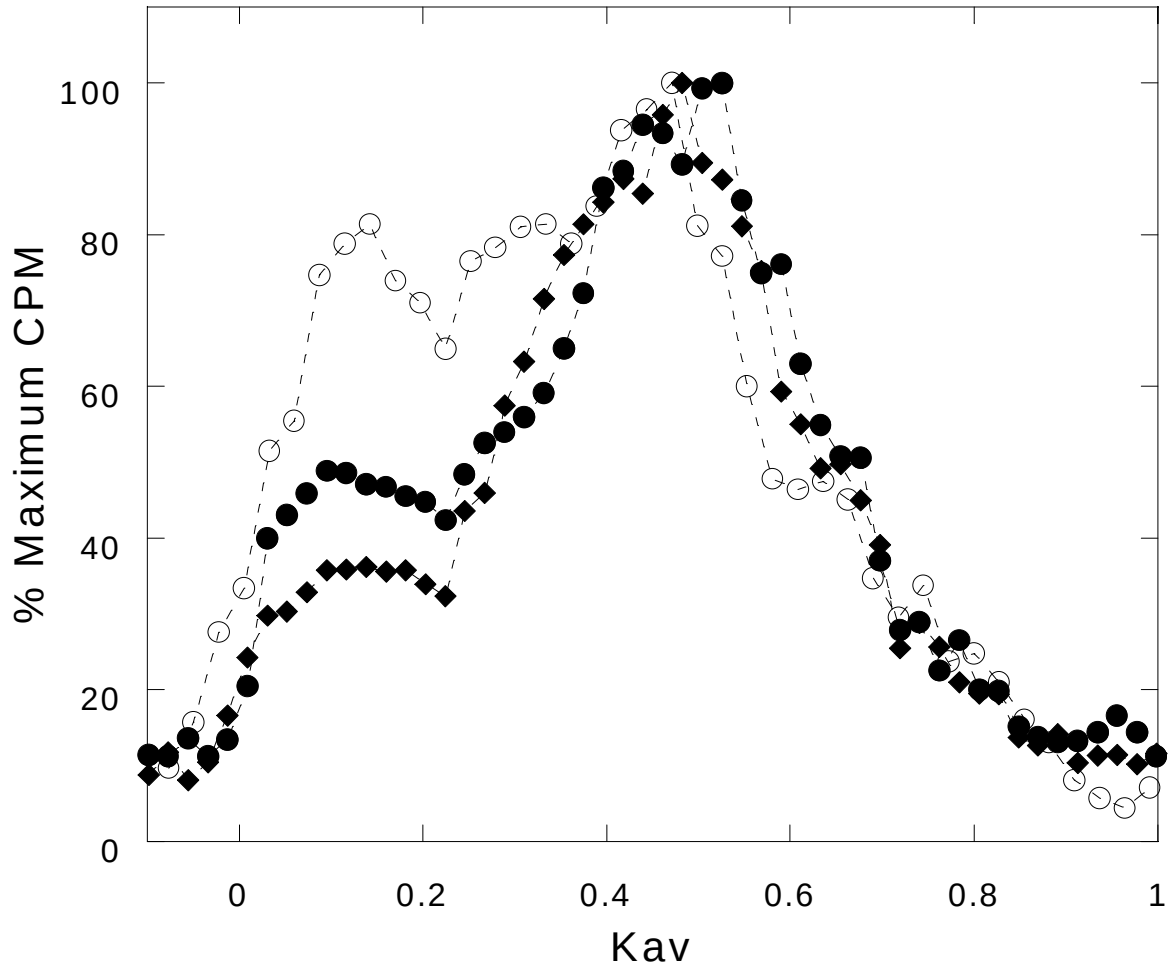

Figure 1. Elution profiles of isolated proteoglycans from the conditioned media of shear and non-shear treated BAEC. Metabolically labeled [^{35}S]proteoglycans were purified as described under Materials and Methods from the conditioned media of shear treated and static cultures of BAEC. Samples were separated on a Sepharose CL-2B column and radioactivity for each fraction was determined with a scintillation analyzer. The results were normalized to the maximum counts obtained from the fractions eluted. No shear (o), low shear (•), and high shear (♦) treated samples represent shear stress treatments of 0, 5±2, and 23±8 dynes/cm^2, respectively. Elution profiles are representative of 3 independent experiments.

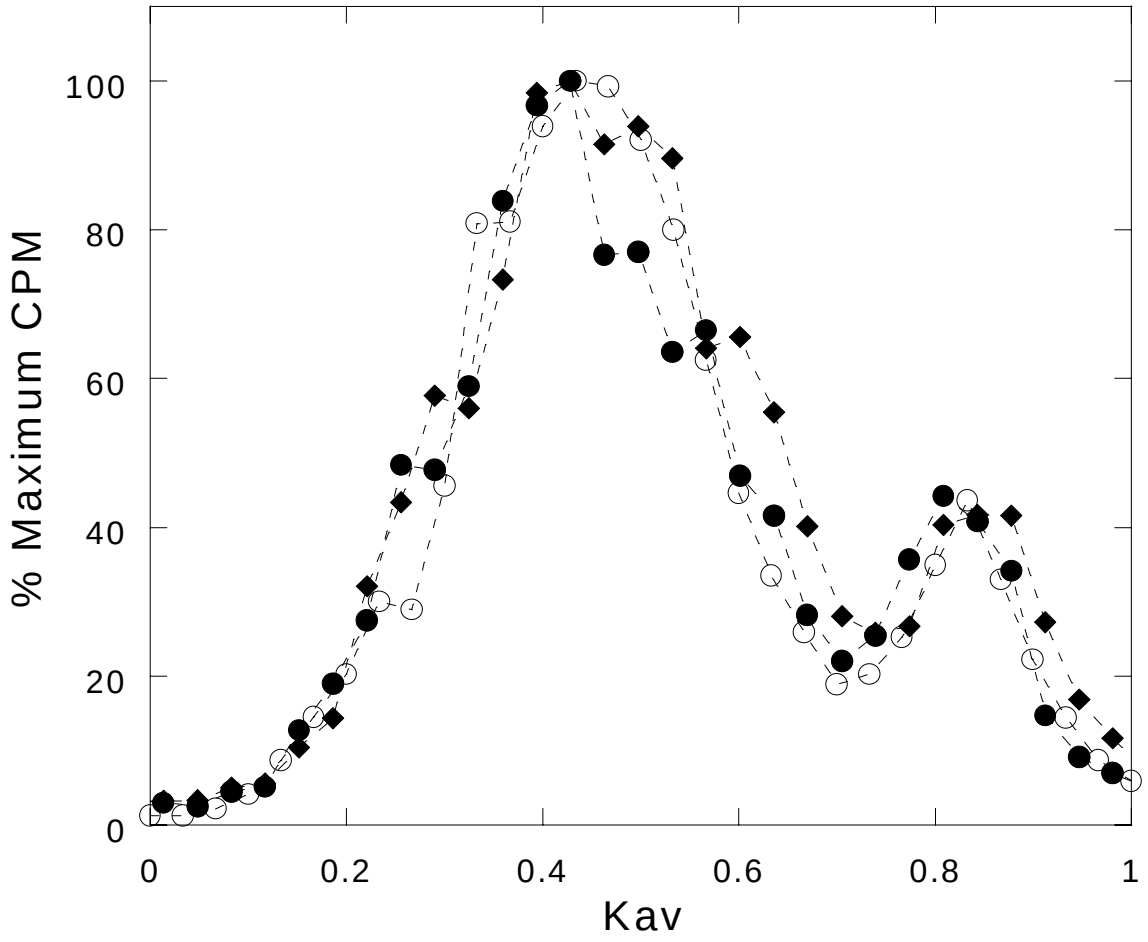

Figure 2. Sepharose CL-6B elution profiles of shear specific glycosaminoglycans from the conditioned media of shear and non-shear treated bovine aortic endothelial cells (BAEC). Metabolically labeled [^{35}S]proteoglycans were purified as described in methods from the conditioned media of shear treated and static cultures of BAEC. Following alkaline borohydride treatment GAGs were separated on a Sepharose CL-6B column and each fraction radioactivity was determined with a scintillation analyzer. The results were normalized to the maximum radioactivity counts obtained from the fractions eluted. No shear (o), low shear (•), and high shear (♦) treated samples represent shear stress treatments of 0, 5±2, and 23±8 dynes/cm^2, respectively. Elution profiles are representative of 3 independent experiments.

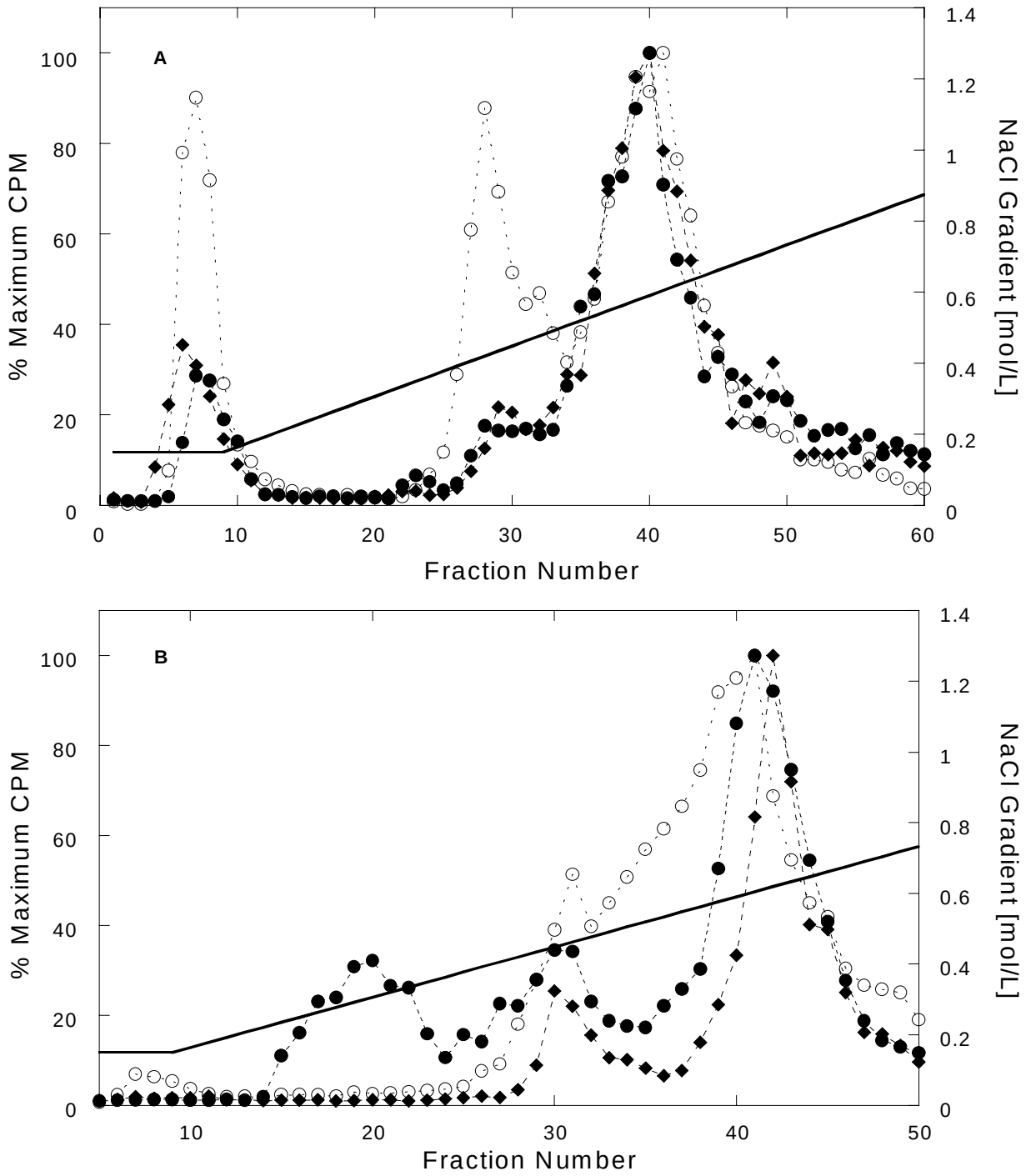

Figure 3. DEAE ion exchange column elution profiles of shear specific GAGs (A) and proteoglycans (B) from the conditioned media of shear and non-shear treated bovine aortic endothelial cells (BAEC). Metabolically labeled [^{35}S]proteoglycans were purified as described in methods from the conditioned media of shear treated and static cultures of BAEC. GAGs samples from β-eliminated proteoglycans and intact proteoglycans were eluted using a NaCl gradient (—) buffer, and each fraction radioactivity was determined with a scintillation analyzer.

The results were normalized to the maximum radioactivity counts obtained from the fractions eluted. No shear (o), low shear (•), and high shear (♦) treated samples represent shear stress treatments of 0, 5±2, and 23±8 dynes/cm^2, respectively. Elution profiles are representative of 3 independent experiments.

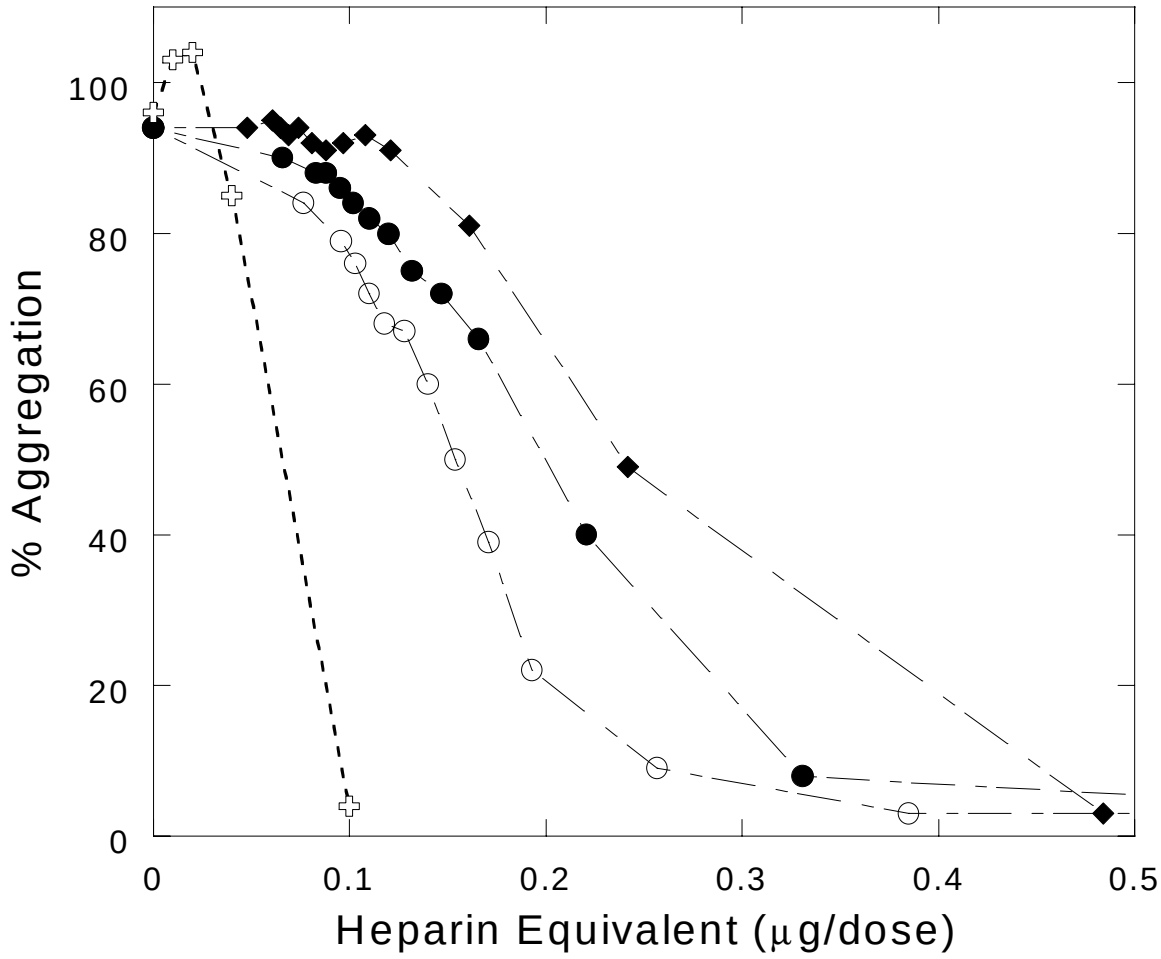

Figure 4. Dose response curves of thrombin induced platelet aggregation versus shear specific proteoglycans from the conditioned media of bovine aortic endothelial cells. Proteoglycans were purified as described under Materials and Methods. Using an aggregometer, samples of 200 μL of platelet rich plasma were incubated with 20 μL of shear specific proteoglycans at various concentrations for 8 minutes (37 °C). Thrombin agonist (20 μL) at a final concentration of 0.5 U/mL is added to the samples at the start of the reading, which was recorded for at least 4 minutes. The following IC_{50} were obtained: No Shear (o) 0.15, low shear (●) 0.20, high shear (♦) 0.24, and heparin (✣) (beef lung) 0.065 μg/dose. Data is representative of 2 independent experiments.

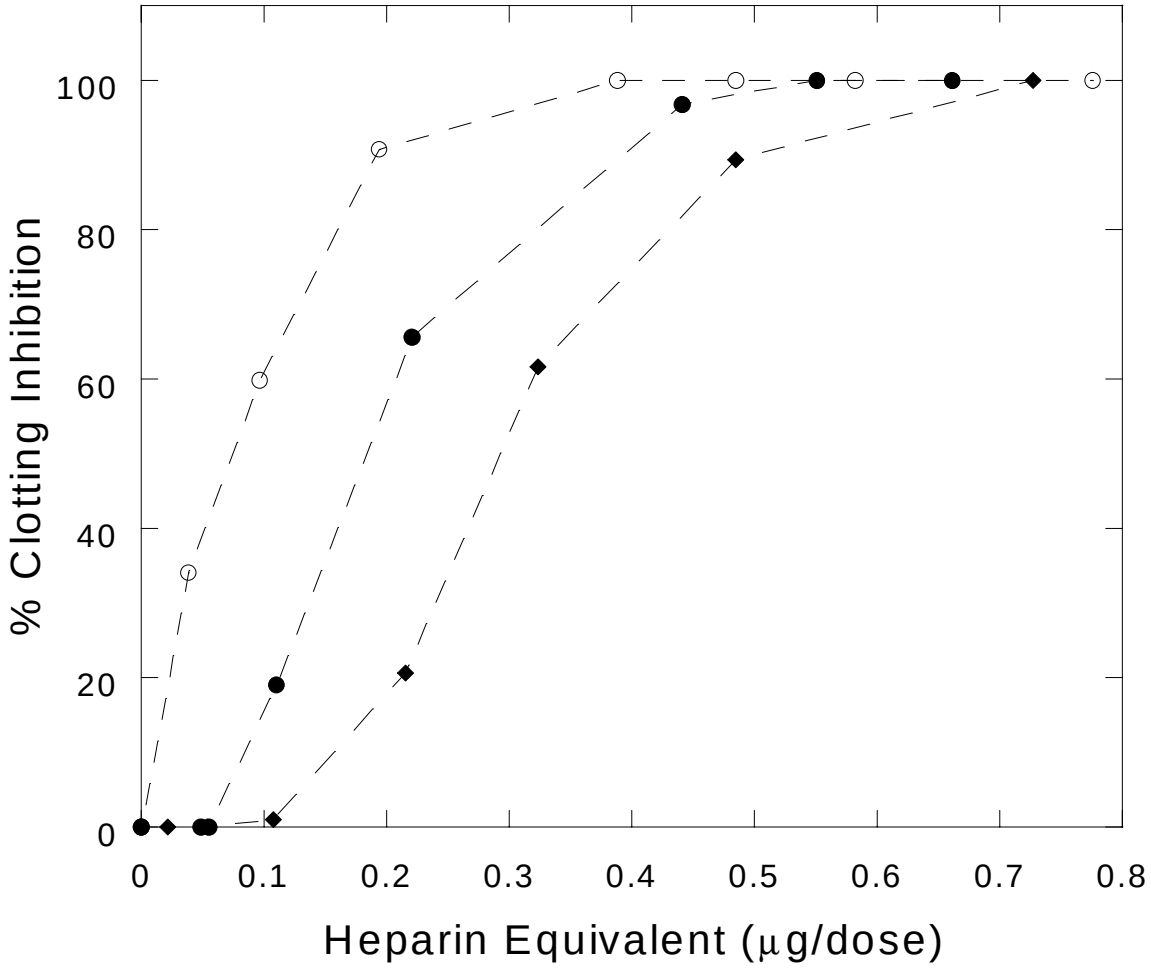

Figure 5. Dose response curves for tissue factor induced blood clot formation versus shear specific proteoglycans from the conditioned media of bovine aortic endothelial cells. Proteoglycans were purified as described in methods. Using a Thromboelastograph®, samples of 315 μL of human whole blood were incubated with 1-20 μL of shear specific proteoglycans and TF agonist (50 μL) at a final concentration of 4 μg/mL. Samples peak rigidity was recorded for at least 45 minutes at 37 °C. Un-exposed plain media negative controls did not inhibit significantly aggregation under the same conditions. The following IC_{50} were obtained: No Shear (o) 0.080, low shear (•) 0.18, and high shear (♦) 0.30 μg/dose. Data is representative of 2 independent experiments.

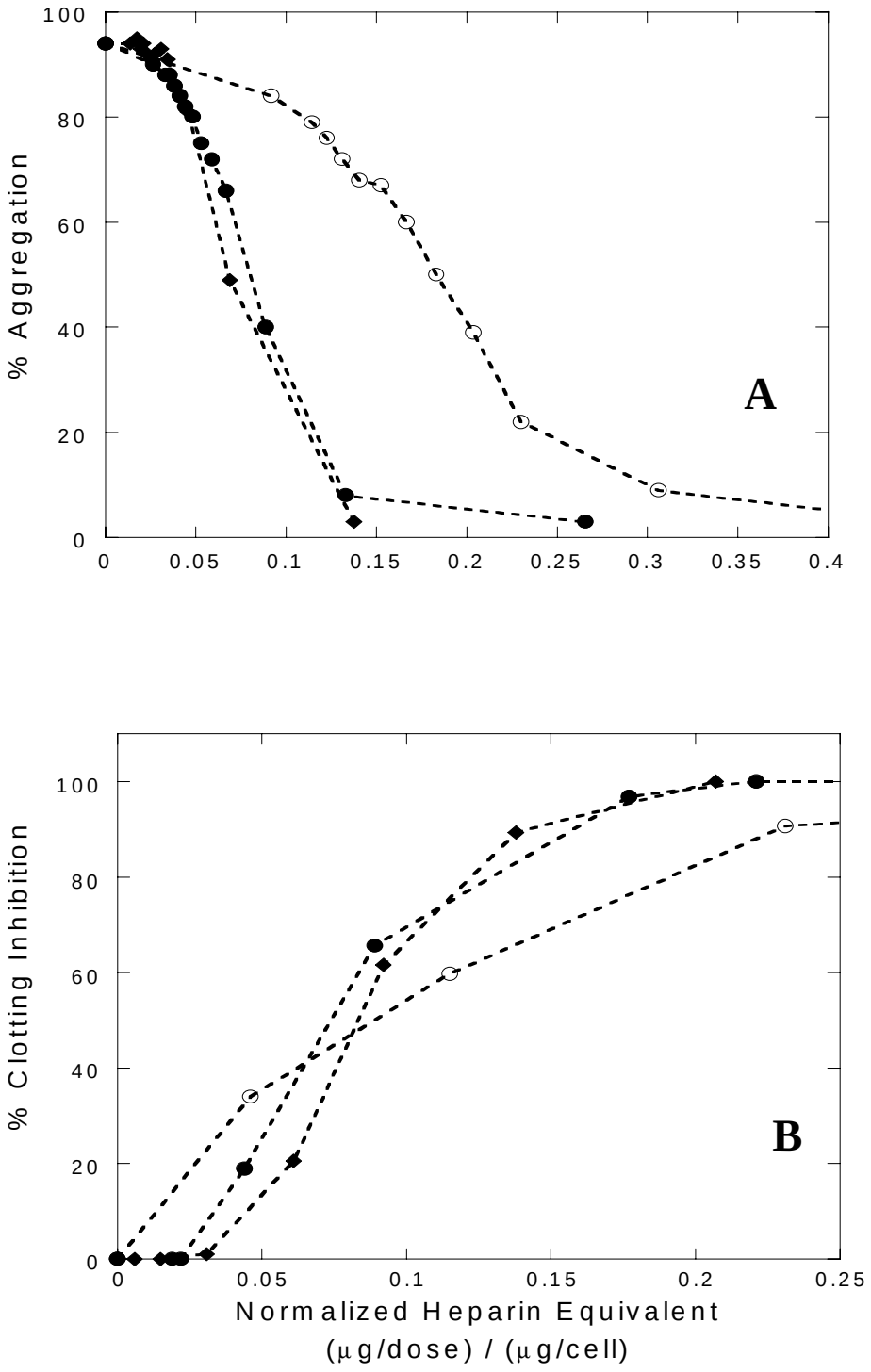

Figure 6. Normalized dose response curves for inhibition of thrombin induced human platelet aggregation (A) and tissue factor induced human blood clot formation (B) using purified proteoglycans from no shear (o), low shear (•), and high shear (♦) treated BAEC. Figures 4 and 5 were reploted and normalized by the amount of released proteoglycans per cell. See captions in figures 4 and 5 for experimental details. Data is representative of 2 independent experiments.

Chapter V: Chronic Pulsatile Shear Stress Increases Insulin Like Growth Factor-I (IGF-I) and IGF Binding Protein Release *in vitro*

Selim Elhadj, R. Michael Akers, Kimberly E. Forsten

Abstract

Insulin like growth factor -1 (IGF-I) is a potent smooth muscle cells mitogen and favors vascular proliferation. Insulin like growth factor binding proteins (IGFBPs) mediate the action of IGF-I within the IGF-I axis. Since hemodynamics have been linked to vascular proliferative disorders, we studied how pulsatile low venous-level (5±2 dynes/cm^2) and high arterial-level (23±8 dynes/cm^2) shear stresses could impact IGF-I and IGFBPs metabolism in bovine aortic endothelial cells (BAEC). Static no shear BAEC cultures were used as controls. Using a radioimmunoassay we determined that IGF-I expression was significantly increased over static culture control and that higher shear stresses reduced IGF-I released. The same trends were obtained from IGF-I mRNA message. Under shear stress BAEC released an additional IGFBP (likely IGFBP-3) that does not appear under static conditions, where only two IGFBPs were detected (likely IGFBP-4 and -2). The identity of the IGFBP-2 and -4 were suggested by MW determination and Western immunoaffinity blotting. Using thymidine incorporation studies, we found that conditioned media from shear and non-shear treated BAEC increased vascular smooth muscle cells (VSMC) proliferation over plain media controls. Further, low and high shear conditioned media were more potent in stimulating VSMCs proliferation than no shear media. The fact that IGF-I and IGFBPs metabolism is regulated by shear stress may point to a mechanism by which shear stress can contribute to the development of atherosclerotic plaques, and how it could also compromise vascular interventions by favoring pathologies such as restenosis, and arterial wall thickening.

Introduction

While the liver is the primary source of insulin-like growth factor-I (IGF-I) and IGF binding proteins (IGFBPs) in the blood stream, vascular cells are capable of secreting them locally [152, 159, 200-202]. IGF-I belongs to the IGF peptide hormone family along with insulin

and IGF-II [203] and is predominately found in the blood stream as a complex with IGF binding protein-3 (IGFBP-3) and a protein known as the acid labile subunit [200]. IGFBP-3 is one of six known IGFBPs capable of modulating IGF-I activity [200] and it, as well as IGFBP-2 and IGFBP-4 are known to be secreted by endothelial cells [147]. IGF-I binding to IGFBPs can increase IGF-I half-life as well as sequester it from cell surface IGF receptors (IGF-IR), thus altering its biological functions within the IGF-I axis [147, 159, 200]. Furthermore, IGF-I has been shown to enhance smooth muscle cells proliferation [152, 204] and migration [205], particularly following vascular injury or intervention [206, 207] suggesting a possible role in arterial wall response to injury and a link to intimal hyperplasia characteristic of restenosis. Pretreatment *ex vivo* of allografts from rat aorta with IGF-I led to an increase in the expression of IGF-I and IGF-IR within the vascular wall, while also up-regulating IGFBP-3 and various other growth factors [77]. It was speculated that this change in IGF-I availability could, in part, explain the occurrence of accelerated transplant arteriosclerosis [208, 209], especially given that up-regulation of IGF-I has been observed following balloon injury in the rabbit model [210]. Further, atherosclerotic plaque specimens from humans were found to have increased IGF-IR, IGF-I, and IGFBPs expression [153] indicating that the IGF-I axis may also have a role in the formation of atherosclerotic lesions.

The endothelium constitutes a natural interface between the perfusing blood and the underlying tissue, composed of cells such as smooth muscle cells and fibroblast cells. Disturbed features of blood flow within well-defined region of the vasculature have been correlated with the occurrence of atherosclerotic plaques [181-183]. Endothelial cells, which makeup the endothelium, actively participate in the chronic and acute regulation of the vascular wall metabolism in response to variations in blood flow pattern and mechanics [17, 118, 161, 165, 167, 211]. Acute effects are related to the release of short-lived vasoactive agents [97, 161, 212-214] while chronic effects are linked to wall remodeling [28, 95, 111, 215]. Previous studies have shown that shear stress, via altered endothelial cell response, regulates the release and metabolism of both mitogens and growth inhibitors [17]. Hence, paracrine and autocrine factors, such as IGF-I, could be regulated by shear stress. The question is whether mechanical forces stemming from altered blood flow can be linked to IGF-I and IGFBPs metabolism.

We thus sought to determine whether shear stress could affect IGF-I and IGFBP metabolism. In our studies, we have used the Cellmax® capillary system in which endothelial

cells are cultured under shear on the luminal walls of hollow fibers having the general dimensions of blood vessels. Using this model, we investigated the response of bovine aortic endothelial cells (BAEC) cultured under flow conditions resulting in chronic pulsatile shear stresses of either 5±2 or 23±8 dynes/cm^2. We compared our flow system results with results from BAEC cultured in the absence of flow in tissue culture conditions. Levels of IGF-I released in the perfusing and in the stationary media were measured using a radioimmunoassay (RIA), while IGFBPs released were measured using western ligand blotting. IGFBP identity were suggested from MW determination and Western immunoaffinity blotting. To determine if variations in expression were responsible for changes in the levels of IGF-I and IGFBP-3, IGF-I mRNA levels were measured using Northern blotting. Our results show that chronic pulsatile shear stress can increase the expression and protein levels of IGF-I and IGFBPs from BAEC, which could influence growth factor-modulated pathologies such as restenosis, vascular graft failures, and atherosclerosis.

Materials and Methods

Materials

All electrophoresis supplies and general chemicals were obtained from Sigma (St. Louis, MO) unless otherwise stated. Fetal bovine serum (FBS) was purchased from Hyclone (Logan, UT). Media supplements with the exception of acidic fibroblast growth factor (aFGF) and all tissue culture supplies were purchased from Fisher Scientific (Suwanee, GA). aFGF was obtained from GibcoBRL Life Technologies (Carlsbad, CA). The Cellmax® High Flow Quad Artificial Capillary Cell Culture System was obtained from Cellco® Spectrum Laboratories, (Rancho Dominguez, CA). Bovine aortic endothelial cells (BAEC, passage 10), and vascular smooth muscle cells (VSMCs, passage 4-6) were from the Coriell Institute (Camden, NJ). Recombinant human IGF-I (MW 7646) was from GrowPep (Adelaide, Australia). Mouse anti-human IGF-I monoclonal antibody was a kind gift from Dr. Bernard Laarveld (University Saskatchewan, Canada). Mouse anti-mouse IgG was obtained from Sigma (St. Louis, MO). Kodak XAR-5 film was from Eastman Kodak (Rochester, NY). Hybond-N Nylon transfer membranes were from Amersham (Buckinghamshire, UK). TRI REAGENT was from Life Technologies (Grand Island, NY). Transfer nitrocellulose membrane for ligand blotting was

from Micron Separation Inc. (Westborough, MA). Hoechst 33258 fluorescent dye was obtained from Amersham Pharmacia Biotech (Piscataway, NJ).

Media Collection

BAEC were seeded at 2.9×10^4 cells/cm^2 on the luminal surface of pronectin-F™ coated polypropylene capillaries contained within a sealed cartridge as described previously [98]. A total of 50 capillaries (13 cm long, 330 μm ID, 150 μm wall, 0.5 μm pore size) are contained within each cartridge used with the cell culture flow apparatus, and the system can simultaneously handle four independent cartridges. Culture media (Ham's F12, supplemented with 10% FBS, 1% L-glutamine, penicillin (100 U/mL), streptomycin (100 μg/mL), and FGF-1 (3.5×10^{-3} μg/mL) was directed within the extra-capillary space to allow for cell attachment for 24 hr before initiating exposure of the cell culture to flow (4 ml/min). Seeding efficiency for the cartridges was ≈ 85%.

The cell cartridges were cultured for 7 days under a nominal shear stress (< 0.5 dynes/cm^2) before ramping up the flow rate to reach the desired low and high shear stress treatment levels. The culture was maintained for 14 days including the treatment shear stresses (final 72 hr). Prior to conditioning, a 1 hr wash with serum-free Ham's F-12 media was then followed by conditioning with serum-free Ham's F-12 at the desired flow rate. The conditioned media was collected 24 hr later and centrifuged (Jouan CR412, Wincester, VA) at 1800 × g for 10 min at 4 °C to remove any cell debris. The treatment shear stresses were 5±2 and 23±8 dynes/cm^2. The pulsatile flows had similar frequencies for low and high shear treatments of ≈0.3 Hz and were essentially sinusoidal. The intraluminal average pressure gradients across the cartridges for low (5±2 dynes/cm) and high (23±8 dynes/cm^2) shear cultures were 9.6 and 26 mmHg, respectively.

The non-flow cultures involved seeding BAEC on polypropylene membranes placed in 12 well tissue culture plates at an identical seeding density as used in shear stress cultures. Cells were grown for 7 days including the 1 hr wash and 24 hr conditioning with serum-free media. As a comparison with the 7 day growth in static cultures, we cultured cells under low shear stress (5±2 dynes/cm^2) for 7 days, including the 1 hr wash and 24 hr conditioning. Except for the difference in growth time, the same protocol was followed for the 1 wk study as in the 2 wk

studies for low shear stress treatments. Following collection, all conditioned media was centrifuged to remove any cell debris, frozen at -80 °C, and thawed as needed. Total DNA was quantified using Hoechst fluorescent dye and a DyNA Quant 200 fluorometer (Amersham Pharmacia Biotech, Piscataway, NJ).

Radioimmunoassay

The media IGF-I detection was performed using a radioimmunoassay as described previously by Shimamoto *et al* [216] and Weber *et al* [217]. Briefly, recombinant human ^{125}IGF-I was iodinated as described previously [218] and used as a competitive standard against samples of IGF-I which, after immunoprecipitation and radioactive counting (Cobra™II Auto-Gamma®, Packard Instruments Company, CT), was related to IGF-I present in the perfused media. Immunoprecipitation was achieved using a primary mouse anti-human IGF-I monoclonal antibody, followed by incubation with an anti-mouse secondary antibody. Specific activity of IGF-I averaged 73 μCi/μg. For analysis, conditioned media samples were lyophilized and concentrated 20-30 fold. IGFBPs were separated from the IGF-I using a method described by Breier *et al*. [219]. Briefly, 100-200 μl of the concentrated solution was mixed with 900 μl of acid ethanol (87.5% ethanol and 12.5% 2 M HCl, v/v) and incubated at room temperature for 1 hour. The samples were then centrifuged (12,000 x g) for 10 minutes and the supernatant was mixed with 0.855 M Tris-base in a 2/5 ratio (v/v) and frozen for 1 hour at -20°C. Following centrifugation (1,500 x g) at 4°C for 20 minutes, the supernatant was retained for assay. Negative controls of plain Ham-F12 media were processed and assayed similarly.

RNA extraction and Northern Blotting

Following collection of the conditioned media, cultured cells were treated by perfusion of 0.1 ml/cm^2 TRI REAGENT per luminal surface area for 4 min. Total RNA was then extracted using chloroform and isopropanol for separation and precipitation, respectively. Fifteen to twenty μg of total RNA were loaded for each lane and electrophoresed on a 1% agarose-0.66 M formaldehyde gel and transferred to a nylon membrane by capillary transfer. Detection of IGF-I mRNA was performed by hybridization overnight at 42 °C with a 0.7-kb [^{32}P]UTP-labeled IGF-I cDNA [220]. Blots were then exposed to Kodak XAR-5 film at -80 ºC with intensifying screens. Blots were stripped and were reprobed with an 18S cDNA to adjust for loading differences.

Western Ligand Blotting

IGFBPs released into the conditioned media of EC cultures were quantified using a method described in Weber *et al* [221]. Using western ligand blotting [222], conditioned media samples were dissolved in SDS-PAGE buffer and electrophoretically separated in a 12.5 % gel at 16 V/cm. The proteins were then blotted onto a nitrocellulose membrane. Blots, which include liver and mammary standards, were incubated overnight with human recombinant [^{125}I]IGF-I with a MW of 7,646 and exposed to Kodak XAR-5 film at –80 °C for 5-7 days with intensifying screens. IGFBP relative amounts were determined using scanning densitometry (Gelworks 1D Image Analysis Software UVP®, Inc., CA)

VSMCs Proliferation: Thymidine Incorporation

Bovine vascular smooth muscle cells (VSMCs) (passage 4) proliferation was assayed using tritiated thymidine incorporation. Briefly, VSMCs were seeded on gelatin coated wells at 5.3×10^4 cells/cm^2 in 24 well-plates and cultured in complete MEM α-medium media (20% FBS) for 24 hours. After aspirating the media, the wells were washed with phosphate buffer saline (PBS) and the PBS was replaced with plain MEM α-medium media for 24 hr. Following a wash with PBS, plain MEM α-medium media with 40% by volume of shear and non-shear conditioned media with or without IGFBP-3 (2.8 μg/mL) was included. VSMCs were incubated for 24 hr with ^{3}H-thymidine (2 μCi/mL) added for the final 16 hr. The media was then removed and cells lysed with 0.3 N NaOH following washes with PBS supplemented with 0.1% BSA. Quantification was done using a Packard Liquid Scintillation Analyzer 2100 TR (Meriden, CT).

Statistics

Means were compared for significance using a Tukey test for comparisons of multiple means.

Results

Specific features of blood flow mechanics have been correlated with the occurrence of intimal hyperplasia, restenosis, and other vascular pathologies [2, 4-6, 223]. Since IGF-I is a potent proliferation and migratory factor for VSMCs, we wanted to determine if shear stress could affect its synthesis and release from BAEC. To address this question, we cultured BAEC within hollow fiber units under flow and collected conditioned media and quantified the IGF-I

present. Both shear and static culture samples contained IGF-I (Figure 1) and shear stress samples had significantly ($p<0.01$) higher levels of IGF-I compared to static culture. However, while there was no statistically significant difference between IGF-I levels between low shear (5 ± 2 dynes/cm^2) and high shear (23 ± 8 dynes/cm^2) samples, there was a tendency for reduced IGF-I levels with increased shear stress treatment observed in three independent experiments. Cells cultured under low shear for a period of only one week also showed an increase of IGF-I release compared to static controls.

To verify that the increased IGF-I from shear exposed BAEC was due to increased expression, we isolated RNA and used Northern blot analysis to examine message levels. IGF-I message was found in both shear treated and static culture samples (Figure 2). Relative mRNA IGF-I levels were ascertained using densitometry readings of autoradiography film bands and the results paralleled those found with protein expression. mRNA levels for shear treated BAEC were significantly greater than those from non-shear treated BAEC ($p<0.01$), while mRNA levels were not significantly different between low shear and high shear treated BAEC. However, a tendency for decreased levels with increased shear stress treatment was observed in two independent experiments, similar to what was observed for IGF-I protein levels.

Since IGFBPs play a significant role in regulating IGF-I activity [200], we sought to determine if the type or amount of IGFBPs released were altered by shear stress. Conditioned media from shear and non-shear treated cells were collected and analyzed using Western ligand blotting with iodinated IGF-I as a probe. Two bands appeared for the non-shear conditioned media indicating the presence of two IGFBPs with apparent molecular weights of approximately 29 kDa and 34 kDa respectively (Figure 3). In contrast, conditioned media from shear-treated (both low and high shear) BAEC exhibited three bands, two of which have the same position as in the non-shear treated samples, while the third band has an apparent MW of ≈ 44 kDa (Figure 3). This third band was also present in cells grown under low shear stress for one week (Figure 3). Densitometry readings of the bands normalized to total DNA indicated that shear stress led to up-regulation of the IGFBPs (Table 1). While there was an increase in both the 34 kDa and 44 kDa proteins and a decrease in the 29 kDa protein with increased shear suggesting some small effects, no significant difference was found.

Since differences were found between both the released IGF-I levels and the IGFBP profiles of shear and non-shear treated BAEC, we wanted to determine if these changes resulted in an altered functional response to the conditioned media. We focused on the impact of conditioned media on VSMC proliferation. Incorporation of tritiated thymidine in VSMC incubated with conditioned media (40% by volume) from samples obtained under shear (low and high) or non-shear conditions was determined and a significant increase in response ($p<0.05$) was found in all cases (Figure 4). Shear-treated samples led to an increase in ^{3}H-thymidine over non-shear samples. The assay however was based on conditioned media which likely contains other regulatory molecules besides IGF-I and IGFBPs. Unfortunately, no IGF-IR blocking antibody to the bovine receptor is available and so, to address specificity, we included exogenous recombinant IGFBP-3 capable of reducing proliferation of VSMC by recombinant IGF-I (Figure 4). While there was some inhibition, the reduction was not statistically significant suggesting that either non-IGF-I components secreted by BAEC affect VSMC proliferation or that the recombinant IGFBP-3 was not able to completely eliminate IGF-I-induced stimulation. Based on our RIA results, IGF-I concentration in treatment media were 0, 0.24±0.04, 5.68±0.73, and 4.68±0.23 ng/mL for control (unexposed plain media), no shear, low shear, and high shear conditioned media, respectively. These increased concentrations parallel the observed increased proliferation, where higher IGF-I concentrations resulting from higher shear stress treatments (Figure 1) correlate with increased VSMCs proliferation.

Discussion

Growth factors regulate vascular cells proliferation and migration [25, 153, 205] that can ultimately lead to atherosclerotic plaques [7, 147, 198], restenosis following vascular intervention [210] [148], and graft failure [77, 224]. While systemic factors are important, the spatial localization of diseased vascular tissue correlates with specific features of disturbed blood flow [2, 4-6, 223]. For example, sustained high shear stress areas within the vasculature are typically devoid of atherosclerotic plaques, while studies indicate low average shear stresses can be atherogenic [157]. Since IGF-I can stimulate both proliferation and migration of vascular cells [25, 153, 205], this study focused on the question of whether sustained shear stress affects the IGF-I axis via altered IGF-I or IGFBP secretion.

Using a biomechanical experimental model that allows for the culture of BAEC under chronic pulsatile shear stress, we collected conditioned media from cells cultured under low venous-level shear stress (5±2 dynes/cm^2) and high arterial-level shear stress (23±8 dynes/cm^2). The release of IGF-I in the conditioned media was then measured along with IGFBPs released and compared with those from no shear static cultures typical of the tissue culture environment. IGF-I release was significantly increased with shear stress treatment (Figure 1) compared to static cultures ($p<0.01$) and a parallel increase in mRNA for IGF-I from shear-treated samples compared to static culture was observed (Figure 2). Growth culture time did not alter this increase of IGF-I expression with shear since cells grown under low shear stress for only 1 week (same as for the static cultures) also had an increased IGF-I expression compared to static cultures (data not shown).

Further, a decrease in IGF-I released at the higher shear treatment (23±8 dynes/cm^2) when compared to samples from the low shear treatment (5±2 dynes/cm^2) was observed in three independent experiments (Figure 1) which was validated with mRNA analysis (Figure 2). The static culture model, however, has a significantly reduced IGF-I release compared to BAEC exposed to shear. Amongst shear treated BAEC, increased shear seems to decrease released IGF-I based on trends shown for IGF-I expression and IGF-I mRNA levels. Although the liver is the main source of IGF-I in the circulation, shear mediated changes in the magnitudes of the IGF-I released by endothelial cells may be physiologically relevant with respect to focalization of growth factor induced vascular pathologies. For example, coronary atherectomy specimens from ischemic patients exhibited increased expression of IGF-I and IGFBPs [153], and exogenous IGF-I led to the development of transplant arteriosclerosis in the rat aorta [225]. The atherogenic nature of the lower level shear stresses (comparable to those used in our *in vitro* study) could be linked to the increased local concentration of IGF-I, perhaps in synergy with other growth factors such as platelet derived growth factor (PDGF) [205, 226], which is also known to be regulated by shear stress in BAEC [109].

These results would also be consistent with previous studies where lower shear stresses up-regulate growth stimulators such as endothelin-1 [92, 93] and platelet derived growth factors [109, 227]. However those studies exposed endothelial cells to acute shear stress treatments for 24 hr or less. In contrast, our studies focused on the baseline response to chronic shear stresses for

prolonged period of time, thus avoiding potential artifacts resulting from possible cell injury response to sudden increases in shear stress, or from reduction of the effective magnitude of shear stress at the surface of the cells following changes in cell topology [81, 85, 228]. Hence our results support the idea that higher chronic shear stresses should favor a baseline vascular response that would decrease the release of mitogenic factors from the endothelium, leading to a more atheroprotective environment [8].

Increase of IGF-I release resulting from shear treatment is consistent with reports of vasorelaxation effects of IGF-I by its induction of NO secretion [229, 230]. Endothelial cells act locally to maintain a "setpoint" shear stress at the vascular wall [17]. When transient increases in shear occur endothelial cells release vasodilators [19, 55, 231, 232] that increase luminal diameter and thus reduce the effective wall shear stress (shear stress being inversely related to the cube of the vessel radius). With sustained increases in shear, wall remodeling is mediated via, in part, growth factor release [65, 92, 93, 99, 215] that alter vascular cell growth ultimately leading to a vascular physiology under the constraint of a "setpoint" shear stress. Endothelial cells actively and locally participate in this regulatory process by being the primary blood flow sensor and by using paracrine secretion of growth factors [95], and thus the increased vasodilatory IGF-I release in our study would fit that model. Conversely, excessive shear stresses may tend to decrease the vasodilatory signals from endothelial cells thereby decreasing wall shear stress to normal values which would be consistent with the decrease IGF-I release when going from low shear to high shear as our data suggests (Figure 1). The shear stress dependent switch between increased and decreased release of IGF-I by endothelial cells is possibly dependent on which vascular bed they originated, since baseline shear stresses vary with position within the vasculature.

The action of IGF-I is contextual in particular with respect to IGF-I-IGFBPs interaction. We thus sought to determine whether levels of these proteins were also affected by shear stress. Using Western ligand blotting, we found that, under static culture conditions, only two IGFBPs were detectable (Figure 3) with MW of 29 kDa and 34 kDa, consistent with either a glycosylated form of IGFBP-4 [233], IGFBP-5, or IGFBP-6 and IGFBP-2 [202], respectively. IGFBP-6 with a MW 30-25 kDa would not have been detected using iodinated IGF-I as a probe since it has a weak affinity for IGF-I, and previous analysis of the conditioned media of BAEC reported only limited IGFBP-6 mRNA and undetectable concentrations of IGFBP-6 in the media using

immunoprecipitation [234]. Thus the 29 kDa band that we detected suggests the presence of glycosylated IGFBP-4 and/or IGFBP-5, but can not exclude the presence of IGFBP-6. Using Western blot immunoaffinity, we confirmed the presence of IGFBP-2 and -4 and the absence of IGFBP-5 in the no shear conditioned media (data not shown). Therefore, the 29 and 34 kDA bands are likely IGFBP-4 and IGFBP-2 for the shear and the no shear samples since these two bands migrated at the same positions for all shear treatments (Figure 3). IGFBP-1 is known to be produced by BAEC as has been reported in numerous studies [146, 202, 234] hence its presence is unlikely. In addition to the two IGFBPs found in the conditioned media of static cultures, BAEC exposed to either low shear or high shear also released a 44 kDa IGFBP that is likely unglycosylated IGFBP-3 [146, 234], and that migrated similarly as IGFBP-3 controls (data not shown).

The lack of IGFBP-3 release in static cultures is in disagreement with previous reports [146, 147, 235] and may be the result of differences in the length of culture time between shear (14 days) and non-shear treated BAEC (7 days). Delafonataine *et al*. [146] have shown that proliferating BAEC did not synthesize IGFBP-3 in contrast with confluent BAEC (Figure 3). Under the assumption that the no shear BAEC were in a proliferative state, IGF-I expression would have been expected to be larger than that of shear treated confluent cells since IGF-I release from proliferative porcine aortic endothelial cells were found to increase almost two fold over confluent controls [236]. It was also reported by Gajdusek *et al.* [237] that a large increase in secreted IGF-I from subconfluent BAEC occurred compared to confluent BAEC, which does not concur with our results since shear treated BAEC cultured for 14 days had a larger IGF-I release (Figure 1).

Nevertheless, shear treatment may have acted to increase IGF-I release beyond that of subconfluent endothelial cells. It should be noted that no significant differences were found between the amount of DNA or cell number per surface area in either of the shear or non-shear treated BAEC, however, even at confluency, static BAEC grown for only 7 days could still be closer to a proliferative phenotype than the shear BAEC grown for 14 days. For example, IGFBP-3 mRNA message was only detected in cells incubated for 2 to 6 days *following* confluency with sustained and increased expression over this time-span. However, it should be noted that in low shear treated cells grown for a total of 1 wk (static cultures were also grown for

a total of 1 wk), IGFBP-3 was found in contrast with static cultures where no IGFBP-3 was detected (Figure 3). In summary, differences in growth culture time rather than shear stress treatment may have contributed to the lack of IGFBP-3 expression in static cultures, however, differences in growth culture time could not explain the observed changes in IGF-I release because 1) cells cultured under shear for the same amount of time had different amount of IGF-I release and, 2) lower growth culture time would have favored an increase in IGF-I release rather than a decrease as was observed in our experiment.

Shear stress significantly up-regulated all IGFBPs over static control however no significant differences were found between low and high shear treatments (Table 1) similar to what was found with IGF-I levels. Since IGFBPs regulate IGF-I via binding and complex formation [159], we compared how shear stress treatment affected the ratios of IGFBPs to IGF-I released in the conditioned media. Shear stress had no significant effect in altering IGFBP-4 to IGF-I ratios compared to static cultures (Table 2). However, considering the possibility that both IGFBP-4 and -5 are present as the detected 29 kDa band, their relative amounts would be unknown and thus does not allow for a definite interpretation of this result. IGFBP-2 to IGF-I ratio was decreased compared to that of static cultures with no significant differences between shear stress treatments. This shear stress effect indicates a phenotypic difference between shear and non-shear treated BAEC, and thus stresses the relevance of shear in analyzing IGFBPs-IGF-I expression profiles in vascular cells. Further, IGFBP-2 was found to mediate IGF-I dependent migration and proliferation in bovine vascular smooth muscle cells (VSMC) [158], and thus may have implication in the progression of human restenotic lesions that exhibit significant IGFBP-2 mRNA [153].

In contrast, while no IGFBP-3 was detected under static conditions, high shear stress increased almost 5 fold the relative amounts of IGFBP-3 to IGF-I released compared to low shear stress. As has been proposed by Hodgson [238], under equilibrium conditions, IGF-I mitogenic effects are decreased upon binding to IGFBPs including IGFBP-3. Further, it was shown that IGFBP-3 reduces IGF-I dissociation rates under saturating binding of the IGF-I receptors. An increased rate of dissociation was found to decrease IGF-I mediated mitogenesis in human breast cancer cell lines. Hence, IGFBP-3, by binding excess IGF-I, would increase the residence time at the cell surface receptor and thus promote IGF-I-IGF-IR signaling and

mitogenic effect. Based on this data, it can be inferred that the observed increase in IGFBP-3 release relative to IGF-I at high shear stress (Table 2) acts to potentiate IGF-I activity. Under non saturating conditions, when only a fraction of IGF-IR are occupied, IGFBP-3 would decrease IGF-I activity by sequestering IGF-I from its site of action at the cell surface receptor. This IGFBP-3 induced inhibition was observed in studies by Delafontaine *et al.* [146] in which post-confluent BAEC demonstrated onset of IGFBP-3 release that maintained BAEC in a growth arrested state. Since our data indicates that high shear stress correlates with a relative increase of IGFBP-3:IGF-I compared to low shear stress, it suggests that higher shear stresses favor a more quiescent phenotype of the cells under paracrine and autocrine control, and would thus favor a more atheroprotective environment.

The physiological implications of these changes in IGF-I to IGFBPs are not clear, however the impact of IGFBP-3 increased release at higher shear stresses is more significant since over 90% of the IGF-I in the circulation is carried by IGFBP-3 [200]. It is probable that an increase in released IGF-I leads to an up-regulation of IGFBPs as has been show previously for IGFBP-3 and -4 [239-242] in various systems. This feedback regulation may thus be important with regard to IGF-I availability by sequestering IGF-I from its receptors on BAEC surface and reducing its transport across the vascular bed [201]. Hence up-regulation of the released IGFBPs may depend more on IGF-I feedback up-regulation of IGFBPs than shear stress itself. Further, IGFBP-3, by sequestering, IGF-I, reduces IGF-I binding and the IGF-I dependent down regulation of cell surface receptor IGF-I receptor (IGF-IR) thus sustaining cell sensitivity to IGF-I stimulation in fibroblast cells [243]. In contrast, chronic IGF-I secretion has also been reported to limit IGF-I action in mammary epithelial cells by desensitizing cells to IGF-I-IGF-IR signaling, a process that was inhibited by IGFBP-3 sequestration of IGF-I [244]. In support of this inhibitory effect on IGF-I is a study by Delafonataine *et al.*[146] where incubation with IGFBP-3 antibody increased DNA synthesis in BAEC. Hence, the physiological relevance of IGFBP up-regulation that relates to increased IGF-I release by shear treatment is to be interpreted in the context of endothelial cells paracrine and autocrine action, and modulated by IGFBPs in a cell specific manner.

Another shear stress dependent factors that could have caused variations in IGFBP profiles is transforming growth factor-β1. TGF-β1, a potent inhibitor of VSMC growth, has

been known to increase in endothelial cells with increasing shear stress [110], and can cause changes in IGFBPs metabolism in BAEC as described by Dahlfors *et al.* [245]. In this latter study, TGF-β1 inhibited IGFBP-3 and -4 mRNA expression and IGFBP-3 release under static conditions, therefore the increased IGFBP-3 observed in our study would have occurred in spite of a possible increase in TGF-β1 concentration and thus inhibition of IGFBP-3 release. IGFBP-4 and -5 release were not affected by TGF-β1 in that study, thus a possible role of TGF-β1 in the observed increase in expression of the 29 kDa band representing either glycosylated IGFBP-4 or IGFBP-5 is excluded. Finally, IGFBP-2 was at the detection limit of their assay and thus no conclusions were drawn on the effects of TGF-β1 on IGFBP-2 release. Considering the data presented above it is unlikely that TGF-β1 could have completely negated the effects seen in our experiments, since TGF-β1 either has no effect or inhibits IGFBPs release, which does not agree with our own finding of systematic increase over static controls.

Having shown that IGF-I and IGFBPs metabolism were affected by shear stress, we sought to determine if shear and non-shear treated conditioned media from BAEC would alter VSMCs proliferation. VSMCs proliferation in the presence or absence of exogenous IGFBP-3 conditioned media was indeed increased compared to control (unexposed plain media) but no significant differences were observed amongst all conditioned media (Figure 4). There is a trend however showing an increase proliferation from shear treated conditioned media compared to static culture conditioned media. Unknown factors within the conditioned media may have contributed to this response, however these results are consistent with our finding that higher shear stresses increase IGF-I release. Since IGFBP-3 generally inhibits IGF-I mediated proliferation [246-249], we wanted to know if SMC proliferation could be reduced by adding IGFBP-3 to the treatment media of VSMCs. Exogenous IGFBP-3 systematically reduced proliferation within each shear treatment group (Figure 4) in two independent experiments, thus further reinforcing the possible role of IGF-I in the observed increases in VSMCs proliferation. The relative lack of responsiveness of VSMCs to the conditioned media from shear and non-shear treated cells, which was not expected since significant changes in IGF-I/IGFBPs profiles were observed, may stem from the relatively low IGF-I concentrations available in treatment BAEC conditioned media that may not be sufficient to elicit a significant growth response from VSMCs. Further, reported increase in TGF-β1 release with shear stress [110] could have inhibited

any IGF-I mediated stimulation of VSMCs since TGF-β1is a SMC growth inhibitor. While shear variations where not discernible, the significant increase over control is consistent with the presence of IGF-I in the BAEC conditioned media. However, additional research is required to clarify a possible link between varying shear stress levels and IGFBP-3:IGF-I profiles that could point to a mechanism by which shear stress may be atheroprotective or atherogenic with regard to proliferative vascular diseases.

In summary, we have shown 1) that while shear stresses increased IGF-I release over static cultures, a higher shear stress of 23±8 dynes/cm^2 seem to reduce IGF-I release compared to a low shear stress of 5±2 dynes/cm^2, 2) that this increase is likely related to an increase in IGF-I mRNA that also shows higher IGF-I mRNA levels at high shear stress compared to low shear stress, 3) that under no shear BAEC released only two IGFBPs likely a glycosylated form of IGFBP-4 or -5 and -2 (with MW of 29 kDA and 34 kDa, respectively) and that the lack of IGFBP-3 released in static cultures may be the results of shorter growth time, 4) that an additional IGFBP appears only from shear treated BAEC with a MW of 44 kDa likely IGFBP-3, 5) that there is an increase in IGFBPs released compared to static cultures, 6) that the IGF-I to IGFBPs relative amounts are significantly different for shear treated BAEC compared to static cultures and, specifically, IGFBP-2 is decreased while IGFBP-3 is increased with shear stress compared to IGF-I released but no significant change was observed for IGFBP-4, 7) that IGF-I increase with shear stress is consistent with results from VSMCs proliferation studies showing an increase in proliferation with shear treated conditioned media. These findings may have implications in how shear stress can exacerbate common pitfalls of vascular intervention and atherosclerosis, since most result from an exaggerated response to injury modulated by growth factors such as IGF-I.

Tables

Table 1. Levels of IGFBPs in conditioned media from shear and non-shear treated BAEC were determined using Western ligand blotting and scanning densitometry. Results were normalized to total DNA and referenced to either no shear (29 and 34 kDa bands) or low shear (44 kDa band) for comparison. Based on MW and Western immunoaffinity blotting of no shear conditioned media 29, 34, and 44 kDA IGFBP are likely IGFBP-4, -2, and 3, respectively. Values are means obtained from two 12-well plates and two shear cartridges for each shear treatment. Error bars represent one standard deviation (n=2). Data is representative of three independent experiments.

IGFBP, MW (kDa)	29	34	44
No shear	1.00±0.39	1.00±0.05	ND[¶]
Low shear	57.2±10.5*	13.3±5.6*	1.00±0.14
High shear	33.9±2.1*	21.4±9.9*	3.75±1.16

*$p<0.05$, low and high shear vs no shear
[¶]Not detected

Table 2. Ratios of IGFBPs to IGF-I released in the conditioned media of shear and non-shear treated BAEC. Autoradiography films from Western ligand blots were analyzed using a scanning densitometer and scaled to the volume of conditioned media. The scanning results were divided by the total IGF-I released to obtain a measure of the total IGFBP to total IGF-I released. The results were referenced to either no shear (29 and 34 kDa bands) or low shear (44 kDa band) for comparison. Based on MW and Western immunoaffinity blotting of no shear conditioned media 29, 34, and 44 kDA IGFBP are likely IGFBP-4, -2, and 3, respectively. Values are means obtained from two 12-well plates and two shear cartridges for each shear treatment. Error bars represent one standard deviation (n=2). Data is representative of three independent experiments.

IGFBP, MW (kDa)	29	34	44
No shear	1.00±0.43	1.00±0.17	ND[¶]
Low shear	0.98±0.22	0.23±0.10*	1.00±0.19
High shear	0.71±0.06	0.44±0.21*	4.55±1.42[§]

*$p<0.05$, low and high shear vs no shear
[§]$p<0.05$, high shear vs low shear
[¶]Not detected

Figures

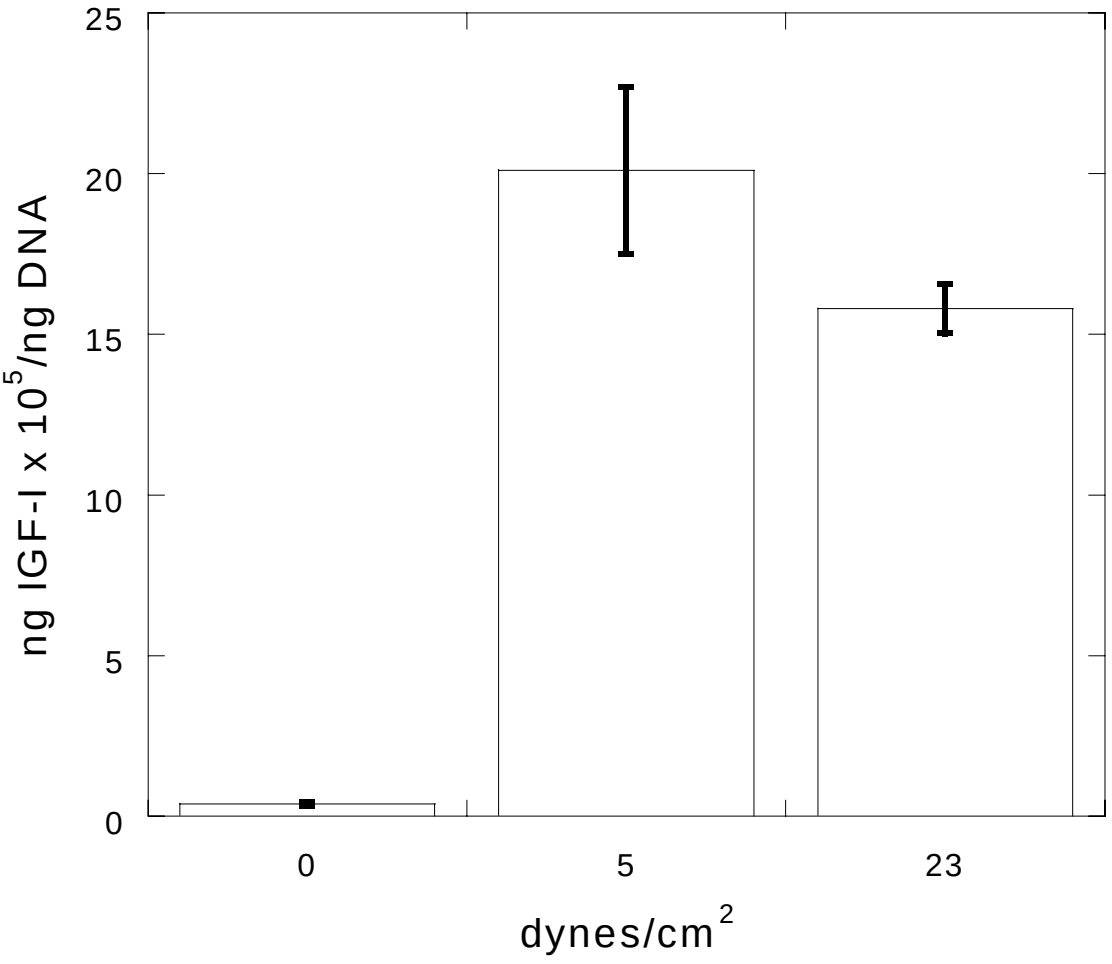

Figure 1. RIA of conditioned media from shear and non-shear treated BAEC. Cells were cultured in plain Ham's F12 for 24 hr and media collected for estimation by RIA. Values are means obtained from two 12-well plates and two shear cartridges for each shear treatment and were normalized to total DNA. Error bars represent one standard deviation (n=3). Data is representative of three independent experiments.

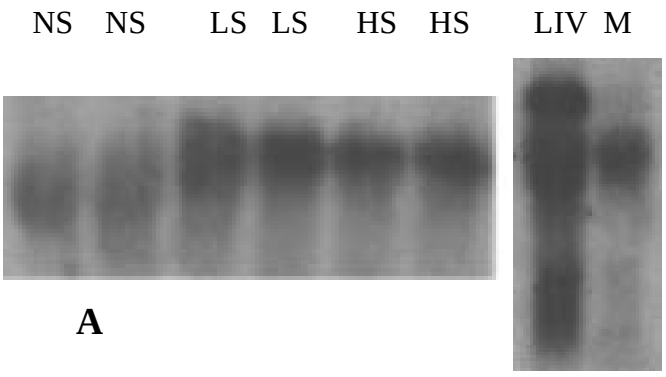

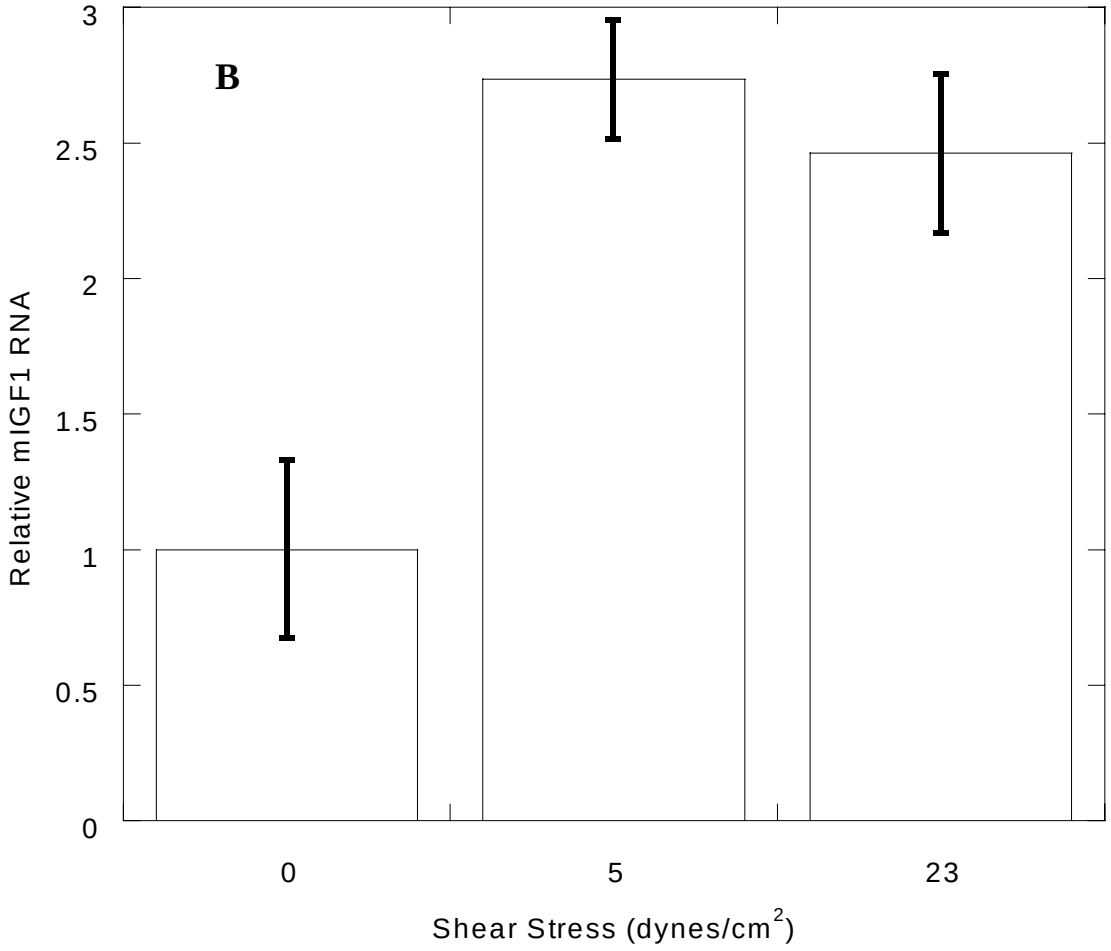

Figure 2. IGF-I Northern blot (A) and densitometry results (B) from shear and non-shear treated BAEC. Cells were cultured in plain Ham's F12 for 24 hr and total RNA was extracted using a Tri Reagent and chloroform/isopropanol for separation and precipitation. Values are means obtained from two 12-well plates and two shear cartridges for each shear treatment (NS= no shear, LS= low shear, HS= high shear, LIV= liver samples, M= mammary epithelial cells

samples). Error bars represent one standard deviation (n=2). Data is representative of two independent experiments.

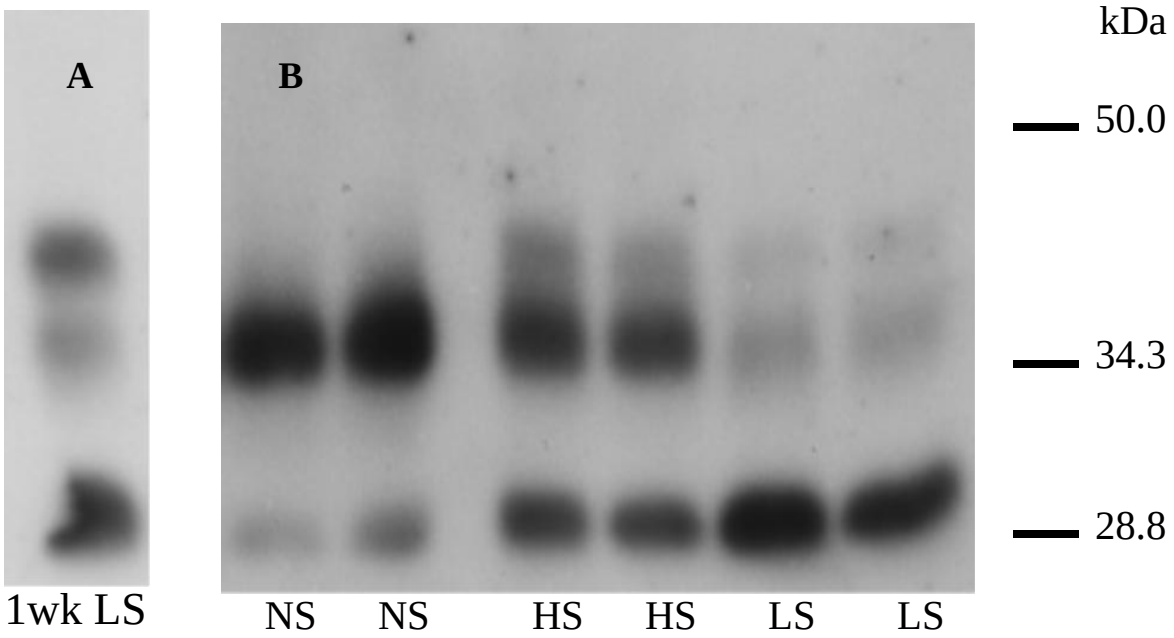

Figure 3. Western Ligand blot of IGF binding proteins secreted into the conditioned media of shear and non-shear treated BAEC. Cells were grown for a total of 1 (A) or 2 wk (B), conditioned for 24 hr in plain Ham's F12 media, and the media collected for ligand blot analysis. Proteins were separated by SDS-PAGE and transferred to nitrocellulose membranes. Blot were probed with iodinated IGF-I ([^{125}I]I-IGF-I) and each lane represents sample from one cartridge for each shear treatment (NS= no shear, LS= low shear, HS= high shear, 1 wk LS= 1 week growth under low shear). Standard molecular weights migrated as indicated (kDa). See Table 1 for densitometry results. Figure is representative of three independent experiments.

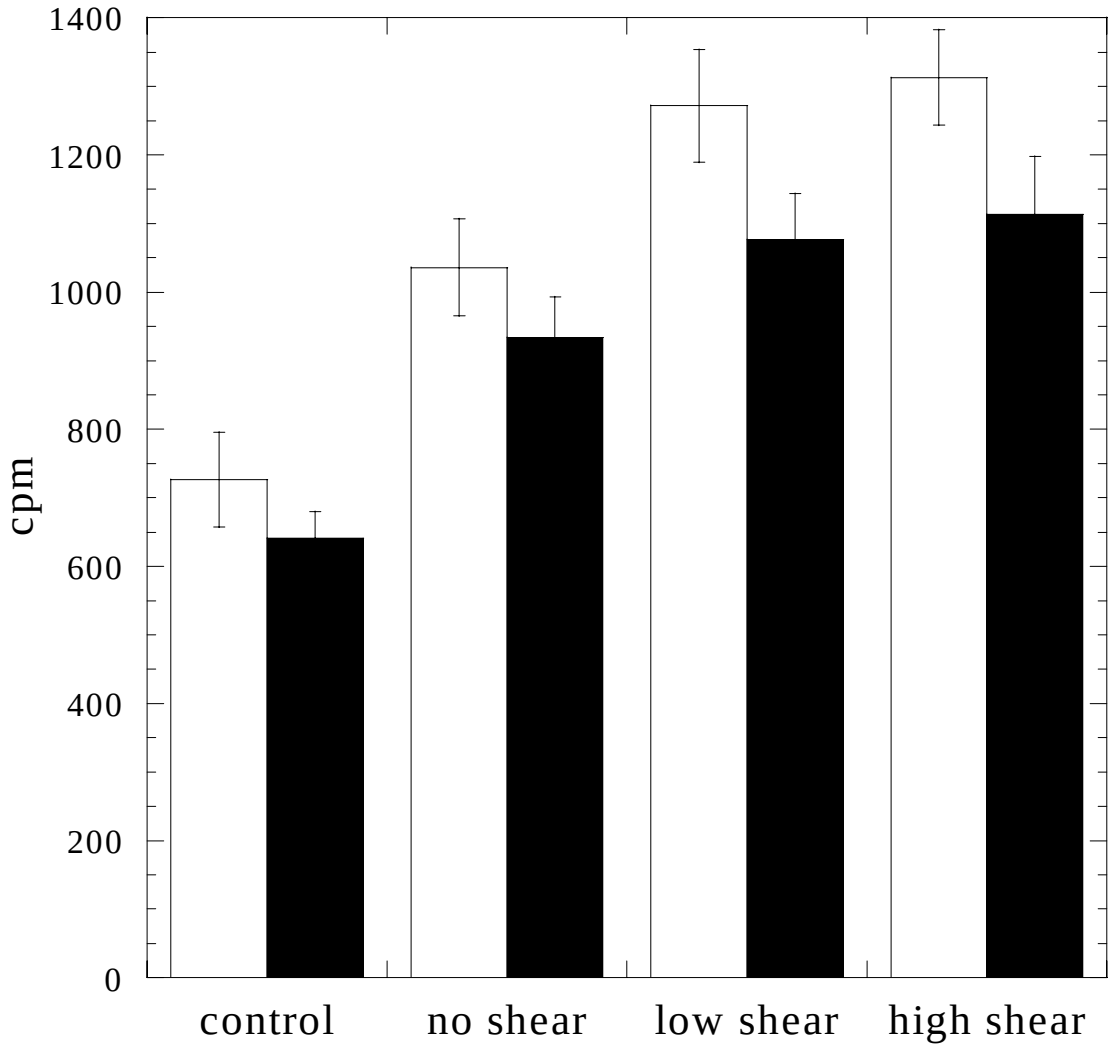

Figure 4. Effect of shear and non-shear treated conditioned media from BAEC on VSMC proliferation. Conditioned media (40% v/v) was added to MEM α-medium with (■) or without (□) IGFBP-3 (2.8 μg/mL). VSMCs were incubated for 24 hr and ^{3}H-thymidine (2 μCi/mL) added for the final 16 hr. Error bars represent one standard error from three wells. Data are representative of two independent experiments.

Chapter VI: Conclusions and Future Work

Mechanical forces on vascular cells generate a host of physiological and metabolic effects that can either promote or inhibit vascular disorders. For example, in atherosclerotic plaque development, wall thickening, vessel occlusion, fatty streaks, and thrombus formation tend to occur in locations within the vasculature where low average shear stresses, oscillatory flow, and disturbed blood flow occur [3, 22]. Experimental studies seeking to elucidate the mechanisms underlying blood flow mechanics relationship to vascular physiology must therefore duplicate the *in vivo* blood flow features and hemodynamic forces, and then relate them to changes in vascular cell metabolism. Compared to the *in vivo* environment, only the simpler hemodynamic features of blood flow are currently duplicated *in vitro* using various experimental models such as the parallel flow chamber and the plate-and-cone model [179]. These models include shear stress as a determinant factor in cellular response to blood flow. However, additional features can also include pulsatile flow, hydrostatic pressure, strain, or a combination of these factors. The standard static cell culture model is often used as a reference but is not the ideal physiological model since, under most conditions, some level of blood flow is maintained throughout the vasculature.

The Cellmax® cell culture system is a relatively new biomechanical model that was used in this research to study chronic shear stress effects on endothelial cells. This model can achieve the sustained growth of cells while providing controlled levels of shear stress of cells seeded on the luminal side of capillaries. Four cartridges with multiple capillaries per cartridge can be run simultaneously with different flow rates in each cartridge depending on the pump configuration. The cylindrical geometry of the capillaries duplicates the arrangement normally found in the vasculature *in vivo*. Thus, using this model, we investigated the effects of chronic shear stress treatment on endothelial cells. Endothelial cells are a natural choice in the study of shear stress effects since they interface directly with blood flow at the arterial wall lumen *in vivo*. As the primary blood flow sensors, endothelial cells transduce mechanical forces into cellular signals that can eventually lead to paracrine and autocrine signaling and regulated cellular growth.

Alterations of the metabolic product of these cells by chronic shear stress treatment are thus the main focus of this dissertation. The chronic aspect of the shear stress treatment was important to emphasize cell response to long term shear stress treatment, which avoids any

artifactual result that may occur with acute shear stress treatments. For example, a large step increase in shear stress can mechanically injure endothelial cells and so response to injury rather than response to shear stress itself will result. Further, after onset of flow, cells tend to profile and elongate in the direction of the main flow direction, which results in a reduction of the effective shear stress at the microscopic level on the cell surface [81]. Therefore, any alteration in cell response during the time frame of an acute shear stress treatment can reflect a reduction in the conditioning signal rather than a normal metabolic adjustment to a sustained mechanical signal. In our model, shear stress was increased in multiple incremental steps over a total of 14 days of cell culture and shear stress treatment so as to minimize the step size. Therefore our model allows cells time to acclimate to their hemodynamic environment so that baseline cell response to shear could be achieved.

Two main physiological shear stress levels were selected to treat endothelial cells: a low shear stress of 5±2 dynes/cm^2 and a high shear stress of 23±8 dynes/cm^2. Static cell culture plates were used as reference. Since flow dynamics would determine the shear environment, the first step in this study was to define and characterize the type of flow in the Cellmax® system. The main issues to consider were whether the flow was laminar, what the magnitude, frequency, and amplitude of shear stress were, and whether any capillary strains could be occurring under the pressure driven flow in the Cellmax®. The positive displacement pumps used in the Cellmax® system are inherently pulsatile and, while the average flow rates could be specified, the frequency and amplitude could not be set independently. We thus measured the pressure drop across the capillaries to determine the extent of pulsatility in the flow. The pressure drop could then be linked to the instantaneous flow rate and, therefore, to the wall shear stress with the solution to the Navier-Stokes equations. Pressure was monitored during cell culture using a custom build data acquisition system and a pressure transducer. The digitized pressure waveforms were represented analytically using a Fourier series (Chapt. II) and the flow was modeled with the Womersley solution of the Navier-Stokes equations. Wall shear stress and volumetric flow rates were then calculated from these model equations.

The power spectrum of the data revealed that the pressure waveforms at the varying levels of shear stress treatments used were primarily pure sine waves at a frequency of approximately 0.3 Hz. This frequency reflects the pump characteristics in the Cellmax® and

could not be specified, thus pointing to a limitation of this particular experimental model. Future experimental models should include the ability to select more physiological frequency, amplitude, and pressure waveforms similar to those measured in arterial segments *in vivo* such as the aorta. Further, the dynamic range of flow rates achievable where limited by the pump configuration so that very low shear stresses (<4 dynes/cm^2) could not be attained simultaneously with high shear stress (>20 dynes/cm^2). Another parameter of physiological interest was the phase angle difference between the pressure and the flow waveforms. The phase angle was obtained from the measured pressure and the calculated flow and was determined to be negligible. Thus, while a spectrum of physiological phase angle difference are known to occur *in vivo* (including a negligible phase angle)[156], our model, given the magnitude of the Womersley number (a dimensionless number that characterizes pulsatility), would not produce any significant phase angle difference for either low or high shear experiments. It is important to note that one requirement of the model equation used to determine shear stress levels and flow rates is that the flow must be laminar. We verified that laminar flow was present from the measured pressure drop, which was in good agreement with the expected pressure drop based on a laminar flow model. The model equations could also accurately predict the measured average flow rates (Chapt. II).

Once the flow in our experimental was fully characterized, we investigated the possibility that the polypropylene (a flexible plastic) capillaries in the Cellmax® could deform when subjected to the pulse pressure during our low and high shear experiments. This has important implications since endothelial cells are known to respond to strain, which is ubiquitously present *in vivo* [91, 156]. Using our data acquisition system we added a custom built laser occlusion technique that allowed for the dynamic determination of the radial strain of the capillaries. Capillary deformation was negligible under experimental transluminal pressure gradients mainly due to the high elastic modulus of polypropylene and the relatively thick capillary walls (Chapt. III). The Pharmed® (an elastomer or rubber) vessel tube tested for validation of our apparatus demonstrated measurable strain levels even for relatively low pressure loading. The strains at the various luminal pressure measured were used to calculate the Pharmed® elastic modulus, which was in good agreement with that provided by the manufacturer (Norton Performance Plastic Co.) thus validating the performance of the laser occlusion apparatus. More importantly, we were

able to reject the possibility of any strain effects on endothelial cells during shear stress treatment. However, the inclusion of strain in the biomechanical model could possibly work to enhance or antagonize the vascular cell response to shear stress and would improve the biomechanical model "realism". An alternative membrane system, which might allow for strain could be considered for future studies.

The mechanics of our experimental model having been defined, we carried out experiments to determine the functional relationship between chronic shear stress treatment of bovine aortic endothelial cells and the release of particular bioregulatory molecules, specifically proteoglycans/glycosaminoglycans and IGF-I/IGFBPs. Both proteoglycans and growth factors are known modulators of endothelial cells function particularly as they relate to hemostasis [136] and vascular proliferative disorders [11, 25], respectively. While the link between proteoglycans and hemostasis *in vivo* remains speculative at this point, our findings demonstrate that shear stress can be a significant regulator of proteoglycans metabolism. Previous studies by Arisaka *et al.* (1995) and Grimm *et al.* (1988) did find an effect of shear stress on endothelial cell proteoglycans synthesis. The specific results of those two studies were contradictory likely due, at least in part, to differences in the experimental models used. For example, whereas Grimm *et al.* found a decrease in proteoglycans released with increased shear stress, Arisaka *et al.* found an increase. The latter authors suggested that longer shear treatment time in their experiments might have caused the discrepancy.

Regardless, these experiments were carried out under acute conditions where cells were not cultured under shear stress prior to shear treatment, in contrast with our own studies where the cells were cultured under shear prior to conditioning. We did, however, find that increased chronic shear stress led to an increase in the proteoglycans released thus agreeing with the work by Arisaka *et al.* with their longer acute studies (Chapt. IV, Table 1). Further, for the first time, we report that there is an inverse relationship between the level of shear stress used to obtain the purified proteoglycans from shear treated endothelial cells and their potency in inhibiting thrombin induced human platelet aggregation (Chapt. IV, Figure 4) and tissue factor induced human blood coagulation (Chapt. IV, Figure 5). Therefore this differential effect suggests that lower shear treatment can lead to an endothelial cell proteoglycans secretion profile that reduces blood clot formation potency in the vasculature. The implications *in vivo* are uncertain since

higher level of proteoglycans were secreted at higher shear stresses even though these purified high shear proteoglycans were less potent in inhibiting coagulation.

To determine if the increased amount of proteoglycans secreted with increasing shear stress treatment could compensate for a corresponding decrease in their specific potency, we normalized the aggregation and blood coagulation inhibition curves based on the amounts of proteoglycans secreted on a per cell basis (Chapt. IV, Figure 6A and 6B). These normalized curves would thus provide an indication of the overall inhibitory potency which would take into account not only the specific potency of these proteoglycans but also how much was secreted by the BAEC under a given shear stress treatment. Interestingly, dose response curves for low and high shear proteoglycans inhibition of blood clot formation and platelet aggregation collapsed when the doses were normalized. The no shear treatment curves did not however collapse, with the overall potency in blood clot inhibition decreasing compared to low and high shear treatments. Thus, while the specific potencies of the proteoglycans varied depending on shear treatment, the overall inhibitory activity was not altered between low and high shear stress in contrast with no shear proteoglycans where a decrease in the overall potency occurred.

It is uncertain if the secreted proteoglycans can remain in the blood long enough so that shear stress regulated proteoglycans secretion can have a differential or shear specific effect on hemostasis locally. Alternatively, changes in shear mediated release of proteoglycans can reflect increase turnover of the cell surface or matrix proteoglycans as shear stress treatment is increased. Cell surface proteoglycans contribute to the antithrombic endothelial cells surface lining, therefore, future studies should include a measurement of the cell surface and matrix proteoglycans at varying shear stress levels. Results would help shed some light into whether the increased media concentration observed in our studies are a reflection of increased *de novo* proteoglycans synthesis and release or increased shedding from endothelial cell surface and/or extracellular cellular matrix.

Regardless, chronic shear stress does impact proteoglycans release and distribution based on size exclusion (SEC) and ion exchange chromatography separation (Chapt. IV, Figure 1-3). The most significant results being that a unique proteoglycans fraction was found amongst the low shear proteoglycans that did not occur in either high or no shear proteoglycans and that, with two primary proteoglycans identified from SEC separation, the relative amounts of the high MW

fraction decreased continuously with shear stress. Further analysis of these proteoglycans fractions should be undertaken in the future in light of the aforementioned blood coagulation and platelet aggregation studies. Also, while enzyme digestion of the pooled proteoglycans did not reveal any significant differences in their chondroitin/dermatan sulfate and heparan sulfate content (Chapt. IV, Table 2), the analysis of the *isolated* fractions could indicate differences in glycosaminoglycan, sulfate, and/or carboxyl group content. These highly anionic groups are likely at the origin of the separation profiles observed in ion exchange separation, especially since the glycosaminoglycans chains were found to be of similar size (Chapt. IV, Figure II). Analyses of the disaccharide products formed from the specific enzyme digestions, nitrous acid, and alkaline borohydride treatment of the glycosaminoglycans, should prove valuable in determining chain composition, including the extent of sulfation and carboxyl content.

Proteoglycans structural differences may prove to be key in determining their function. For example, the high MW proteoglycans fractions were significantly more potent inhibitors of FGF-2 stimulated smooth muscle cells (SMC) growth in studies by Forsten *et al.* (1997) compared to the low MW fractions. Interestingly, the relative amounts of this high MW fraction increased with decreasing shear stress (Chapt. IV, Figure 1). This observation suggests that higher shear stress treatment in our experimental model would seem to lead to a more pathogenic endothelial cells phenotype, presumably, since fewer of these proteoglycans would be available to inhibit vascular proliferative type disorders resulting from paracrine growth factor stimulation. This interpretation would be contrary to the current view indicating that low shear stresses are atherogenic and hence that the higher shear stress model used in our studies results in a more pathogenic phenotype of the endothelial cells. The pulsatile nature of our flow that is more pronounced in the high shear stress experiments with larger pressure wave amplitudes, could explain this apparent inconsistency. Indeed, disturbed blood flow conditions such as large spatial and temporal shear stress gradients are thought to be important in the focal localization of atherosclerotic plaques. An approach to resolve this issue would thus be to add a non-pulsatile flow system to possibly differentiate between pulsatile and non-pulsatile effects *in vitro*. The addition of a damping chamber to remove the oscillatory component of the pressure/flow waveform at the inlet of the capillaries can readily achieve this goal and should be considered in future experiments.

In contrast, the results from the IGF-I studies suggested that higher shear stress would lead to a more atheroprotective phenotype of the endothelial cells. From our data, the secretion of IGF-I indicated that a higher shear stress reduced the amount of media IGF-I compared to low shear stress treatment (Chapt. V, Figure 1). IGF-I mRNA was similarly down regulated by increased shear stress (Chapt. V, Figure 2). IGF-I being a stimulator of SMC proliferation and migration, this decrease suggests that higher shear stresses could reduce paracrine stimulation of SMC by IGF-I, thus reducing the likelihood of vascular proliferative disorders *in vivo*. The IGFBP release profiles indicated that shear stress has a significant impact on IGFBP metabolism (Chapt. V, Table 1-2). In static culture even more dramatic differences were observed in the amount of IGF-I and IGFBP released, suggesting that the typical static culture model for the study of vascular cells may not be physiologically relevant, especially in studies of paracrine and autocrine stimulation. The effect of IGFBP on cell stimulation is highly contextual. IGFBP can inhibit or accentuate the mitogenic activities of IGF-I depending upon the experimental model used [238]. Therefore interpreting the results from IGFBP release profiles can be meaningful only in a specific context that would indicate, for example, the state of saturation of the IGF-I receptors at the endothelial cells surface.

With the realization from our own data that proteoglycans and IGF-I metabolism are influenced by shear stress, the question of whether proteoglycans and growth factors can interact to either promote or inhibit vascular growth is intriguing. While it is unlikely that IGF-I can interact with proteoglycans since it is not a heparin-binding growth factor, other growth factors such as VEGF, FGF-2, and FGF-1 known to bind to heparin could be of interest. The implication on vascular proliferative disorders is obvious and its study is suggested by data from this laboratory (Forsten *et al.* (1997)) since media released endothelial cell proteoglycans are known to inhibit FGF-2 mediated smooth muscle cell growth. SMC are normally found in the medial regions of the vascular wall not in contact with blood flow, therefore a static cell culture model would be appropriate (even though strain effects would be neglected) to study the effects of endothelial cells shear conditioned media. The addition of specific growth factor antibodies could isolate any given growth factor effect observed from that of other components of the raw endothelial cells conditioned media. Also, since we have established that the proteoglycans and glycosaminoglycan composition was predominantly heparan sulfate and, to a lesser extent,

chondroitin/dermatan sulfate, the use of exogenous specific enzymes would likely inactivate their ability to interact with these growth factors as has been shown for FGF-2. Binding studies with labeled growth factors could establish the role of the glycosaminoglycan chains in growth factor-proteoglycans interactions. Hence, enzymatic treatment of the secreted proteoglycans would determine their contribution in growth factor mediated cell proliferation.

This part of a future research could also be contrasted with the effects of exogenous heparin, which is a commonly prescribed glycosaminoglycan anticoagulant post intervention. Heparin-growth factor interaction could thus be analyzed in light of the numerous failures resulting from restenosis at sites of vascular surgical intervention. The hypothesis would be that heparin treatment might, in addition to its anticoagulant properties, help reduce SMC proliferation. Similarly, ion exchange and SEC shear proteoglycans fractions described in this dissertation (Chapt. IV) could also be isolated and studied separately in their effect on blood coagulation and SMC growth regulation. Assays already described in this thesis could be utilized to quantitate these effects. Specifically, aggregometry and thromboelastography are valuable to study coagulation effects and thymidine or cell number counting can be used to determine the stimulating or inhibiting effects of the proteoglycans fractions.

Another aspect to consider would likely be the transport of growth factors to the cell surface by convection/diffusion and across the endothelial cells by transcytosis, so that paracrine dynamics on the underlying SMC can be studied. The current Cellmax® configuration does allow for coculturing of smooth muscle on the extra capillary space and endothelial cells on the luminal side, thus the growth factor transport dynamics can be validated with a measure of SMC growth in coculture. Ultimately, the results could shed some light on the role of various growth factors and proteoglycans in vascular proliferative disorders that often occur as chronic pathologies or following acute disturbance post vascular intervention.

References

1. Frangos SG, Gahtan V, Sumpio B. Localization of atherosclerosis: role of hemodynamics. Arch Surg 1999; 134:1142-9.
2. Greenwald SE, Berry CL. Improving vascular grafts: the importance of mechanical and hemodynamic properties. J Pathol 2000; 190:292-9.
3. Asakura T, Karino T. Flow patterns and spatial distribution of atherosclerotic lesions in human coronary arteries. Circ Res 1990; 66:1045-66.
4. Chiu JJ, Wang DL, Chien S, Skalak R, Usami S. Effects of disturbed flow on endothelial cells. J Biomech Eng 1998; 120:2-8.
5. Nagel T, Resnick N, Dewey CF, Jr., Gimbrone MA, Jr. Vascular endothelial cells respond to spatial gradients in fluid shear stress by enhanced activation of transcription factors. Arterioscler Thromb Vasc Biol 1999; 19:1825-34.
6. Phelps JE, DePaola N. Spatial variations in endothelial barrier function in disturbed flows in vitro. Am J Physiol Heart Circ Physiol 2000; 278:H469-76.
7. Schwartz CJ, Valente AJ, Sprague EA, Kelley JL, Nerem RM. The pathogenesis of atherosclerosis: an overview. Clin Cardiol 1991; 14:I1-16.
8. Traub O, Berk BC. Laminar shear stress: mechanisms by which endothelial cells transduce an atheroprotective force. Arterioscler Thromb Vasc Biol 1998; 18:677-85.
9. Rudic RD, Shesely EG, Maeda N, Smithies O, Segal SS, Sessa WC. Direct evidence for the importance of endothelium-derived nitric oxide in vascular remodeling. J Clin Invest 1998; 101:731-6.
10. Ross R. Smooth muscle cells and atherosclerosis. In: Moore S, ed. Vascular Injury and Athrosclerosis. Vol. 9. New York: Marcel Dekker, Inc., 1981:53-73.
11. Ross R. Cell biology of atherosclerosis. Annu Rev Physiol 1995; 57:791-804.
12. Nollert MU, Diamond SL, McIntire LV. Hydrodynamic shear stress and mass transport modulation of endothelial cell metabolism. Biotechnology and Bioengineering 1991; 38:588-602.
13. DeBakey ME, Lawrie GM. Combined coronary artery and peripheral vascular disease: recognition and treatment. J Vasc Surg 1984; 1:605-7.
14. Balaram SK, Agrawal DK, Allen RT, Kuszynski CA, Edwards JD. Cell adhesion molecules and insulin-like growth factor-1 in vascular disease. J Vasc Surg 1997; 25:866-76.
15. Bobik A, Agrotis A, Kanellakis P, et al. Distinct patterns of transforming growth factor-beta isoform and receptor expression in human atherosclerotic lesions. Colocalization implicates TGF-beta in fibrofatty lesion development. Circulation 1999; 99:2883-91.
16. Cybulsky MI, Gimbrone MA, Jr. Endothelial expression of a mononuclear leukocyte adhesion molecule during atherogenesis. Science 1991; 251:788-91.
17. Davies PF. Flow-mediated endothelial mechanotransduction. Physiol Rev 1995; 75:519-60.
18. Evanko SP, Angello JC, Wight TN. Formation of hyaluronan- and versican-rich pericellular matrix is required for proliferation and migration of vascular smooth muscle cells. Arterioscler Thromb Vasc Biol 1999; 19:1004-13.
19. Gattullo D, Pagliaro P, Marsh NA, Losano G. New insights into nitric oxide and coronary circulation. Life Sci 1999; 65:2167-74.
20. Gibson CM, Diaz L, Kandarpa K, et al. Relation of vessel wall shear stress to atherosclerosis progression in human coronary arteries. Arterioscler Thromb 1993; 13:310-5.

21. Irace C, Carallo C, Crescenzo A, et al. NIDDM is associated with lower wall shear stress of the common carotid artery. Diabetes 1999; 48:193-7.

22. Pedersen EM, Oyre S, Agerbaek M, et al. Distribution of early atherosclerotic lesions in the human abdominal aorta correlates with wall shear stresses measured in vivo. Eur J Vasc Endovasc Surg 1999; 18:328-33.

23. Pritchard WF, Davies PF, Derafshi Z, et al. Effects of wall shear stress and fluid recirculation on the localization of circulating monocytes in a three-dimensional flow model. J Biomech 1995; 28:1459-69.

24. Ravensbergen J, Ravensbergen JW, Krijger JK, Hillen B, Hoogstraten HW. Localizing role of hemodynamics in atherosclerosis in several human vertebrobasilar junction geometries. Arterioscler Thromb Vasc Biol 1998; 18:708-16.

25. Ross R. Cellular and molecular studies of atherogenesis. Atherosclerosis 1997; 131 Suppl:S3-4.

26. Sampath R, Kukielka GL, Smith CW, Eskin SG, McIntire LV. Shear stress-mediated changes in the expression of leukocyte adhesion receptors on human umbilical vein endothelial cells in vitro. Ann Biomed Eng 1995; 23:247-56.

27. Stanton AV. Hemodynamics, wall mechanics and atheroma: a clinician's perspective. Proc Inst Mech Eng [H] 1999; 213:385-90.

28. Tardy Y, Resnick N, Nagel T, Gimbrone MA, Jr., Dewey CF, Jr. Shear stress gradients remodel endothelial monolayers in vitro via a cell proliferation-migration-loss cycle. Arterioscler Thromb Vasc Biol 1997; 17:3102-6.

29. Topper JN, Cai J, Falb D, Gimbrone MA, Jr. Identification of vascular endothelial genes differentially responsive to fluid mechanical stimuli: cyclooxygenase-2, manganese superoxide dismutase, and endothelial cell nitric oxide synthase are selectively up-regulated by steady laminar shear stress. Proc Natl Acad Sci U S A 1996; 93:10417-22.

30. Wight TN. Cell biology of arterial proteoglycans. Arteriosclerosis 1989; 9:1-20.

31. Wilson RF, Marcus ML, White CW. Prediction of the physiologic significance of coronary arterial lesions by quantitative lesion geometry in patients with limited coronary artery disease. Circulation 1987; 75:723-32.

32. Grimm J, Keller R, de Groot PG. Laminar flow induces cell polarity and leads to rearrangement of proteoglycan metabolism in endothelial cells. Thromb Haemost 1988; 60:437-41.

33. Kinsella MG, Wight TN. Structural characterization of heparan sulfate proteoglycan subclasses isolated from bovine aortic endothelial cell cultures. Biochemistry 1988; 27:2136-44.

34. Oohira A, Wight TN, Bornstein P. Sulfated proteoglycans synthesized by vascular endothelial cells in culture. J Biol Chem 1983; 258:2014-21.

35. Lookene A, Savonen R, Olivecrona G. Interaction of lipoproteins with heparan sulfate proteoglycans and with lipoprotein lipase. Studies by surface plasmon resonance technique. Biochemistry 1997; 36:5267-75.

36. Forsten KE, Courant NA, Nugent MA. Endothelial proteoglycans inhibit bFGF binding and mitogenesis. J Cell Physiol 1997; 172:209-20.

37. Lowe-Krentz LJ, Thompson K, Patton WAd. Heparin releasable and nonreleasable forms of heparan sulfate proteoglycan are found on the surfaces of cultured porcine aortic endothelial cells. Mol Cell Biochem 1992; 109:51-60.

38. McCarty MF. Glucosamine may retard atherogenesis by promoting endothelial production of heparan sulfate proteoglycans. Med Hypotheses 1997; 48:245-51.

39. Ciolino HP, Vijayagopal P, Berenson GS. Endothelial cell-conditioned medium modulates the synthesis and structure of proteoglycans in vascular smooth muscle cells [published erratum appears in Biochim Biophys Acta 1993 May 8;1177(1):107]. Biochim Biophys Acta 1992; 1135:129-40.

40. Klein DJ, Cohen RM, Rymaszewski Z. Proteoglycan synthesis by bovine myocardial endothelial cells is increased by long-term exposure to high concentrations of glucose. J Cell Physiol 1995; 165:493-502.

41. Ramasamy S, Lipke DW, McClain CJ, Hennig B. Tumor necrosis factor reduces proteoglycan synthesis in cultured endothelial cells. J Cell Physiol 1995; 162:119-26.

42. Mas-Oliva J, Arnold KS, Wagner WD, Phillips DR, Pitas RE, Innerarity TL. Isolation and characterization of a platelet-derived macrophage-binding proteoglycan. J Biol Chem 1994; 269:10177-83.

43. Ho G, Broze GJ, Jr., Schwartz AL. Role of heparan sulfate proteoglycans in the uptake and degradation of tissue factor pathway inhibitor-coagulation factor Xa complexes. J Biol Chem 1997; 272:16838-44.

44. Sivaram P, Obunike JC, Goldberg IJ. Lysolecithin-induced alteration of subendothelial heparan sulfate proteoglycans increases monocyte binding to matrix. J Biol Chem 1995; 270:29760-5.

45. Olsson U, Bondjers G, Camejo G. Fatty acids modulate the composition of extracellular matrix in cultured human arterial smooth muscle cells by altering the expression of genes for proteoglycan core proteins. Diabetes 1999; 48:616-22.

46. Kaji T, Yamada A, Miyajima S, et al. Cell density-dependent regulation of proteoglycan synthesis by transforming growth factor-beta(1) in cultured bovine aortic endothelial cells. J Biol Chem 2000; 275:1463-70.

47. Neufeld G, Cohen T, Gengrinovitch S, Poltorak Z. Vascular endothelial growth factor (VEGF) and its receptors. Faseb J 1999; 13:9-22.

48. Clasper S, Vekemans S, Fiore M, et al. Inducible expression of the cell surface heparan sulfate proteoglycan syndecan-2 (fibroglycan) on human activated macrophages can regulate fibroblast growth factor action. J Biol Chem 1999; 274:24113-23.

49. Vlodavsky I, Korner G, Ishai-Michaeli R, Bashkin P, Bar-Shavit R, Fuks Z. Extracellular matrix-resident growth factors and enzymes: possible involvement in tumor metastasis and angiogenesis. Cancer Metastasis Rev 1990; 9:203-26.

50. Chang MY, Potter-Perigo S, Tsoi C, Chait A, Wight TN. Oxidized low density lipoproteins regulate synthesis of monkey aortic smooth muscle cell proteoglycans that have enhanced native low density lipoprotein binding properties. J Biol Chem 2000; 275:4766-73.

51. Potter-Perigo S, Wight TN. Heparin causes the accumulation of heparan sulfate in cultures of arterial smooth muscle cells. Arch Biochem Biophys 1996; 336:19-26.

52. Wang DM, Tarbell JM. Modeling interstitial flow in an artery wall allows estimation of wall shear stress on smooth muscle cells. J Biomech Eng 1995; 117:358-63.

53. Thompson SA, Higashiyama S, Wood K, et al. Characterization of sequences within heparin-binding EGF-like growth factor that mediate interaction with heparin. J Biol Chem 1994; 269:2541-9.

54. Wight TN, Ross R. Proteoglycans in primate arteries. II. Synthesis and secretion of glycosaminoglycans by arterial smooth muscle cells in culture. J Cell Biol 1975; 67:675-86.

55. Arnal JF, Dinh-Xuan AT, Pueyo M, Darblade B, Rami J. Endothelium-derived nitric oxide and vascular physiology and pathology. Cell Mol Life Sci 1999; 55:1078-87.

56. Redmond EM, Cahill PA, Sitzmann JV. Flow-mediated regulation of endothelin receptors in cocultured vascular smooth muscle cells: an endothelium-dependent effect. J Vasc Res 1997; 34:425-35.

57. Anderson AR, Chaplain MA. Continuous and discrete mathematical models of tumor-induced angiogenesis. Bull Math Biol 1998; 60:857-99.

58. Faassen AE, Mooradian DL, Tranquillo RT, et al. Cell surface CD44-related chondroitin sulfate proteoglycan is required for transforming growth factor-beta-stimulated mouse melanoma cell motility and invasive behavior on type I collagen. J Cell Sci 1993; 105:501-11.

59. Turner CE, Burridge K. Transmembrane molecular assemblies in cell-extracellular matrix interactions. Curr Opin Cell Biol 1991; 3:849-53.

60. Wang N, Ingber DE. Control of cytoskeletal mechanics by extracellular matrix, cell shape, and mechanical tension. Biophys J 1994; 66:2181-9.

61. Gimbrone MA. Vascular endothelium and atheroscelrosis. In: Moore S, ed. Vascular Injury and Athrosclerosis. Vol. 9. New York: Marcel Dekker, Inc., 1981:25-45.

62. Ghinea N, Milgrom E. Transport of protein hormones through the vascular endothelium. J Endocrinol 1995; 145:1-9.

63. Venkatachalam MA, Rennke HG. The structural and molecular basis of glomerular filtration. Circ Res 1978; 43:337-47.

64. Weber G, Fabbrini P, Figura N, Resi L. Prevention by methylprednisolone of the endothelial lesions in rabbits on a hypercholesterolic diet or submitted to immunologic injury. Pathol Eur 1974; 9:303-6.

65. Okahara K, Sun B, Kambayashi J. Upregulation of prostacyclin synthesis-related gene expression by shear stress in vascular endothelial cells. Arterioscler Thromb Vasc Biol 1998; 18:1922-6.

66. Prasad A, Husain S, Quyyumi AA. Abnormal flow-mediated epicardial vasomotion in human coronary arteries is improved by angiotensin-converting enzyme inhibition: a potential role of bradykinin. J Am Coll Cardiol 1999; 33:796-804.

67. Hurt E, Camejo G. Effect of arterial proteoglycans on the interaction of LDL with human monocyte-derived macrophages. Atherosclerosis 1987; 67:115-26.

68. Baumann H, Keller R. Which glycosaminoglycans are suitable for antithrombogenic or athrombogenic coatings of biomaterials? Part II: Covalently immobilized endothelial cell surface heparan sulfate (ESHS) and heparin (HE) on synthetic polymers and results of animal experiments. Semin Thromb Hemost 1997; 23:215-23.

69. Sakariassen KS, Baumgartner HR. Axial dependence of platelet-collagen interactions in flowing blood. Upstream thrombus growth impairs downstream platelet adhesion. Arteriosclerosis 1989; 9:33-42.

70. Jaffe EA, Hoyer LW, Nachman RL. Synthesis of von Willebrand factor by cultured human endothelial cells. Proc Natl Acad Sci U S A 1974; 71:1906-9.

71. Moazzam F, DeLano FA, Zweifach BW, Schmid-Schonbein GW. The leukocyte response to fluid stress [see comments]. Proc Natl Acad Sci U S A 1997; 94:5338-43.

72. Walpola PL, Gotlieb AI, Cybulsky MI, Langille BL. Expression of ICAM-1 and VCAM-1 and monocyte adherence in arteries exposed to altered shear stress [published erratum appears in Arterioscler Thromb Vasc Biol 1995 Mar;15(3):429]. Arterioscler Thromb Vasc Biol 1995; 15:2-10.

73. Schwartz SM, deBlois D, O'Brien ER. The intima. Soil for atherosclerosis and restenosis. Circ Res 1995; 77:445-65.

74. Ruoslahti E, Yamaguchi Y. Proteoglycans as modulators of growth factor activities. Cell 1991; 64:867-9.

75. Howell M, Orskov H, Frystyk J, Flyvbjerg A, Gronbaek H, Foegh M. Lanreotide, a somatostatin analogue, reduces insulin-like growth factor I accumulation in proliferating aortic tissue in rabbits in vivo. A preliminary study. Eur J Endocrinol 1994; 130:422-5.

76. Lou H, Zhao Y, Delafontaine P, et al. Estrogen effects on insulin-like growth factor-I (IGF-I)-induced cell proliferation and IGF-I expression in native and allograft vessels. Circulation 1997; 96:927-33.

77. Motomura N, Lou H, Orskov H, Ramwell PW, Foegh ML. Exposure of vascular allografts to insulin-like growth factor-I (IGF-I) increases vascular expression of IGF-I ligand and receptor protein and accelerates arteriosclerosis in rats. Transplantation 1998; 65:1024-30.

78. Burke JM, Ross R. Collagen synthesis by monkey arterial smooth muscle cells during proliferation and quiescence in culture. Exp Cell Res 1977; 107:387-95.

79. Moore S, Friedman RJ, Singal DP, Gauldie J, Blajchman MA, Roberts RS. Inhibition of injury induced thromboatherosclerotic lesions by anti-platelet serum in rabbits. Thromb Haemost 1976; 35:70-81.

80. Ritchie JL, Harker LA. Platelet and fibrinogen survival in coronary atherosclerosis. Response to medical and surgical therapy. Am J Cardiol 1977; 39:595-8.

81. Barbee KA, Davies PF, Lal R. Shear stress-induced reorganization of the surface topography of living endothelial cells imaged by atomic force microscopy. Circ Res 1994; 74:163-71.

82. Bell DR, Sabbah HN, Stein PD. Profiles of velocity in coronary arteries of dogs indicate lower shear rate along inner arterial curvature. Arteriosclerosis 1989; 9:167-75.

83. Kirpalani A, Park H, Butany J, Johnston KW, Ojha M. Velocity and wall shear stress patterns in the human right coronary artery. J Biomech Eng 1999; 121:370-5.

84. Paulsen PK, Hasenkam JM. Three-dimensional visualization of velocity profiles in the ascending aorta in dogs, measured with a hot-film anemometer. J Biomech 1983; 16:201-10.

85. Davies PF, Mundel T, Barbee KA. A mechanism for heterogeneous endothelial responses to flow in vivo and in vitro. J Biomech 1995; 28:1553-60.

86. Krams R, Wentzel JJ, Oomen JA, et al. Evaluation of endothelial shear stress and 3D geometry as factors determining the development of atherosclerosis and remodeling in human coronary arteries in vivo. Combining 3D reconstruction from angiography and IVUS (ANGUS) with computational fluid dynamics. Arterioscler Thromb Vasc Biol 1997; 17:2061-5.

87. Xu XY, Long Q, Collins MW, Bourne M, Griffith TM. Reconstruction of blood flow patterns in human arteries. Proc Inst Mech Eng [H] 1999; 213:411-21.

88. Brown TD. Techniques for mechanical stimulation of cells in vitro: a review. J Biomech 2000; 33:3-14.

89. Liu SQ, Fung YC. Indicial functions of arterial remodeling in response to locally altered blood pressure. Am J Physiol 1996; 270:H1323-33.

90. Thoumine O, Nerem RM, Girard PR. Oscillatory shear stress and hydrostatic pressure modulate cell-matrix attachment proteins in cultured endothelial cells. In Vitro Cell Dev Biol Anim 1995; 31:45-54.

91. Benbrahim A, L'Italien GJ, Milinazzo BB, et al. A compliant tubular device to study the influences of wall strain and fluid shear stress on cells of the vascular wall. J Vasc Surg 1994; 20:184-94.

92. Ziegler T, Bouzourene K, Harrison VJ, Brunner HR, Hayoz D. Influence of oscillatory and unidirectional flow environments on the expression of endothelin and nitric oxide synthase in cultured endothelial cells. Arterioscler Thromb Vasc Biol 1998; 18:686-92.

93. Yoshizumi M, Kurihara H, Sugiyama T, et al. Hemodynamic shear stress stimulates endothelin production by cultured endothelial cells. Biochem Biophys Res Commun 1989; 161:859-64.

94. Sawchuk AP, Unthank JL, Dalsing MC. Drag reducing polymers may decrease atherosclerosis by increasing shear in areas normally exposed to low shear stress. J Vasc Surg 1999; 30:761-4.

95. Malek AM, Izumo S. Control of endothelial cell gene expression by flow. J Biomech 1995; 28:1515-28.

96. Mattsson EJ, Kohler TR, Vergel SM, Clowes AW. Increased blood flow induces regression of intimal hyperplasia. Arterioscler Thromb Vasc Biol 1997; 17:2245-9.

97. Shen J, Luscinskas FW, Connolly A, Dewey CF, Jr., Gimbrone MA, Jr. Fluid shear stress modulates cytosolic free calcium in vascular endothelial cells. Am J Physiol 1992; 262:C384-90.

98. Redmond EM, Cahill PA, Sitzmann JV. Perfused transcapillary smooth muscle and endothelial cell co-culture--a novel in vitro model. In Vitro Cell Dev Biol Anim 1995; 31:601-9.

99. Redmond EM, Cahill PA, Sitzmann JV. Flow-mediated regulation of G-protein expression in cocultured vascular smooth muscle and endothelial cells. Arterioscler Thromb Vasc Biol 1998; 18:75-83.

100. Cappadona C, Redmond EM, Theodorakis NG, et al. Phenotype dictates the growth response of vascular smooth muscle cells to pulse pressure in vitro. Exp Cell Res 1999; 250:174-86.

101. Hendrickson RJ, Cappadona C, Yankah EN, Sitzmann JV, Cahill PA, Redmond EM. Sustained pulsatile flow regulates endothelial nitric oxide synthase and cyclooxygenase expression in co-cultured vascular endothelial and smooth muscle cells. J Mol Cell Cardiol 1999; 31:619-29.

102. Hendrickson RJ, Okada SS, Cahill PA, Yankah E, Sitzmann JV, Redmond EM. Ethanol inhibits basal and flow-induced vascular smooth muscle cell migration in vitro. J Surg Res 1999; 84:64-70.

103. Redmond EM, Cullen JP, Cahill PA, et al. Endothelial cells inhibit flow-induced smooth muscle cell migration: role of plasminogen activator inhibitor-1. Circulation 2001; 103:597-603.

104. Womersley. Method for the calculation of velocity, rate of flow and viscous drag in arteries when the pressure gradient is known. Journal of Physiology 1955; 127:553-563.

105. Hale JF, McDonald DA, Womersley JR. Velocity profiles of oscillating arterial flow, with some calculations of viscous drag and the Reynolds number. Journal of Physiology 1955; 128:629-640.

106. Arisaka T, Mitsumata M, Kawasumi M, Tohjima T, Hirose S, Yoshida Y. Effects of shear stress on glycosaminoglycan synthesis in vascular endothelial cells. Ann N Y Acad Sci 1995; 748:543-54.

107. Davies PF, Robotewskyj A, Griem ML. Quantitative studies of endothelial cell adhesion. Directional remodeling of focal adhesion sites in response to flow forces. J Clin Invest 1994; 93:2031-8.

108. Zhao S, Suciu A, Ziegler T, et al. Synergistic effects of fluid shear stress and cyclic circumferential stretch on vascular endothelial cell morphology and cytoskeleton. Arterioscler Thromb Vasc Biol 1995; 15:1781-6.

109. Resnick N, Collins T, Atkinson W, Bonthron DT, Dewey CF, Jr., Gimbrone MA, Jr. Platelet-derived growth factor B chain promoter contains a cis-acting fluid shear-stress-responsive element [published erratum appears in Proc Natl Acad Sci U S A 1993 Aug 15;90(16):7908]. Proc Natl Acad Sci U S A 1993; 90:4591-5.

110. Ohno M, Cooke JP, Dzau VJ, Gibbons GH. Fluid shear stress induces endothelial transforming growth factor beta-1 transcription and production. Modulation by potassium channel blockade. J Clin Invest 1995; 95:1363-9.

111. Ballermann BJ, Dardik A, Eng E, Liu A. Shear stress and the endothelium. Kidney Int Suppl 1998; 67:S100-8.

112. Ballermann BJ, Ott MJ. Adhesion and differentiation of endothelial cells by exposure to chronic shear stress: a vascular graft model. Blood Purif 1995; 13:125-34.

113. Dardik A, Liu A, Ballermann BJ. Chronic in vitro shear stress stimulates endothelial cell retention on prosthetic vascular grafts and reduces subsequent in vivo neointimal thickness. J Vasc Surg 1999; 29:157-67.

114. Standley PR, Obards TJ, Martina CL. Cyclic stretch regulates autocrine IGF-I in vascular smooth muscle cells: implications in vascular hyperplasia. Am J Physiol 1999; 276:E697-705.

115. McIntire LV. 1992 ALZA Distinguished Lecture: bioengineering and vascular biology. Ann Biomed Eng 1994; 22:2-13.

116. Gaver DP, 3rd, Kute SM. A theoretical model study of the influence of fluid stresses on a cell adhering to a microchannel wall. Biophys J 1998; 75:721-33.

117. Xu J, Liu M, Liu J, Caniggia I, Post M. Mechanical strain induces constitutive and regulated secretion of glycosaminoglycans and proteoglycans in fetal lung cells. J Cell Sci 1996; 109:1605-13.

118. Davies PF, Tripathi SC. Mechanical stress mechanisms and the cell. An endothelial paradigm. Circ Res 1993; 72:239-45.

119. Yan C, Takahashi M, Okuda M, Lee JD, Berk BC. Fluid shear stress stimulates big mitogen-activated protein kinase 1 (BMK1) activity in endothelial cells. Dependence on tyrosine kinases and intracellular calcium. J Biol Chem 1999; 274:143-50.

120. Fink CC, Slepchenko B, Moraru, II, Schaff J, Watras J, Loew LM. Morphological control of inositol-1,4,5-trisphosphate-dependent signals. J Cell Biol 1999; 147:929-36.

121. Fink CC, Slepchenko B, Loew LM. Determination of time-dependent inositol-1,4,5-trisphosphate concentrations during calcium release in a smooth muscle cell. Biophys J 1999; 77:617-28.

122. Takahashi M, Berk BC. Mitogen-activated protein kinase (ERK1/2) activation by shear stress and adhesion in endothelial cells. Essential role for a herbimycin-sensitive kinase. J Clin Invest 1996; 98:2623-31.

123. Wang N, Butler JP, Ingber DE. Mechanotransduction across the cell surface and through the cytoskeleton [see comments]. Science 1993; 260:1124-7.

124. Houston P, White BP, Campbell CJ, Braddock M. Delivery and expression of fluid shear stress-inducible promoters to the vessel wall: applications for cardiovascular gene therapy. Hum Gene Ther 1999; 10:3031-44.

125. Resnick N, Gimbrone MA, Jr. Hemodynamic forces are complex regulators of endothelial gene expression. Faseb J 1995; 9:874-82.

126. Papadaki M, Eskin SG. Effects of fluid shear stress on gene regulation of vascular cells. Biotechnol Prog 1997; 13:209-21.

127. Gosling M, Golledge J, Turner RJ, Powell JT. Arterial flow conditions downregulate thrombomodulin on saphenous vein endothelium. Circulation 1999; 99:1047-53.

128. Jackson RL, Busch SJ, Cardin AD. Glycosaminoglycans: molecular properties, protein interactions, and role in physiological processes. Physiol Rev 1991; 71:481-539.

129. Bernfield M, Kokenyesi R, Kato M, et al. Biology of the syndecans: a family of transmembrane heparan sulfate proteoglycans. Annu Rev Cell Biol 1992; 8:365-93.

130. Lander AD, Selleck SB. The elusive functions of proteoglycans: in vivo veritas. J Cell Biol 2000; 148:227-32.

131. Sperinde GV, Nugent MA. Heparan sulfate proteoglycans control intracellular processing of bFGF in vascular smooth muscle cells. Biochemistry 1998; 37:13153-64.

132. Reiland J, Rapraeger AC. Heparan sulfate proteoglycan and FGF receptor target basic FGF to different intracellular destinations. J Cell Sci 1993; 105:1085-93.

133. Klein-Soyer C, Beretz A, Cazenave JP, et al. Sulfated polysaccharides modulate effects of acidic and basic fibroblast growth factors on repair of injured confluent human vascular endothelium. Arteriosclerosis 1989; 9:147-53.

134. Nugent MA, Nugent HM, Iozzo RV, Sanchack K, Edelman ER. Perlecan is required to inhibit thrombosis after deep vascular injury and contributes to endothelial cell-mediated inhibition of intimal hyperplasia. 1999.

135. Nader HB, Pinhal MA, Bau EC, et al. Development of new heparin-like compounds and other antithrombotic drugs and their interaction with vascular endothelial cells. Braz J Med Biol Res 2001; 34:699-709.

136. Bourin MC, Lindahl U. Glycosaminoglycans and the regulation of blood coagulation. Biochem J 1993; 289:313-30.

137. Nader HB, Buonassisi V, Colburn P, Dietrich CP. Heparin stimulates the synthesis and modifies the sulfation pattern of heparan sulfate proteoglycan from endothelial cells. J Cell Physiol 1989; 140:305-10.

138. Pinhal MA, Walenga JM, Jeske W, et al. Antithrombotic agents stimulate the synthesis and modify the sulfation pattern of a heparan sulfate proteoglycan from endothelial cells. Thromb Res 1994; 74:143-53.

139. Pinhal MA, Santos IA, Silva IF, Dietrich CP, Nader HB. Minimum fragments of the heparin molecule able to produce the accumulation and change of the sulfation pattern of an antithrombotic heparan sulfate from endothelial cells. Thromb Haemost 1995; 74:1169-74.

140. Almeida RA, Fang W, Oliver SP. Adherence and internalization of Streptococcus uberis to bovine mammary epithelial cells are mediated by host cell proteoglycans. FEMS Microbiol Lett 1999; 177:313-7.

141. Ugolini S, Mondor I, Sattentau QJ. HIV-1 attachment: another look. Trends Microbiol 1999; 7:144-9.

142. Nishimura M, Yan W, Mukudai Y, et al. Role of chondroitin sulfate-hyaluronan interactions in the viscoelastic properties of extracellular matrices and fluids. Biochim Biophys Acta 1998; 1380:1-9.

143. Edelman ER, Adams DH, Karnovsky MJ. Effect of controlled adventitial heparin delivery on smooth muscle cell proliferation following endothelial injury. Proc Natl Acad Sci U S A 1990; 87:3773-7.

144. Mousa SA. Comparative efficacy of different low-molecular-weight heparins (LMWHs) and drug interactions with LMWH: implications for management of vascular disorders. Semin Thromb Hemost 2000; 26:39-46.

145. Bar RS, Boes M, Dake BL, Erondu NE, Booth BA. Growth Regulation 1994; 4:S13.

146. Delafontaine P, Ku L, Anwar A, Hayzer DJ. Insulin-like growth factor 1 binding protein 3 synthesis by aortic endothelial cells is a function of cell density. Biochem Biophys Res Commun 1996; 222:478-82.

147. Delafontaine P. Insulin-like growth factor I and its binding proteins in the cardiovascular system. Cardiovasc Res 1995; 30:825-34.

148. Hayry P, Myllarniemi M, Aavik E, et al. Stabile D-peptide analog of insulin-like growth factor-1 inhibits smooth muscle cell proliferation after carotid ballooning injury in the rat. Faseb J 1995; 9:1336-44.

149. Goldspink G. Changes in muscle mass and phenotype and the expression of autocrine and systemic growth factors by muscle in response to stretch and overload. J Anat 1999; 194:323-34.

150. Khachigian LM, Anderson KR, Halnon NJ, Gimbrone MA, Jr., Resnick N, Collins T. Egr-1 is activated in endothelial cells exposed to fluid shear stress and interacts with a novel shear-stress-response element in the PDGF A-chain promoter. Arterioscler Thromb Vasc Biol 1997; 17:2280-6.

151. Malek AM, Greene AL, Izumo S. Regulation of endothelin 1 gene by fluid shear stress is transcriptionally mediated and independent of protein kinase C and cAMP. Proc Natl Acad Sci U S A 1993; 90:5999-6003.

152. Arnqvist HJ, Bornfeldt KE, Chen Y, Lindstrom T. The insulin-like growth factor system in vascular smooth muscle: interaction with insulin and growth factors. Metabolism 1995; 44:58-66.

153. Grant MB, Wargovich TJ, Ellis EA, et al. Expression of IGF-I, IGF-I receptor and IGF binding proteins-1, -2, -3, -4 and -5 in human atherectomy specimens. Regul Pept 1996; 67:137-44.

154. Nerem RM. Hemodynamics and the vascular endothelium. J Biomech Eng 1993; 115:510-4.

155. Taber LA. A model for aortic growth based on fluid shear and fiber stresses. J Biomech Eng 1998; 120:348-54.

156. Qiu Y, Tarbell JM. Interaction between wall shear stress and circumferential strain affects endothelial cell biochemical production. J Vasc Res 2000; 37:147-57.

157. Malek AM, Alper SL, Izumo S. Hemodynamic shear stress and its role in atherosclerosis. Jama 1999; 282:2035-42.

158. Gockerman A, Prevette T, Jones JI, Clemmons DR. Insulin-like growth factor (IGF)-binding proteins inhibit the smooth muscle cell migration responses to IGF-I and IGF-II. Endocrinology 1995; 136:4168-73.

159. Bayes-Genis A, Conover CA, Schwartz RS. The insulin-like growth factor axis: A review of atherosclerosis and restenosis. Circ Res 2000; 86:125-30.

160. Nollert MU, McIntire LV. Convective mass transfer effects on the intracellular calcium response of endothelial cells [published erratum appears in J Biomech Eng 1992 Nov;114(4):496]. J Biomech Eng 1992; 114:321-6.

161. Dull RO, Davies PF. Flow modulation of agonist (ATP)-response (Ca2+) coupling in vascular endothelial cells. Am J Physiol 1991; 261:H149-54.

162. Hornbeck R. Laminar flow in the entrance region of a pipe. Applied Science Research 1964; 13:224-232.

163. O'neil P. Advanced Engineering Mathematics. In: Scanlan-Rohrer A, ed. Belmont: Wadsworth, 1995.

164. Qiu Y, Tarbell JM. Numerical simulation of pulsatile flow in a compliant curved tube model of a coronary artery. J Biomech Eng 2000; 122:77-85.

165. Barakat AI, Davies PF. Mechanisms of shear stress transmission and transduction in endothelial cells. Chest 1998; 114:58S-63S.

166. Salacinski HJ, Goldner S, Giudiceandrea A, et al. The mechanical behavior of vascular grafts: a review. J Biomater Appl 2001; 15:241-78.

167. Dewey CF, Jr., Bussolari SR, Gimbrone MA, Jr., Davies PF. The dynamic response of vascular endothelial cells to fluid shear stress. J Biomech Eng 1981; 103:177-85.

168. Nauman EA, Risic KJ, Keaveny TM, Satcher RL. Quantitative assessment of steady and pulsatile flow fields in a parallel plate flow chamber. Ann Biomed Eng 1999; 27:194-9.

169. Brown DC, Larson RS. Improvements to parallel plate flow chambers to reduce reagent and cellular requirements. BMC Immunol 2001; 2:9.

170. Freyberg MA, Kaiser D, Graf R, Buttenbender J, Friedl P. Proatherogenic flow conditions initiate endothelial apoptosis via thrombospondin-1 and the integrin-associated protein. Biochem Biophys Res Commun 2001; 286:141-9.

171. Gan L, Sjogren LS, Doroudi R, Jern S. A new computerized biomechanical perfusion model for ex vivo study of fluid mechanical forces in intact conduit vessels. J Vasc Res 1999; 36:68-78.

172. Megerman J, Hasson JE, Warnock DF, L'Italien GJ, Abbott WM. Noninvasive measurements of nonlinear arterial elasticity. Am J Physiol 1986; 250:H181-8.

173. Brant AM, Rodgers GJ, Borovetz HS. Measurement in vitro of pulsatile arterial diameter using a helium-neon laser. J Appl Physiol 1987; 62:679-83.

174. Bergel D. The dynamic elastic properties of the arterial wall. journal of Physiology 1961; 156:458-469.

175. Ramesh KT, Narasimhan S. Finite deformations and the dynamic measurement of radial strains in compression Kolsky bar experiments. International Journal of Solids Structures 1996; 33:3723-3738.

176. Dobrin PB. Mechanical properties of arterises. Physiol Rev 1978; 58:397-460.

177. Dowling N. Mechanical Behavior of Materials. New Jersey: Prentice-Hall, Inc., 1993.

178. Branddrup J, Immergut E. Polymer Handbook. In: Branddrup J, Immergut E, eds. NewYork: John Wiley & Sons, 1989.

179. Liu SQ. Biomechanical basis of vascular tissue engineering. Crit Rev Biomed Eng 1999; 27:75-148.

180. DeBakey ME, Lawrie GM, Glaeser DH. Patterns of atherosclerosis and their surgical significance. Ann Surg 1985; 201:115-31.

181. Jiang Y, Kohara K, Hiwada K. Low wall shear stress contributes to atherosclerosis of the carotid artery in hypertensive patients. Hypertens Res 1999; 22:203-7.

182. Buchanan JR, Jr., Kleinstreuer C, Truskey GA, Lei M. Relation between non-uniform hemodynamics and sites of altered permeability and lesion growth at the rabbit aorto-celiac junction. Atherosclerosis 1999; 143:27-40.

183. Eskin SG, McIntire LV. Hemodynamic effects on atherosclerosis and thrombosis. Semin Thromb Hemost 1988; 14:170-4.

184. Marsden PA, Danthuluri NR, Brenner BM, Ballermann BJ, Brock TA. Endothelin action on vascular smooth muscle involves inositol trisphosphate and calcium mobilization. Biochem Biophys Res Commun 1989; 158:86-93.

185. Cornwell TL, Arnold E, Boerth NJ, Lincoln TM. Inhibition of smooth muscle cell growth by nitric oxide and activation of cAMP-dependent protein kinase by cGMP. Am J Physiol 1994; 267:C1405-13.

186. Kjellen L, Lindahl U. Proteoglycans: structures and interactions [published erratum appears in Annu Rev Biochem 1992;61:following viii]. Annu Rev Biochem 1991; 60:443-75.

187. Farndale RW, Buttle DJ, Barrett AJ. Improved quantitation and discrimination of sulphated glycosaminoglycans by use of dimethylmethylene blue. Biochim Biophys Acta 1986; 883:173-7.

188. Bassols A, Massague J. Transforming growth factor beta regulates the expression and structure of extracellular matrix chondroitin/dermatan sulfate proteoglycans. J Biol Chem 1988; 263:3039-45.

189. Ohno H, Blackwell J, Jamieson AM, Carrino DA, Caplan AI. Calibration of the relative molecular mass of proteoglycan subunit by column chromatography on Sepharose CL-2B. Biochem J 1986; 235:553-7.

190. Wasteson A. A method for the determination of the molecular weight and molecular-weight distribution of chondroitin sulphate. J Chromatogr 1971; 59:87-97.

191. Prydz K, Dalen KT. Synthesis and sorting of proteoglycans. J Cell Sci 2000; 113 Pt 2:193-205.

192. Zaman AG, Osende JI, Chesebro JH, et al. In vivo dynamic real-time monitoring and quantification of platelet-thrombus formation : use of a local isotope detector [In Process Citation]. Arterioscler Thromb Vasc Biol 2000; 20:860-5.

193. Bakker SJ, Gans RO. About the role of shear stress in atherogenesis [editorial; comment]. Cardiovasc Res 2000; 45:270-2.

194. Hellums JD. 1993 Whitaker Lecture: biorheology in thrombosis research. Ann Biomed Eng 1994; 22:445-55.

195. Wysokinski WE, McBane RD, 2nd, Owen WG. Individual propensity for arterial thrombosis. Arterioscler Thromb Vasc Biol 1999; 19:883-6.

196. Cattaneo M, Gachet C. ADP receptors and clinical bleeding disorders. Arterioscler Thromb Vasc Biol 1999; 19:2281-5.

197. Gachet C, Cattaneo M, Ohlmann P, et al. Purinoceptors on blood platelets: further pharmacological and clinical evidence to suggest the presence of two ADP receptors. Br J Haematol 1995; 91:434-44.

198. Ross R. The pathogenesis of atherosclerosis--an update. N Engl J Med 1986; 314:488-500.

199. Klagsbrun M, Edelman ER. Biological and biochemical properties of fibroblast growth factors. Implications for the pathogenesis of atherosclerosis. Arteriosclerosis 1989; 9:269-78.

200. Baxter RC. Insulin-like growth factor binding proteins in the human circulation: a review. Horm Res 1994; 42:140-4.

201. Kelley KM, Oh Y, Gargosky SE, et al. Insulin-like growth factor-binding proteins (IGFBPs) and their regulatory dynamics. Int J Biochem Cell Biol 1996; 28:619-37.

202. Moser DR, Lowe WL, Jr., Dake BL, et al. Endothelial cells express insulin-like growth factor-binding proteins 2 to 6. Mol Endocrinol 1992; 6:1805-14.

203. Daughaday WH, Rotwein P. Insulin-like growth factors I and II. Peptide, messenger ribonucleic acid and gene structures, serum, and tissue concentrations. Endocr Rev 1989; 10:68-91.

204. Chen Y, Bornfeldt KE, Arner A, et al. Increase in insulin-like growth factor I in hypertrophying smooth muscle. Am J Physiol 1994; 266:E224-9.

205. Bornfeldt KE, Raines EW, Nakano T, Graves LM, Krebs EG, Ross R. Insulin-like growth factor-I and platelet-derived growth factor-BB induce directed migration of human arterial smooth muscle cells via signaling pathways that are distinct from those of proliferation. J Clin Invest 1994; 93:1266-74.

206. Schwartz RS, Murphy JG, Edwards WD, Camrud AR, Vliestra RE, Holmes DR. Restenosis after balloon angioplasty. A practical proliferative model in porcine coronary arteries. Circulation 1990; 82:2190-200.

207. Farb A, Sangiorgi G, Carter AJ, et al. Pathology of acute and chronic coronary stenting in humans. Circulation 1999; 99:44-52.

208. Foegh ML. Chronic rejection--graft arteriosclerosis. Transplant Proc 1990; 22:119-22.

209. Ewel CH, Foegh ML. Chronic graft rejection: accelerated transplant arteriosclerosis. Immunol Rev 1993; 134:21-31.

210. Grant MB, Wargovich TJ, Bush DM, et al. Expression of IGF-1, IGF-1 receptor and TGF-beta following balloon angioplasty in atherosclerotic and normal rabbit iliac arteries: an immunocytochemical study. Regul Pept 1999; 79:47-53.

211. Papadaki M, Eskin SG, Ruef J, Runge MS, McIntire LV. Fluid shear stress as a regulator of gene expression in vascular cells: possible correlations with diabetic abnormalities. Diabetes Res Clin Pract 1999; 45:89-99.

212. Nakao M, Ono K, Fujisawa S, Iijima T. Mechanical stress-induced Ca2+ entry and Cl- current in cultured human aortic endothelial cells. Am J Physiol 1999; 276:C238-49.

213. Buga GM, Gold ME, Fukuto JM, Ignarro LJ. Shear stress-induced release of nitric oxide from endothelial cells grown on beads. Hypertension 1991; 17:187-93.

214. Ganz P, Davies PF, Leopold JA, Gimbrone MA, Jr., Alexander RW. Short- and long-term interactions of endothelium and vascular smooth muscle in coculture: effects on cyclic GMP production. Proc Natl Acad Sci U S A 1986; 83:3552-6.

215. Gosgnach W, Challah M, Coulet F, Michel JB, Battle T. Shear stress induces angiotensin converting enzyme expression in cultured smooth muscle cells: possible involvement of bFGF [see comments]. Cardiovasc Res 2000; 45:486-92.

216. Shimamoto GT, Byatt JC, Jennings MG, Comens-Keller PG, Collier RJ. Destripeptide insulin-like growth factor-I in milk from bovine somatotropin-treated cows. Pediatr Res 1992; 32:296-300.

217. Weber MS, Boyle PL, Corl BA, Wong EA, Gwazdauskas FC, Akers RM. Expression of ovine insulin-like growth factor-1 (IGF-1) stimulates alveolar bud development in mammary glands of transgenic mice. Endocrine 1998; 8:251-9.

218. Akers RM, McFadden TB, Beal WE, Guidry AJ, Farrell HM. Radioimmunoassay for measurement of bovine alpha-lactalbumin in serum, milk and tissue culture media. J Dairy Res 1986; 53:419-29.

219. Breier BH, Gallaher BW, Gluckman PD. Radioimmunoassay for insulin-like growth factor-I: solutions to some potential problems and pitfalls. J Endocrinol 1991; 128:347-57.

220. Ohlsen SM, Dean DM, Wong EA. Characterization of multiple transcription initiation sites of the ovine insulin-like growth factor-I gene and expression profiles of three alternatively spliced transcripts. DNA Cell Biol 1993; 12:243-51.

221. Weber MS, Purup S, Vestergaard M, Akers RM, Sejrsen K. Nutritional and somatotropin regulation of the mitogenic response of mammary cells to mammary tissue extracts. Domest Anim Endocrinol 2000; 18:159-64.

222. Hossenlopp P, Seurin D, Segovia-Quinson B, Hardouin S, Binoux M. Analysis of serum insulin-like growth factor binding proteins using western blotting: use of the method for titration of the binding proteins and competitive binding studies. Anal Biochem 1986; 154:138-43.

223. Liu SQ. Prevention of focal intimal hyperplasia in rat vein grafts by using a tissue engineering approach. Atherosclerosis 1998; 140:365-77.

224. Gronbaek H, Skjaerbaek C, Nielsen B, et al. Growth hormone and insulin-like growth factor-I: a suggested role in renal transplantation and graft vessel disease. Transplant Proc 1995; 27:2133-6.

225. Motomura N, Lou H, Maurice P, Foegh ML. Acceleration of arteriosclerosis of the rat aorta allograft by insulin growth factor-I. Transplantation 1997; 63:932-6.

226. Banskota NK, Taub R, Zellner K, King GL. Insulin, insulin-like growth factor I and platelet-derived growth factor interact additively in the induction of the protooncogene c-myc and cellular proliferation in cultured bovine aortic smooth muscle cells. Mol Endocrinol 1989; 3:1183-90.

227. Hsieh HJ, Li NQ, Frangos JA. Pulsatile and steady flow induces c-fos expression in human endothelial cells. J Cell Physiol 1993; 154:143-51.

228. Helmlinger G, Geiger RV, Schreck S, Nerem RM. Effects of pulsatile flow on cultured vascular endothelial cell morphology. J Biomech Eng 1991; 113:123-31.

229. Hasdai D, Rizza RA, Holmes DR, Jr., Richardson DM, Cohen P, Lerman A. Insulin and insulin-like growth factor-I cause coronary vasorelaxation in vitro. Hypertension 1998; 32:228-34.

230. Muniyappa R, Walsh MF, Rangi JS, et al. Insulin like growth factor 1 increases vascular smooth muscle nitric oxide production. Life Sci 1997; 61:925-31.

231. Davis MJ, Hill MA. Signaling mechanisms underlying the vascular myogenic response. Physiol Rev 1999; 79:387-423.

232. Zhang Z, Xiao Z, Diamond SL. Shear stress induction of C-type natriuretic peptide (CNP) in endothelial cells is independent of NO autocrine signaling. Ann Biomed Eng 1999; 27:419-26.

233. Ververis J, Ku L, Delafontaine P. Fibroblast growth factor regulates insulin-like growth factor-binding protein production by vascular smooth muscle cells. Am J Med Sci 1994; 307:77-81.

234. Tucci M, Nygard K, Tanswell BV, Farber HW, Hill DJ, Han VK. Modulation of insulin-like growth factor (IGF) and IGF binding protein biosynthesis by hypoxia in cultured vascular endothelial cells. J Endocrinol 1998; 157:13-24.

235. Erondu NE, Dake BL, Moser DR, Lin M, Boes M, Bar RS. Regulation of endothelial IGFBP-3 synthesis and secretion by IGF-I and TGF-beta. Growth Regul 1996; 6:1-9.

236. Taylor WR, Alexander RW. Autocrine control of wound repair by insulin-like growth factor I in cultured endothelial cells. Am J Physiol 1993; 265:C801-5.

237. Gajdusek CM, Luo Z, Mayberg MR. Sequestration and secretion of insulin-like growth factor-I by bovine aortic endothelial cells. J Cell Physiol 1993; 154:192-8.

238. Hodgson DR. Free-ligand accelerated dissociation of insulin-like growth factor 1 (IGF-1) from the type I IGF receptor is reduced by insulin-like growth factor binding protein 3. Regul Pept 2000; 90:33-7.

239. Huynh H. Post-transcriptional and post-translational regulation of insulin-like growth factor binding protein-3 and -4 by insulin-like growth factor-I in uterine myometrial cells. Growth Horm IGF Res 2000; 10:20-7.

240. Villafuerte BC, Zhang WN, Phillips LS. Insulin and insulin-like growth factor-I regulate hepatic insulin-like growth factor binding protein-3 by different mechanisms. Mol Endocrinol 1996; 10:622-30.

241. Lemmey AB, Glassford J, Flick-Smith HC, Holly JM, Pell JM. Differential regulation of tissue insulin-like growth factor-binding protein (IGFBP)-3, IGF-I and IGF type 1 receptor mRNA levels, and serum IGF-I and IGFBP concentrations by growth hormone and IGF-I. J Endocrinol 1997; 154:319-28.

242. Cohick WS, Turner JD. Regulation of IGF binding protein synthesis by a bovine mammary epithelial cell line. J Endocrinol 1998; 157:327-36.

243. Conover CA, Powell DR. Insulin-like growth factor (IGF)-binding protein-3 blocks IGF-I-induced receptor down-regulation and cell desensitization in cultured bovine fibroblasts. Endocrinology 1991; 129:710-6.

244. Romagnolo D, Akers RM, Byatt JC, Wong EA, Turner JD. Regulation of expression of IGF-I-induced IGFBP-3 and IGF-I-receptor by constitutive vs regulated expression of recombinant IGF-I in transfected mammary epithelial cells. Mol. Cell. Endocrinology 1994.

245. Dahlfors G, Arnqvist HJ. Vascular endothelial growth factor and transforming growth factor-beta1 regulate the expression of insulin-like growth factor-binding protein-3, -4, and -5 in large vessel endothelial cells. Endocrinology 2000; 141:2062-7.

246. Karas M, Danilenko M, Fishman D, LeRoith D, Levy J, Sharoni Y. Membrane-associated insulin-like growth factor-binding protein-3 inhibits insulin-like growth factor-I-induced insulin-like growth factor-I receptor signaling in ishikawa endometrial cancer cells. J Biol Chem 1997; 272:16514-20.

247. Mohseni-Zadeh S, Binoux M. Insulin-like growth factor (IGF) binding protein-3 interacts with the type 1 IGF receptor, reducing the affinity of the receptor for its ligand: an alternative mechanism in the regulation of IGF action. Endocrinology 1997; 138:5645-8.

248. Matsumoto T, Tsurumoto T, Goldring MB, Shindo H. Differential effects of IGF-binding proteins, IGFBP-3 and IGFBP-5, on IGF-I action and binding to cell membranes of immortalized human chondrocytes. J Endocrinol 2000; 166:29-37.

249. van der Ven LT, Van Buul-Offers SC, Gloudemans T, et al. Modulation of insulin-like growth factor (IGF) action by IGF-binding proteins in normal, benign, and malignant smooth muscle tissues. J Clin Endocrinol Metab 1996; 81:3629-35.

Vita

Selim Elhadj was born in Algiers, Algeria to Margaret and Haoussine Elhadj. He earned his B.S., M.E., and Ph.D. in chemical engineering from Virginia Tech.